Recent developments in the asymptotic theory of separated flows

Leverhulme Lectures – Lecture Notes

Stefan Braun
Institute of Fluid Mechanics and Heat Transfer,
Vienna University of Technology,
Resselgasse 3/E322, 1040 Wien, Austria
stefan.braun@tuwien.ac.at
http://www.fluid.tuwien.ac.at/

Manchester, Aug. 2006

Contents

Introduction, Acknowledgement **1**

1 Classical boundary layer theory and its breakdown **2**

1.1 Motivation 2

1.2 Second order boundary layer theory 4

1.3 Displacement effect 6

1.4 Example: flow past airfoil 7

1.5 Boundary layer behaviour near a point of vanishing skin friction 9

2 The concept of viscous/inviscid interaction (triple deck): Flat plate trailing edge flow **10**

2.1 Local analysis 10

2.2 Interaction 13

3 Marginal separation **18**

3.1 Experimental observations 18

3.2 DNS results 19

3.3 Benchmark problem: channel flow 21

3.4 Theory of marginal separation 24

3.4.1 Classical boundary layer at the verge of separation 24

3.4.2 Interaction 28

3.4.3 Extension to unsteady, 3D interacting flows including control devices 31

3.5 Bifurcation analysis 35

3.6 Flow control 39

4 Fisher's equation **43**

4.1 2D flow 43

4.2 3D flow 47

4.3 Blow-up asymptotics 52

5 Bifurcations in triple deck flows **56**

5.1 Subsonic expansion ramp flow 56

5.2 Subsonic symmetric wedge shaped trailing edge flow 62

References **63**

Introduction

Although Prandtl's seminal contribution to the understanding of viscous flows at high Reynolds numbers dates back one century significant problems in the context of boundary layer separation and laminar-turbulent boundary layer transition remain still unsolved. The clarification of these open questions is desirable not only from a theoretical point of view but is also essential for practical purposes such as accurate numerical computations with a minimum amount of model assumptions.

A milestone in the development of boundary layer theory is, among others, the introduction of viscous-inviscid interaction by Neiland, Stewartson, Williams and Messiter 1969/70. This approach turned out to be very successful in the description of various fundamental flow problems but could not resolve Goldstein's singularity associated with (strong) boundary layer separation, Stewartson 1970. However, as demonstrated by Ruban 1981 and Stewartson, Smith and Kaups 1982 the strength of Goldstein's singularity can be reduced by varying a parameter controlling the adverse pressure gradient acting on the boundary layer. The limiting case of so-called marginal separation can then be treated successfully with the interaction concept and enables the description of small reverse flow regions. While steady flow problems of this type seemed to be analysed adequately, another breakdown in the form of finite time blow-up appeared in the investigations of the equation of marginal separation extended to include unsteady effects. This breakdown then was associated with a sudden change of the global flow structure.

However, more recent investigations with special emphasis on the well-known non-uniqueness and branching behaviour of steady solutions showed that in the vicinity of the bifurcation point unsteady three-dimensional perturbations of the flow field are governed by an evolution equation of Fisher's type known from mathematical biology. The existence of singular travelling waves interpreted as vortex sheets suggest that solutions of the Fisher equation leading to the formation of finite time singularities may be extended beyond the blow-up time, thereby generating vortical structures qualitatively similar to those emerging in direct numerical simulations and experimental investigations of transitional separation bubbles.

Acknowledgement

This script was prepared during a 10 hour lecture course in the context of a visiting professorship at The University of Manchester, School of Mathematics, 15.02.–14.12.2006, supported by *The Leverhulme Trust* under award reference number F00120AK, the *Manchester Institute for Mathematical Sciences (MIMS)* and proposed by Prof. A.I. Ruban, Manchester, UK.

1 Classical boundary layer theory and its breakdown

1.1 Motivation

- J. Zierep, Symposium Transsonicum IV, 2002: how precisely is it possible to determine the drag of an airfoil – is the accuracy 1%, 10% or 100%?
- *used methodology:* perturbation techniques, laminar boundary layer theory of L. Prandtl (1904) and its extensions,
- *face difficulties:* real high Reynolds-number flows are turbulent in general and tend to separate from solid surfaces (see e.g. [7]),
- *aim:* insight into underlying physics.

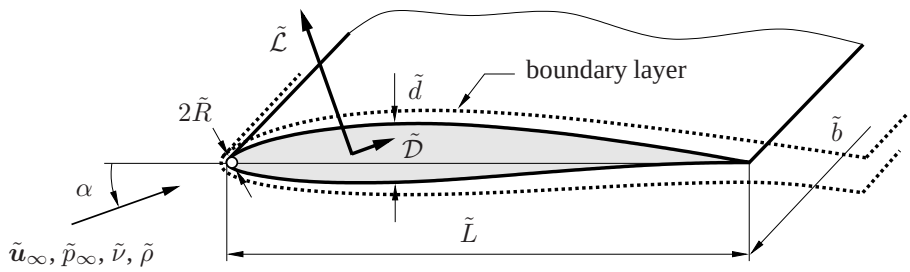

Figure 1: Airfoil at an angle of attack α: free-stream velocity $\tilde{\boldsymbol{u}}_\infty$ and pressure $\tilde{p}_\infty$, kinematic viscosity $\tilde{\nu}$, density $\tilde{\rho}$, chord/reference length $\tilde{L}$, wing span $\tilde{b}$, thickness $\tilde{d}$, nose radius $\tilde{R}$, lift $\tilde{\mathcal{L}}$, drag $\tilde{\mathcal{D}}$.

main assumptions about

flow characteristics:

$$Re = \frac{|\tilde{\boldsymbol{u}}_\infty|\tilde{L}}{\tilde{\nu}} \to \infty\,, \quad M_\infty^2 \ll 1\,, \tag{1}$$

geometry:

$$d = \tilde{d}/\tilde{L} \ll 1\,, \quad R = \tilde{R}/\tilde{L} \sim O(d^2)\,, \quad \Lambda = \tilde{b}/\tilde{L} \to \infty\,, \quad \alpha \ll 1\,. \tag{2}$$

aerodynamic coefficients:

$$\text{lift coefficient} \quad c_l = \frac{\tilde{\mathcal{L}}}{\dfrac{\tilde{\rho}|\tilde{\boldsymbol{u}}_\infty|^2}{2}\,\tilde{L}\tilde{b}} \sim O(\alpha)\,, \tag{3}$$

$$\text{drag coefficient} \quad c_d = \frac{\tilde{\mathcal{D}}}{\dfrac{\tilde{\rho}|\tilde{\boldsymbol{u}}_\infty|^2}{2}\,\tilde{L}\tilde{b}} \gtrsim O(Re^{-1/2})\,, \tag{4}$$

$$\text{pressure coefficient} \quad c_p = \frac{\tilde{p} - \tilde{p}_\infty}{\dfrac{\tilde{\rho}|\tilde{\boldsymbol{u}}_\infty|^2}{2}} \sim O(1)\,. \tag{5}$$

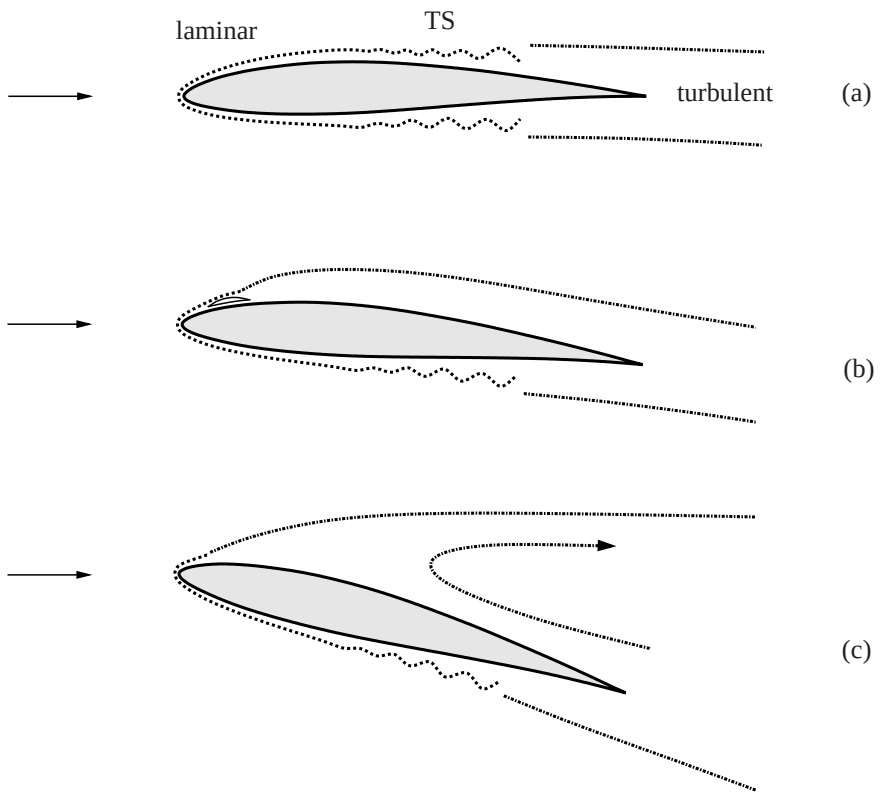

Figure 2: Phenomenology (schematic, $d \lesssim 0.12$): (a) $\alpha \approx 0$, 'slow' laminar/turbulent transition mechanism due to amplification of (external) disturbances ($\rightarrow$ 'receptivity' problem), TS ... Tollmien–Schlichting waves, (b) $\alpha \gtrsim \alpha_c$, leading edge separation with fast (bypass) transition, (c) $\alpha > \alpha_c$, stall.

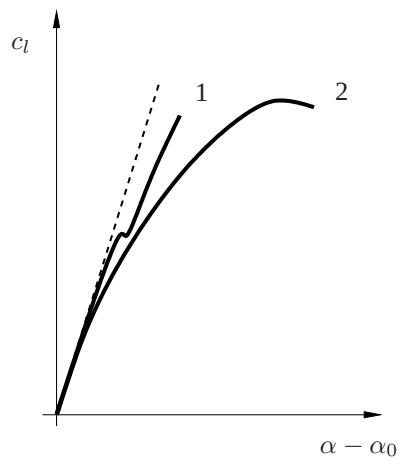

Figure 3: Airfoil lift curve (schematic): dashed – leading order inviscid ($c_l \sim 2\pi\alpha$), 1: $d \lesssim 0.12$, dominant effect: leading edge separation 2: $d \gtrsim 0.15$, trailing edge separation; zero lift angle α_0.

1.2 Second order boundary layer theory

basic equations for incompressible, steady flow:

$$\begin{gathered}\boldsymbol{\nabla}\cdot\boldsymbol{u}=0\,,\quad \boldsymbol{u}\cdot\boldsymbol{\nabla}\boldsymbol{u}=-\boldsymbol{\nabla}p+\frac{1}{Re}\Delta\boldsymbol{u}\,,\\ \text{b.c.:}\quad y\to\infty:\quad u^2+v^2\to 1\,,\quad p\to 0\,;\quad y=0:\quad \boldsymbol{u}=\boldsymbol{0}\,.\end{gathered}\tag{6}$$

$$\boldsymbol{u}=\frac{\tilde{\boldsymbol{u}}}{|\tilde{\boldsymbol{u}}_\infty|}\,,\quad \boldsymbol{x}=\frac{\tilde{\boldsymbol{x}}}{\tilde{L}}\,,\quad p=\frac{\tilde{p}-\tilde{p}_\infty}{\tilde{\rho}|\tilde{\boldsymbol{u}}_\infty|^2}\,,\quad \tilde{\rho},\tilde{\nu}=const.\tag{7}$$

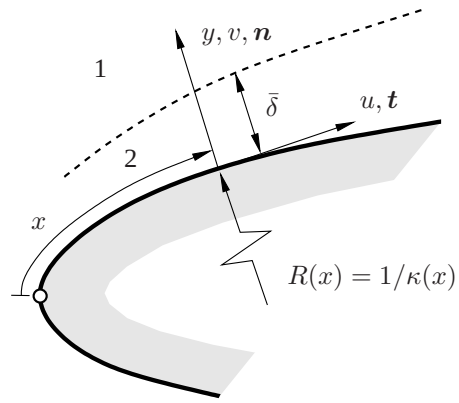

Figure 4: Notations: curvature $\kappa\sim O(1)$, boundary layer thickness $\bar{\delta}$, outer inviscid flow region 1, viscous boundary layer 2.

planar flow, orthogonal curvilinear coordinates, metric coefficient $h=1+\kappa(x)y$:

$$\begin{gathered}\frac{\partial u}{\partial x}+\frac{\partial(hv)}{\partial y}=0\,,\\ \frac{u}{h}\frac{\partial u}{\partial x}+v\frac{\partial u}{\partial y}+\frac{\kappa uv}{h}=-\frac{1}{h}\frac{\partial p}{\partial x}+\frac{1}{Re}\frac{\partial}{\partial y}\left[\frac{1}{h}\left(\frac{\partial(hu)}{\partial y}-\frac{\partial v}{\partial x}\right)\right],\\ \frac{u}{h}\frac{\partial v}{\partial x}+v\frac{\partial v}{\partial y}-\frac{\kappa u^2}{h}=-\frac{\partial p}{\partial y}-\frac{1}{Re}\frac{1}{h}\frac{\partial}{\partial x}\left[\frac{1}{h}\left(\frac{\partial(hu)}{\partial y}-\frac{\partial v}{\partial x}\right)\right].\end{gathered}\tag{8}$$

boundary layer *scaling:*

$$v\sim y\sim\bar{\delta}\sim Re^{-1/2}=:\varepsilon\to 0\,.\tag{9}$$

expansions for outer flow region 1:

$$\boldsymbol{u}\sim\boldsymbol{u}_0(x,y)+\varepsilon\boldsymbol{u}_1(x,y)+\cdots\,,\quad p\sim p_0(x,y)+\varepsilon p_1(x,y)+\cdots\tag{10}$$

and boundary layer 2:

$$\begin{gathered}u\sim U_0(x,\bar{y})+\varepsilon U_1(x,\bar{y})+\cdots\,,\quad v\sim\varepsilon V_0(x,\bar{y})+\varepsilon^2V_1(x,\bar{y})+\cdots\,,\\ p\sim P_0(x,\bar{y})+\varepsilon P_1(x,\bar{y})+\cdots\,,\quad \bar{y}=y/\varepsilon\,.\end{gathered}\tag{11}$$

→ *first order boundary layer theory:*

$$\text{reg. 1}\quad\begin{cases}\Delta\phi_0=0\,,\quad(\boldsymbol{u}_0=\boldsymbol{\nabla}\phi_0)\,,\quad p_0=1/2-(u_0^2+v_0^2)/2\,,\\ \text{b.c.:}\quad y\to\infty:\quad u_0^2+v_0^2\to 1\,,\quad y=0:\quad v_0=0\,;\\ \text{determine:}\quad u_0(x,0)=u_{0w}(x)\,.\end{cases}\tag{12}$$

$$
\text{reg. 2} \quad \begin{cases} U_{0x} + V_{0\bar{y}} = 0\,, \\ U_0 U_{0x} + V_0 U_{0\bar{y}} = -P_{0x} + U_{0\bar{y}\bar{y}}\,, \\ P_{0\bar{y}} = 0\,, \\ \text{b.c.:} \quad \bar{y} \to \infty : \quad U_0 \to u_{0w}(x)\,, \quad \bar{y} = 0 : \quad U_0 = V_0 = 0\,, \quad x = 0 : \quad U_0 = \bar{U}_0(\bar{y})\,; \\ \text{determine:} \quad \tau_w(x)\,,\ \delta^*(x)\,. \end{cases} \tag{13}
$$

consequences:

- *no* curvature effects,
- *no* pressure variation in $\bar{y}$-direction within b.l., i.e. $P_0 = P_0(x)$,
- pressure (gradient) along b.l. *imposed:* $P_0' = -u_{0w} u_{0w}'$,
- b.l. equations of *parabolic* type, i.e. solution at position x depends on upstream behaviour only.

formulation via *stream function* ($u = \psi_y$, $v = -\psi_x$):

$$
\psi(x,y) = \frac{\tilde{\psi}}{|\tilde{\boldsymbol{u}}_\infty|\tilde{L}} = \varepsilon \underbrace{[\Psi_0(x,\bar{y}) + O(\varepsilon)]}_{\Psi} = \varepsilon\, u_{0w} \delta f(x,\eta) + \cdots\,, \quad \eta(x,\bar{y}) = \bar{y}/\delta(x)\,, \tag{14}
$$

so that $\Psi_{0x} = -V_0$, $\Psi_{0\bar{y}} = U_0$; $\delta(x) \sim O(1)$ is a typical (otherwise arbitrary) b.l. thickness and η is a 'pseudo-similarity' variable:

$$
\begin{gathered} f_{\eta\eta\eta} + (u_{0w}\delta\delta' + u_{0w}'\delta^2) f f_{\eta\eta} + u_{0w}'\delta^2(1 - f_\eta^2) + u_{0w}\delta^2(f_x f_{\eta\eta} - f_\eta f_{x\eta}) = 0\,, \\ f(x,0) = f_\eta(x,0) = 0\,, \quad f_\eta(x,\eta \to \infty) \to 1\,. \end{gathered} \tag{15}
$$

the assumption $u_{0w}\delta\delta' + u_{0w}'\delta^2 = 1$[1] leads to

$$
\delta(x) = \frac{1}{u_{0w}} \sqrt{2 \int_0^x u_{0w}(s)\,\mathrm{d}s}\,. \tag{16}
$$

boundary layer characteristics:

- *displacement thickness* δ^**:*

$$
\delta^*(x) = \int_0^\infty \left(1 - \frac{U_0}{u_{0w}}\right) \mathrm{d}\bar{y} = \delta \int_0^\infty (1 - f_\eta)\mathrm{d}\eta = \delta \lim_{\eta\to\infty} (\eta - f)\,, \tag{17}
$$

- *wall shear stress* τ_w*:*

$$
\tau_w(x) = \frac{\tilde{\tau}_w}{\varepsilon\tilde{\rho}|\tilde{\boldsymbol{u}}_\infty|^2} = \left.\frac{\partial U_0}{\partial \bar{y}}\right|_{\bar{y}=0} = \frac{u_{0w}}{\delta}\, f_{\eta\eta}(x,0)\,. \tag{18}
$$

second order boundary layer theory, see e.g. [32]

$$
\text{reg. 1} \quad \begin{cases} \Delta\phi_1 = 0\,, \quad (\boldsymbol{u}_1 = \boldsymbol{\nabla}\phi_1)\,, \quad p_1 = -u_0 u_1 - v_0 v_1\,, \\ \text{b.c.:} \quad y \to \infty : \quad u_1^2 + v_1^2 \to 0\,, \quad y = 0 : \quad v_1 = (u_{0w}\delta^*)'\,; \\ \text{determine:} \quad u_1(x,0)\,, \quad \to \quad p_1(x,0) = -u_{0w} u_1(x,0)\,. \end{cases} \tag{19}
$$

[1] definition of δ; for other possibilities see e.g. [24].

$$
\text{reg. 2} \quad \begin{cases}
U_{1x} + (V_1 + \kappa\bar{y}V_0)_{\bar{y}} = 0\,, \\
U_0U_{1x} + U_1U_{0x} + V_0U_{1\bar{y}} + V_1U_{0\bar{y}} + \kappa(U_0V_0 + \bar{y}V_0U_{0\bar{y}} - \bar{y}U_{0\bar{y}\bar{y}} - U_{0\bar{y}}) = -P_{1x} + U_{1\bar{y}\bar{y}}\,, \\
P_{1\bar{y}} = \kappa U_0^2\,, \\
\text{b.c.:} \quad \bar{y} \to \infty: \quad U_1 \to -\kappa u_{0w}\bar{y} + u_1(x,0)\,, \quad P_1 \to \kappa u_{0w}^2\bar{y} + p_1(x,0)\,, \\
\qquad\qquad \bar{y} = 0: \quad U_1 = V_1 = 0\,.
\end{cases} \tag{20}
$$

notice the *strictly hierarchical structure* of Prandtl's classical b.l. theory.

example: semi infinite flat plate at zero incidence

$$
\begin{aligned}
& u_{0w} = 1\,, \quad P_0 = 0\,, \quad \kappa = 0\,, \\
& f''' + ff'' = 0\,, \quad f(0) = f'(0) = 0\,, \quad f'(\eta \to \infty) \to 1\,; \quad \text{Blasius (1908)} \\
& \delta = \sqrt{2x}\,, \quad \delta^* \approx 1.721\sqrt{x}\,, \quad \tau_w \approx \frac{0.3321}{\sqrt{x}}\,, \\
& v_1(x,0) \approx \frac{1.721}{2\sqrt{x}} \quad \to \quad u_1(x,0) = \phi_{1x}(x,0) = \frac{1}{\pi}\oint_{-\infty}^{\infty} \frac{v_1(s,0)}{x-s}\,\mathrm{d}s = 0\,.
\end{aligned} \tag{21}
$$

as a consequence, in this case (20) has only the trivial solution $P_1 = U_1 = V_1 = 0$ and therefore there is no contribution to the drag coefficient c_d at $O(\varepsilon^2)$.

1.3 Displacement effect

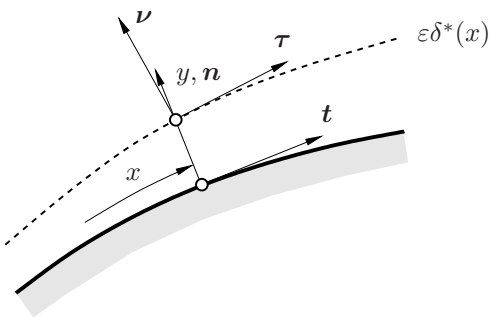

Figure 5: Notation; impermeable solid wall $y = 0$ (= streamline): $v_0 = 0$.

thicken solid body by amount $\varepsilon\delta^*$ and assume at $y = \varepsilon\delta^*$: $\boldsymbol{u}\cdot\boldsymbol{\nu} = 0$,

$$
\boldsymbol{\tau} = \begin{pmatrix} 1 \\ \varepsilon\delta^{*\prime} \end{pmatrix} \frac{1}{\sqrt{1+\varepsilon^2\delta^{*\prime 2}}}\,, \quad \to \quad \boldsymbol{\nu} = \begin{pmatrix} -\varepsilon\delta^{*\prime} \\ 1 \end{pmatrix} \frac{1}{\sqrt{1+\varepsilon^2\delta^{*\prime 2}}}\,; \tag{22}
$$

$$
\boldsymbol{u}\cdot\boldsymbol{\nu} = \frac{1}{\sqrt{\cdots}}\,(-u\varepsilon\delta^{*\prime} + v) = 0\,, \quad \to \quad v(x,\varepsilon\delta^*) = \varepsilon\delta^{*\prime}u(x,\varepsilon\delta^*)\,. \tag{23}
$$

using expansions (10):

$$
v_0(x,0) + \underbrace{v_{0y}(x,0)}_{-u_{0w}'}\,\varepsilon\delta^* + \cdots + \varepsilon v_1(x,0) + \cdots = \varepsilon\delta^{*\prime}(u_{0w}(x) + \cdots)\,,
$$

$$
\begin{aligned}
O(1): \quad & v_0(x,0) = 0\,, \\
O(\varepsilon): \quad & v_1(x,0) = (u_{0w}\delta^*)'\,.
\end{aligned} \tag{24}
$$

1.4 Example: flow past airfoil

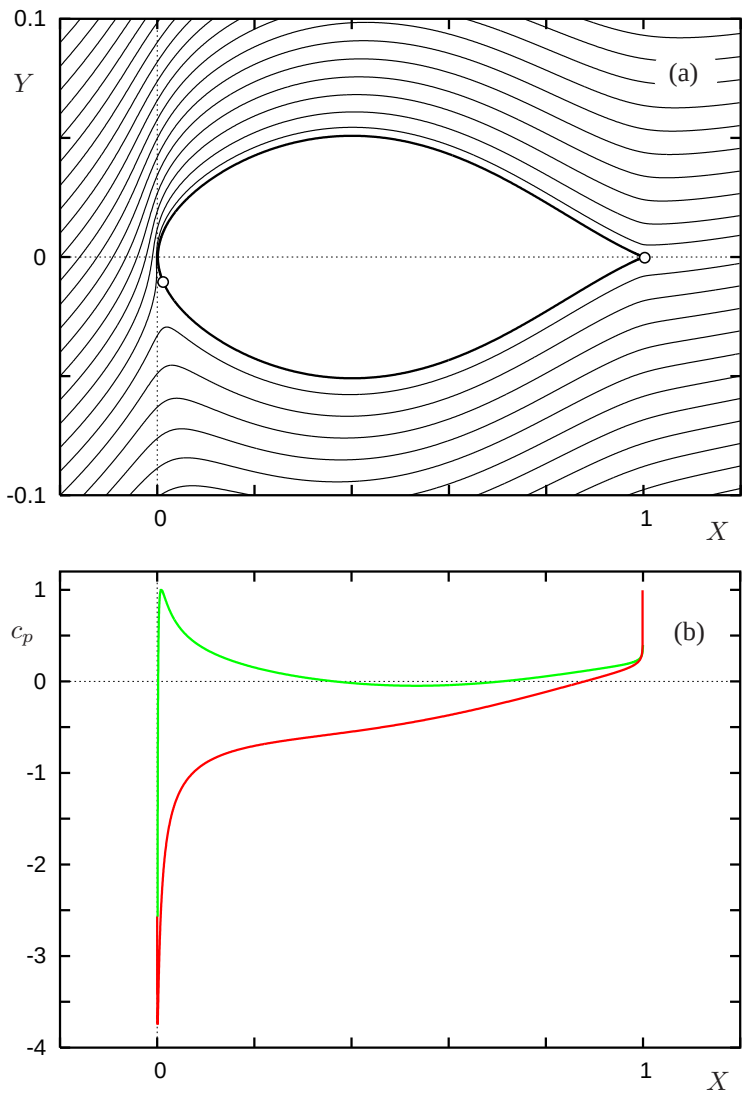

Figure 6: Potential flow past symmetric airfoil at angle of attack (Hess–Smith panel method): $d = 0.1$, $\alpha = 5°$; (a) streamlines, (b) surface pressure distribution, (5).

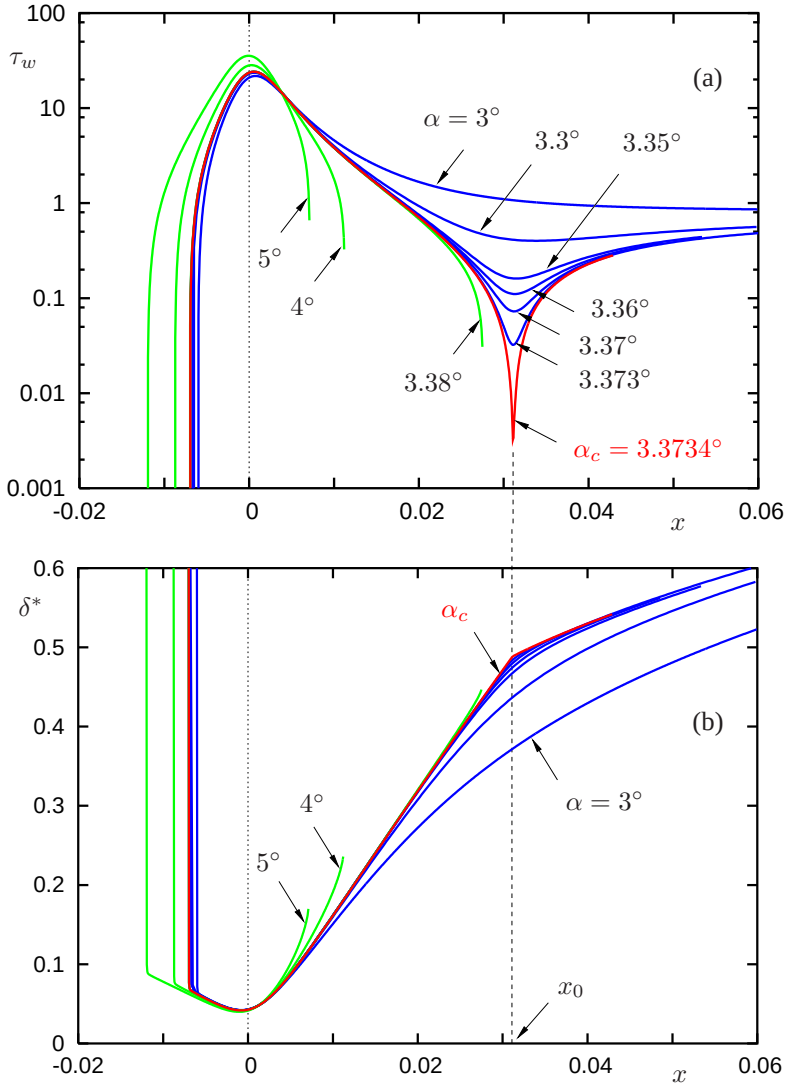

Figure 7: Boundary layer flow past the suction side of the airfoil of Fig. 6 (Keller–box method); (a) wall shear stress $\tau_w(x)$, (18), (b) displacement thickness $\delta^*(x)$, (17); similarity solution at stagnation point: $\delta^* \approx 0.648$; point of marginal separation x_0.

1.5 Boundary layer behaviour near a point of vanishing skin friction

boundary layer equation (subscript '0' omitted):

$$\Psi_{\bar{y}}\Psi_{\bar{y}x} - \Psi_x\Psi_{\bar{y}\bar{y}} = u_w u_w' + \Psi_{\bar{y}\bar{y}\bar{y}} \qquad \left| \frac{\partial^2}{\partial \bar{y}^2} \right. \tag{25}$$

$$\Rightarrow \quad \Psi_{\bar{y}\bar{y}}\Psi_{\bar{y}\bar{y}x} + \Psi_{\bar{y}}\Psi_{\bar{y}\bar{y}\bar{y}x} - \Psi_{x\bar{y}}\Psi_{\bar{y}\bar{y}\bar{y}} - \Psi_x\Psi_{\bar{y}\bar{y}\bar{y}\bar{y}} = \Psi_{\bar{y}\bar{y}\bar{y}\bar{y}\bar{y}}\,; \tag{26}$$

evaluation at the solid boundary $\bar{y} = 0$ where $\Psi = \Psi_x = \Psi_{\bar{y}} = \Psi_{\bar{y}x} = 0$:

$$\frac{1}{2}\frac{\mathrm{d}}{\mathrm{d}x}\underbrace{\Psi_{\bar{y}\bar{y}}^2\Big|_{\bar{y}=0}}_{\tau_w^2(x)} = \Psi_{\bar{y}\bar{y}\bar{y}\bar{y}\bar{y}}\Big|_{\bar{y}=0} =: \chi(x)\,. \tag{27}$$

Taylor series expansion[2] of $\chi(x)$ about x_0 and integration of above formula using $\tau_w(x_0) = 0$ leads to

$$\tau_w(x) \sim \sqrt{-2\chi(x_0)(x_0 - x) + \chi'(x_0)(x - x_0)^2 + \cdots}\,, \quad \text{as} \quad x - x_0 \to 0\,. \tag{28}$$

- in general: $\chi(x_0) < 0$: *Goldstein square-root singularity*, Landau (1944), Goldstein (1948), [11]; for $x > x_0$: $\tau_w \in \mathbb{C} \quad \to \quad$ breakdown of b.l. calculation,
- special case: $\chi(x_0) = 0$: *marginal separation*, Ruban (1981), [21, 22], Stewartson et al. (1982), [29],

$$\tau_w(x \to x_0) \sim a_0|x - x_0| + \cdots\,, \quad a_0 \in \mathbb{R}^+\,, \tag{29}$$

  or *regular separation* with $\tau_w(x \to x_0) \sim a_0(x_0 - x) + \cdots$.

[2] here: assumption; this can be justified by matched asymptotic expansions, see chapter 3.4.1

2 The concept of viscous/inviscid interaction (triple deck): Flat plate trailing edge flow

Stewartson (1969), [27] and Messiter (1970), [20], see also [30].

2.1 Local analysis

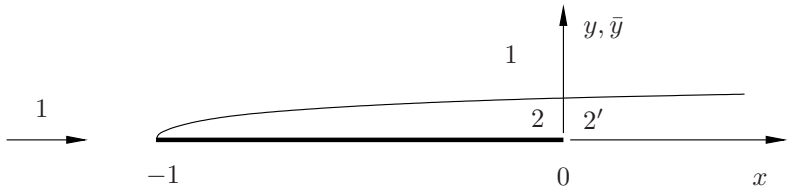

Figure 8: Aligned flat plate of finite length; potential flow region 1, Blasius boundary layer 2, wake $2'$, coordinate shift $x \to x+1$.

expansions up to second order:

$$\begin{aligned} &\text{region 1:} \quad \boldsymbol{u} \sim \boldsymbol{e}_x + \varepsilon \boldsymbol{u}_1(x,y) + \cdots\,, \quad p \sim \varepsilon p_1(x,y) + \cdots\,, \\ &\text{region } 2, 2'\text{:} \quad \Psi \sim \Psi_0(x,\bar{y}) + \varepsilon \Psi_1(x,\bar{y}) + \cdots\,, \quad p \sim \varepsilon P_1(x) + \cdots\,. \end{aligned} \tag{30}$$

region 2:

$$\begin{gathered} \Psi_0 = \sqrt{2(x+1)}\, f(\eta) = \sqrt{x+1}\, F(\bar{\eta})\,, \quad \bar{\eta} = \sqrt{2}\eta = \bar{y}/\sqrt{x+1}\,, \quad x \in [-1,0]\,; \\ 2F''' + FF'' = 0\,, \quad F(0) = F'(0) = 0\,, \quad F'(\bar{\eta} \to \infty) \to 1\,; \\ \tau_w(x) = \frac{F''(0)}{\sqrt{x+1}} = \frac{\lambda}{\sqrt{x+1}}\,, \quad \lambda \approx 0.3321\,; \quad \delta^*(x) = \bar{\beta}_1 \sqrt{x+1}\,, \quad \bar{\beta}_1 \approx 1.721\,. \end{gathered} \tag{31}$$

$$\begin{gathered} \Psi_0(x \to 0^-, \bar{y}) \sim \Psi_0(0,\bar{y}) + \Psi_{0x}\Big|_{x=0} x + \cdots = F(\bar{y}) + \tfrac{1}{2}[F(\bar{y}) - \bar{y}F'(\bar{y})]x + \cdots\,, \\ \to \quad v(x \to 0^-, \bar{y}) \sim -\varepsilon \Psi_{0x} + \cdots = -\varepsilon[F(\bar{y}) - \bar{y}F'(\bar{y})]/2 + \cdots\,. \end{gathered} \tag{32}$$

$$F(\bar{y} \to 0) \sim \frac{\lambda}{2}\bar{y}^2 + O(\bar{y}^5)\,, \quad F(\bar{y} \to \infty) \sim \bar{y} - \bar{\beta}_1 + \text{t.s.t.} \tag{33}$$

continuation of solution into wake requires match $2 - 2'$:

$$\Psi_0(0^-, \bar{y}) = \Psi_0(0^+, \bar{y}) = F(\bar{y})\,. \tag{34}$$

region 3': *Goldstein near wake sub-layer*

seek local similarity behaviour:

$$\Psi \sim x^a g_0(\xi) + \cdots\,, \quad \xi = \bar{y}/x^b\,, \quad x \to 0^+\,; \tag{35}$$

(35) in (25) gives

$$x^{2a-2b-1}[(a-b){g_0'}^2 - a g_0 g_0''] = x^{a-3b} g_0'''\,. \tag{36}$$

matching the shear stress $\Psi_{\bar{y}\bar{y}}$ for regions $3' - 2'$

$$\begin{gathered} x^{a-2b} g_0''(\bar{y}/x^b) + \cdots = F''(x^b \xi) + \cdots \quad \text{as} \quad x \to 0^+\,, \\ \to \quad x^{a-2b} g_0''(\infty) = F''(0) = \lambda \end{gathered} \tag{37}$$

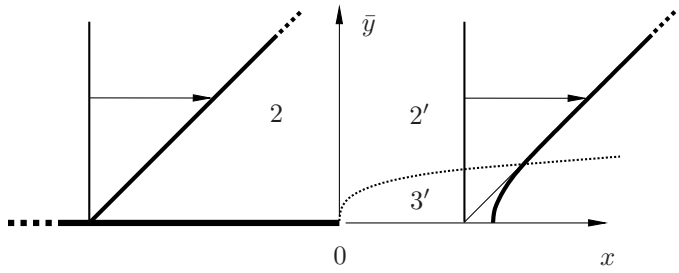

Figure 9: Close up of flat plate trailing edge: Goldstein near wake $3'$; wake centreline $x > 0$, $\bar{y} = 0$: $\Psi = 0$, $\tau = \Psi_{\bar{y}\bar{y}} = 0$ (symmetry condition).

leads to the conditions

$$2a - 2b - 1 = a - 3b\,, \quad a - 2b = 0 \quad \rightarrow \quad a = 2/3\,, \quad b = 1/3\,; \tag{38}$$

therefore:

$$\begin{gathered} \Psi \sim x^{2/3} g_0(\xi) + \cdots\,, \quad \xi = \bar{y}/x^{1/3} \sim O(1)\,, \\ g_0''' + \tfrac{2}{3} g_0 g_0'' - \tfrac{1}{3} {g_0'}^2 = 0\,, \quad g_0(0) = g_0''(0) = 0\,, \quad g_0''(\infty) = \lambda\,; \end{gathered} \tag{39}$$

upper edge of sub-layer:

$$g_0(\xi \to \infty) \sim \frac{\lambda}{2}(\xi + A_0)^2 + \cdots. \tag{40}$$

numerical solution, see Fig. 10:

$$A_0 \approx 0.8920\lambda^{-1/3}\,, \quad g_0'(0) \approx 1.612\lambda^{2/3}\,. \tag{41}$$

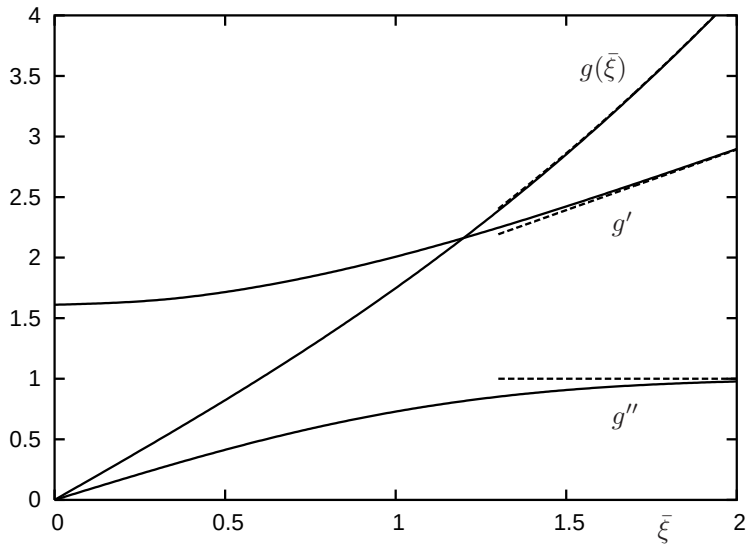

Figure 10: Goldstein near wake similarity solution (39) after transformation (75).

as $\xi \to \infty$:

$$\Psi \sim x^{2/3}\frac{\lambda}{2}(\xi^2 + 2\xi A_0 + \cdots) + \cdots \sim \frac{\lambda}{2}\bar{y}^2 + x^{1/3}\lambda A_0 \bar{y} + \cdots\,, \tag{42}$$

which suggests expansion for

region 2':

$$\Psi \sim F(\bar{y}) + x^{1/3}\Psi_{01}(\bar{y}) + \cdots\,, \quad x \to 0^+\,. \tag{43}$$

substitute above expansion into b.l. equ. (25):

$$F'\Psi_{01}' - \Psi_{01}F'' = 0 \quad \rightarrow \quad \Psi_{01}(\bar{y}) = k_1 F'(\bar{y})\,, \quad k_1 = const. \tag{44}$$

as $\bar{y} \rightarrow 0$ we have $\Psi \sim \lambda\bar{y}^2/2 + \cdots + x^{1/3}\lambda k_1 \bar{y} + \cdots$ and from the match $2' - 3'$, equ. (42)

$$k_1 = A_0\,. \tag{45}$$

an essential result is the *singular behaviour* of v at the trailing edge

$$v = -\varepsilon\Psi_x \sim -\varepsilon x^{-2/3}\frac{A_0}{3}F'(\bar{y}) + \cdots \rightarrow -\infty \quad \text{as} \quad x \rightarrow 0^+\,, \tag{46}$$

indicating a *local breakdown* of the classical b.l. concept.

region 1: second order potential flow

$$u - \mathrm{i}v \sim 1 + \varepsilon w_1(z) + \cdots\,; \quad w_1 = u_1 - \mathrm{i}v_1\,, \quad z = x + \mathrm{i}y = r(\cos\varphi + \mathrm{i}\sin\varphi) \rightarrow 0\,. \tag{47}$$

match $2' - 1$:

$$v_1(x \rightarrow 0^+, 0) \sim -x^{-2/3}A_0/3 + \cdots\,, \tag{48}$$

match $2 - 1$, from (32):

$$v_1(x \rightarrow 0^-, 0) \sim \bar{\beta}_1/2 + \cdots\,. \tag{49}$$

ansatz for w_1; $a = a_r + \mathrm{i}a_i \in \mathbb{C}$:

$$w_1(z \rightarrow 0) \sim az^\alpha + \cdots = [a_r\cos(\alpha\varphi) - a_i\sin(\alpha\varphi)]\,r^\alpha + \mathrm{i}\,[a_r\sin(\alpha\varphi) + a_i\cos(\alpha\varphi)]\,r^\alpha + \cdots\,; \tag{50}$$

$$\begin{aligned} \varphi = 0: &\quad v_1 \sim -x^{-2/3}A_0/3 \sim -a_i\,x^\alpha \quad \rightarrow \quad a_i = A_0/3\,, \quad \alpha = -2/3\,, \\ \varphi = \pi: &\quad v_1 \sim \bar{\beta}_1/2 \sim -(-\sqrt{3}\,a_r/2 - A_0/6)\,|x|^{-2/3} \quad \rightarrow \quad a_r = -A_0/(3\sqrt{3})\,, \end{aligned} \tag{51}$$

finally,

$$w_1(z \rightarrow 0) \sim \frac{A_0}{3}\left(-\frac{1}{\sqrt{3}} + \mathrm{i}\right)z^{-2/3} + O(z^{-1/3})\,. \tag{52}$$

using (19),

$$\begin{aligned} u_1 = -p_1 &\sim \frac{A_0}{3}\left[-\frac{1}{\sqrt{3}}\cos\left(\frac{2\varphi}{3}\right) + \sin\left(\frac{2\varphi}{3}\right)\right]r^{-2/3} + \cdots\,, \\ u_1(x \rightarrow 0^-, 0) &\sim \frac{2A_0}{3\sqrt{3}}\,|x|^{-2/3} + \cdots\,, \quad u_1(x \rightarrow 0^+, 0) \sim -\frac{A_0}{3\sqrt{3}}\,x^{-2/3} + \cdots\,, \end{aligned} \tag{53}$$

which is singular as $x \rightarrow 0$.

region 2: second order b.l. theory

from (20), (30) with $\kappa = 0$:

$$\Psi_{0\bar{y}}\Psi_{1\bar{y}x} + \Psi_{1\bar{y}}\Psi_{0\bar{y}x} - \Psi_{0x}\Psi_{1\bar{y}\bar{y}} - \Psi_{1x}\Psi_{0\bar{y}\bar{y}} = -P_1' + \Psi_{1\bar{y}\bar{y}\bar{y}}\,. \tag{54}$$

match $2 - 1$:

$$P_1(x \rightarrow 0^-) = p_1(x \rightarrow 0^-, 0) \sim -\frac{2A_0}{3\sqrt{3}}\,|x|^{-2/3} + \cdots\,; \tag{55}$$

the balance of the pressure gradient requires $\Psi_{1x} \sim O(|x|^{-5/3})$ since $\Psi_0(x \rightarrow 0^-, \bar{y}) \sim F(\bar{y}) + O(x)$, i.e. $\Psi_1 \sim \Psi_{1\bar{y}\bar{y}\bar{y}} \sim O(|x|^{-2/3}) \quad \rightarrow$ main part 2 of b.l. is *inviscid* to leading order as $x \rightarrow 0^-$ and as a consequence a sub-layer is needed to satisfy the no-slip condition:

region 3: viscous sub-layer

with $\zeta = \bar{y}/|x|^{\sigma} \sim O(1)$, the balance $P_1' \sim \Psi_{1\bar{y}\bar{y}\bar{y}} \sim \Psi_{0\bar{y}}\Psi_{1\bar{y}x} \sim \cdots$ yields $\sigma = 1/3$; hence

$$\Psi \sim \frac{\lambda}{2}|x|^{2/3}\zeta^2 + \cdots + \varepsilon|x|^{-2/3} f_1(\zeta) + \cdots \quad \text{as} \quad x \to 0^- \tag{56}$$

with $f_1(0) = f_1'(0) = 0$ and $f_1(\zeta \to \infty)$: no exponential growth; $f_1(\zeta)$ can be expressed in terms of a confluent hypergeometric function with asymptotic behaviour

$$f_1(\zeta \to \infty) \sim O(\zeta)\,. \tag{57}$$

expansion (56) breaks down if

$$|x|^{2/3} \sim \varepsilon|x|^{-2/3} \quad \to \quad |x| \sim \varepsilon^{3/4} = Re^{-3/8}\,, \tag{58}$$

which leads to the *interaction length scaling*.

2.2 Interaction

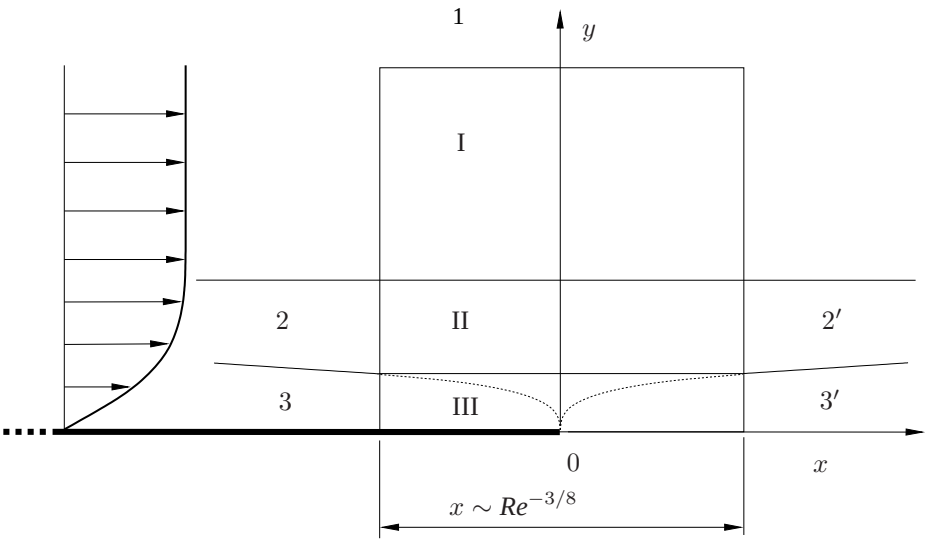

Figure 11: Trailing edge triple deck structure.

region II: *main deck*

cf. 2′: $\Psi \sim F(\bar{y}) + x^{1/3}A_0F'(\bar{y}) + \cdots\,, \quad P_1 \sim O(x^{-2/3}) \quad$ as $x \to 0^+$

$$\begin{aligned} \Rightarrow \quad & \Psi \sim F(\bar{y}) + Re^{-1/8}\Psi_{10}(x^*, \bar{y}) + \cdots\,, \quad x^* = Re^{3/8}x \sim O(1)\,, \\ & p \sim Re^{-1/4}\bar{P}_1(x^*, \bar{y}) + \cdots\,; \end{aligned} \tag{59}$$

into Navier–Stokes equations[3]:

$$\begin{aligned} & F'\Psi_{10\bar{y}x^*} - \Psi_{10x^*}F'' = 0 \quad \to \quad \Psi_{10} = \bar{A}(x^*)F'(\bar{y})\,, \\ & \bar{P}_{1\bar{y}} = 0 \quad \to \quad \bar{P}_1 = \bar{P}(x^*)\,, \end{aligned} \tag{61}$$

[3]

$$x: \quad \Psi_{\bar{y}}\Psi_{\bar{y}x} - \Psi_x\Psi_{\bar{y}\bar{y}} = -p_x + \Psi_{\bar{y}\bar{y}\bar{y}} + \varepsilon^2\Psi_{\bar{y}xx}\,, \quad y: \quad \varepsilon(-\Psi_{\bar{y}}\Psi_{xx} + \Psi_x\Psi_{\bar{y}x}) = -p_{\bar{y}}/\varepsilon - \varepsilon^3\Psi_{xxx} - \varepsilon\Psi_{x\bar{y}\bar{y}} \tag{60}$$

where $\bar{A}(x^*)$, $\bar{P}(x^*)$ remain undetermined at this stage.

- displacement thickness:

$$\delta^*(x \to 0) = \int_0^\infty \left(1 - \frac{\Psi_{\bar{y}}}{u_{0w}}\right) \mathrm{d}\bar{y} \sim \bar{\beta}_1 - Re^{-1/8}\bar{A}(x^*) + \cdots , \tag{62}$$

which suggests notion *displacement function* $\bar{A}$, more precisely, *negative correction of displacement thickness*.

- slope of streamlines:

$$\tan\vartheta = \frac{v}{u} = -\frac{Re^{3/8}\Psi_{x^*}}{Re^{1/2}\Psi_{\bar{y}}} \sim -Re^{-1/8}\frac{Re^{-1/8}\bar{A}'F' + \cdots}{F' + Re^{-1/8}\bar{A}F'' + \cdots} = -Re^{-1/4}\bar{A}'(x^*) + O(Re^{-3/8}) \tag{63}$$

remains *unchanged* across whole reg. II.

- y-velocity component at boundary layer edge:

$$v|_{\bar{y}\to\infty} = -\varepsilon\Psi_x|_{\bar{y}\to\infty} \sim -Re^{-1/4}\bar{A}'(x^*) + \cdots . \tag{64}$$

region III: *lower deck*

from reg. 3: $\Psi \sim \lambda|x|^{2/3}\zeta^2/2 + \cdots + \varepsilon|x|^{-2/3}f_1(\zeta) + \cdots , \quad P_1 \sim (|x|^{-2/3}) \quad$ as $x \to 0^-$,

$$\begin{aligned} &\zeta = \bar{y}/|Re^{-3/8}x^*|^{1/3} \sim O(1) \quad \to \quad \bar{y} \sim O(Re^{-1/8}) \\ &\Rightarrow \quad \Psi \sim Re^{-1/4}\Psi^*(x^*, y^*) + \cdots , \quad y^* = Re^{1/8}\bar{y} = Re^{5/8}y , \\ &\qquad p \sim Re^{-1/4}P_1^*(x^*, y^*) + \cdots ; \end{aligned} \tag{65}$$

into (60):

$$\begin{aligned} &\Psi^*_{y^*}\Psi^*_{y^*x^*} - \Psi^*_{y^*}\Psi^*_{y^*y^*} = -P^*_{1x^*} + \Psi^*_{y^*y^*y^*} , \\ &P^*_{1y^*} = 0 \quad \to \quad P_1^* = P^*(x^*) , \\ &\Psi^*(x^*, 0) = \Psi^*_{y^*}(x^* < 0, 0) = \Psi^*_{y^*y^*}(x^* > 0, 0) = 0 , \end{aligned} \tag{66}$$

i.e. *Prandtl's b.l. equations*.

upper 'b.c.' from match III–II: $\Psi \sim Re^{-1/4}\Psi^*(x^*, y^* \to \infty) + \cdots = F(\bar{y} \to 0) + Re^{-1/8}\bar{A}F'(\bar{y} \to 0) + \cdots$

$$\Rightarrow \quad \Psi^*(x^*, y^* \to \infty) \sim \frac{\lambda}{2}y^{*2} + \lambda\bar{A}(x^*)y^* + \cdots , \quad P^*(x^*) = \bar{P}(x^*) . \tag{67}$$

match III–$(3, 3')$:

$$\begin{aligned} &\Psi^*(x^* \to -\infty, y^*) \sim \frac{\lambda}{2}y^{*2} + |x^*|^{-2/3}f_1\left(\frac{y^*}{|x^*|^{1/3}}\right) + \cdots , \\ &\Psi^*(x^* \to \infty, y^*) \sim x^{*2/3}g_0\left(\frac{y^*}{x^{*1/3}}\right) + \cdots . \end{aligned} \tag{68}$$

region I: *upper deck*

$(x^*, \hat{y}) = Re^{3/8}(x, y) , \quad \hat{y} = Re^{-1/8}\bar{y} ,$

$$u \sim 1 + Re^{-1/4}\hat{u}_1(x^*, \hat{y}) + \cdots , \quad v \sim Re^{-1/4}\hat{v}_1(x^*, \hat{y}) + \cdots , \quad p \sim Re^{-1/4}\hat{p}_1(x^*, \hat{y}) + \cdots \tag{69}$$

into Navier–Stokes eqns. (60):

$$\hat{u}_{1x^*} = -\hat{p}_{1x^*}\,, \quad \hat{v}_{1x^*} = -\hat{p}_{1\hat{y}}\,, \tag{70}$$

i.e. the *linearised Euler equations*; solution in terms of analytical function

$$\hat{w}_1(\hat{z}) = \hat{u}_1 - \mathrm{i}\hat{v}_1 = -\hat{p}_1 - \mathrm{i}\hat{v}_1\,, \quad \hat{z} = x^* + \mathrm{i}\hat{y}\,. \tag{71}$$

match I–1:

$$Re^{-1/4}\hat{w}_1(\hat{z}\to\infty) = Re^{-1/2}w_1(z\to 0) \quad \to \quad \hat{w}_1(\hat{z}\to\infty) \sim \frac{A_0}{3}\left(-\frac{1}{\sqrt{3}} + \mathrm{i}\right)\hat{z}^{-2/3} + \cdots\,. \tag{72}$$

match I–II: $\quad v \sim Re^{-1/4}\hat{v}_1(x^*, \hat{y}\to 0) = -\varepsilon\Psi_x|_{\bar{y}\to\infty} \sim -Re^{-1/4}\bar{A}'F'(\bar{y}\to\infty) + \cdots$

$$\Rightarrow \quad \hat{v}_1(x^*, \hat{y}\to 0) \sim -\bar{A}'(x^*) + \cdots\,, \tag{73}$$

finally,

$$-\hat{u}_1(x^*, 0) = \hat{p}_1(x^*, 0) = \bar{P}(x^*) = P^*(x^*) = \frac{1}{\pi}\oint_{-\infty}^{\infty} \frac{\bar{A}'(s)}{x^* - s}\,\mathrm{d}s\,, \tag{74}$$

representing the *interaction law (Hilbert integral)*, known from thin airfoil theory.

affine transformation

$$\begin{gathered} x^* = \lambda^{-5/4}X\,, \quad y^* = \lambda^{-3/4}Y\,, \quad \Psi^* = \lambda^{-1/2}\Psi\,, \quad P^* = \lambda^{1/2}P\,, \quad \bar{A} = \lambda^{-3/4}A\,, \\ (g_0, f_1) = \lambda^{1/3}(g, f)\,, \quad (\xi, A_0, \zeta) = \lambda^{-1/3}(\bar{\xi}, \bar{A}_0, \bar{\zeta}) \end{gathered} \tag{75}$$

leads to the *canonical form* of the *fundamental problem* of the trailing edge:

$$\begin{gathered} \Psi_Y\Psi_{YX} - \Psi_X\Psi_{YY} = -P' + \Psi_{YYY}\,, \\ Y = 0\,, \quad X < 0: \quad \Psi = \Psi_Y = 0\,, \quad X > 0: \quad \Psi = \Psi_{YY} = 0\,, \\ Y \to \infty: \quad \Psi \sim \frac{Y^2}{2} + AY + \cdots\,, \\ X \to -\infty: \quad \Psi \sim \frac{Y^2}{2} + |X|^{-2/3}f(\bar{\zeta}) + \cdots\,, \quad X \to \infty: \quad \Psi \sim X^{2/3}g(\bar{\xi}) + \cdots\,, \\ P = \frac{1}{\pi}\oint_{-\infty}^{\infty} \frac{A'}{X - s}\,\mathrm{d}s\,. \end{gathered} \tag{76}$$

asymptotic behaviour, from (72)-(74); combining (76), (57) and (40):

$$\begin{gathered} X \to -\infty: \quad P \sim -\frac{2\bar{A}_0}{3\sqrt{3}}\,|X|^{-2/3} + \cdots\,, \quad A \sim O(|X|^{-1})\,, \\ X \to \infty: \quad P \sim \frac{\bar{A}_0}{3\sqrt{3}}\,X^{-2/3} + \cdots\,, \quad A \sim \bar{A}_0\,X^{1/3} + \cdots\,. \end{gathered} \tag{77}$$

centreline velocity, from (68):

$$X \to \infty: \quad U(X, 0) = \Psi_Y|_{Y=0} \sim g'(0)\,X^{1/3} + \cdots\,. \tag{78}$$

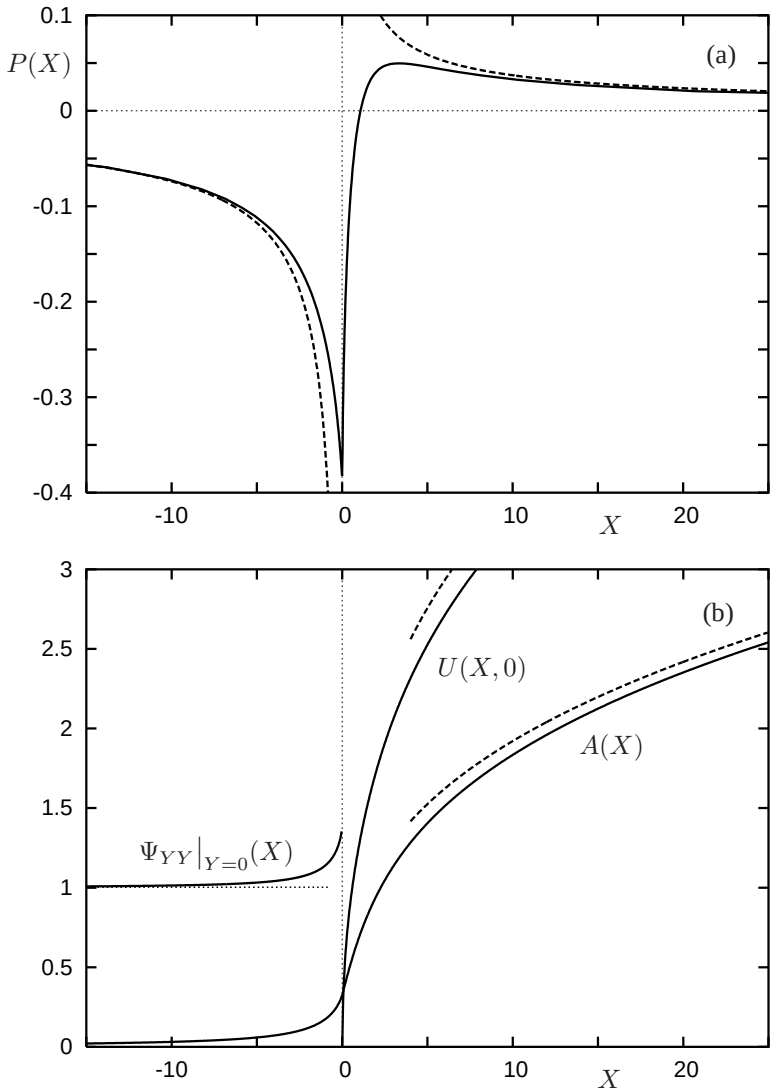

Figure 12: Flat plate trailing edge flow; numerical solution of (76): (a) induced pressure, (b) correction of wall shear, displacement function, wake centreline velocity; dashed lines: asymptotes (77), (78).

drag of finite plate (one side only), evaluation of (4):

$$c_d = 2\varepsilon \int_{-1}^{0} \tau_w(x)\,\mathrm{d}x\,, \tag{79}$$

$$\tau_w \sim \lambda \begin{cases} \dfrac{1}{\sqrt{x+1}} & \text{(Blasius b.l.)}, \\ \Psi_{YY}|_{Y=0} & \text{(TD)} \end{cases} \tag{80}$$

$$\begin{aligned} \rightarrow \quad c_d &\sim 4\lambda Re^{-1/2} + 2\lambda^{-1/4} Re^{-7/8} \int_{-\infty}^{0} (\Psi_{YY}|_{Y=0} - 1)\,\mathrm{d}X + \cdots \\ &\approx 1.328\, Re^{-1/2} + 2.668\, Re^{-7/8} + O(Re^{-1}) \end{aligned} \tag{81}$$

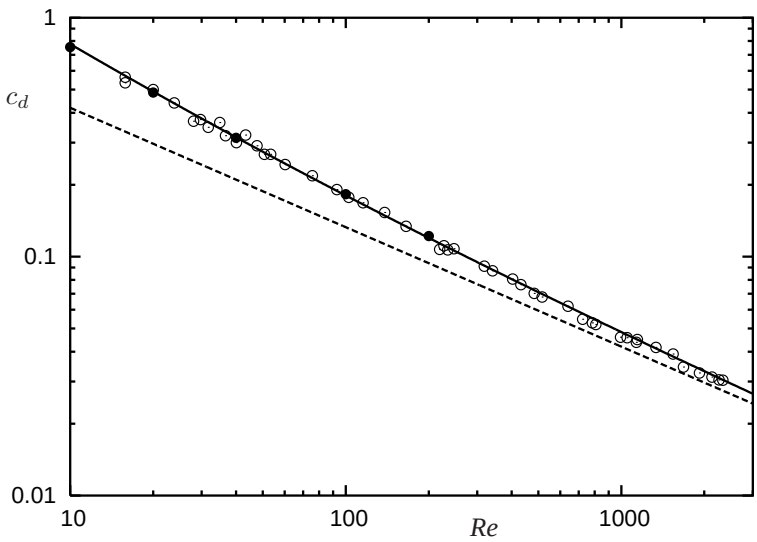

Figure 13: Drag coefficient for flat plate of finite length; ○ experimental data, Janour (1951), ● Navier–Stokes calculations, Dennis (1973), dashed line: Blasius (1908) similarity solution $c_d \sim 1.328\, Re^{-1/2}$, solid line: triple deck correction (81).

3 Marginal separation

3.1 Experimental observations

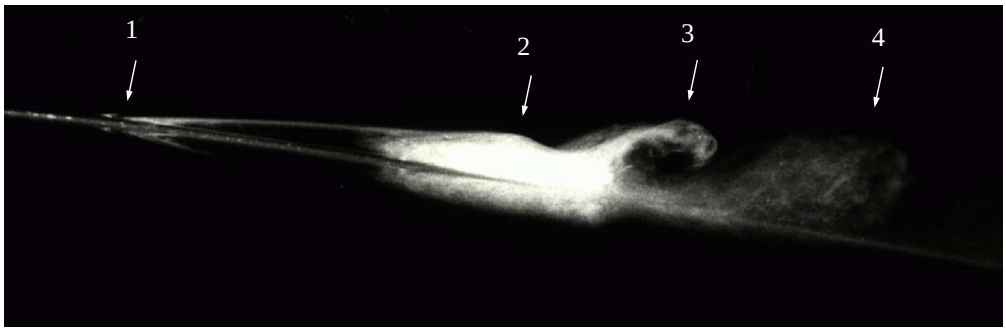

Figure 14: Smoke flow visualisation (snapshot) of a laminar separation bubble on an Eppler 387 airfoil at $\alpha = 2°$ and $Re = 10^5$; 1: nearly steady laminar separation, 2: onset of bursting process, 3: formation of Λ-vortex, 4: vortex breakdown, developing turbulent boundary layer; source: G. Cole, T.J. Mueller, University of Notre Dame, Indiana, USA.

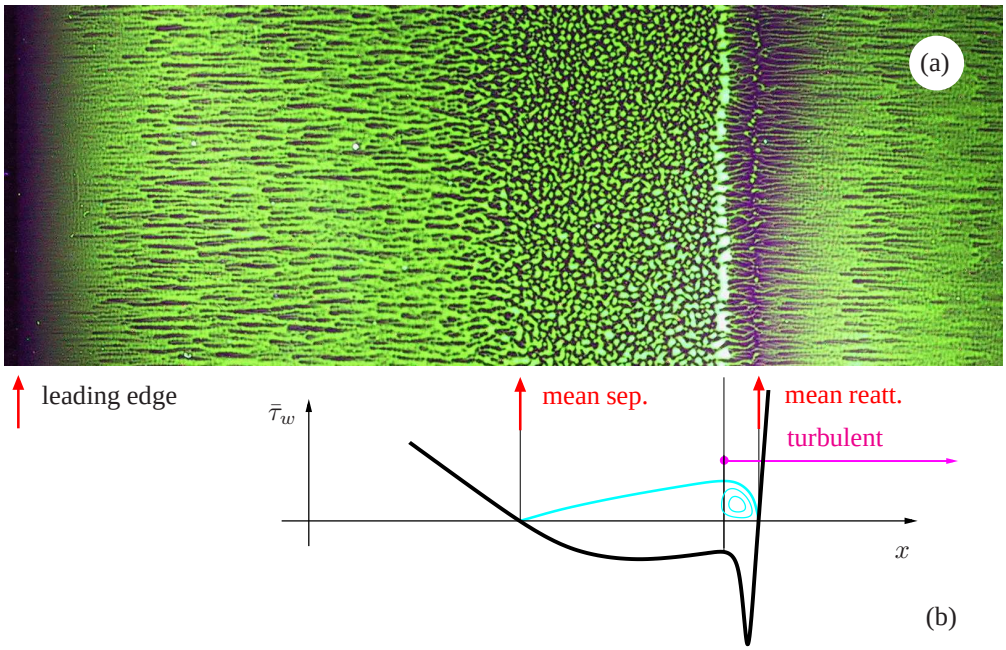

Figure 15: Laminar separation bubble with turbulent reattachment; (a) oil flow pattern on an Eppler 387 airfoil at $\alpha = 2°$ and $Re = 3.5 \times 10^5$ after 15 minutes in the UIUC laminar wind tunnel; source: B.D. McGranahan & M.S. Selig, University of Illinois at Urbana-Champaign, USA, (b) corresponding mean wall shear (qualitative).

3.2 DNS results

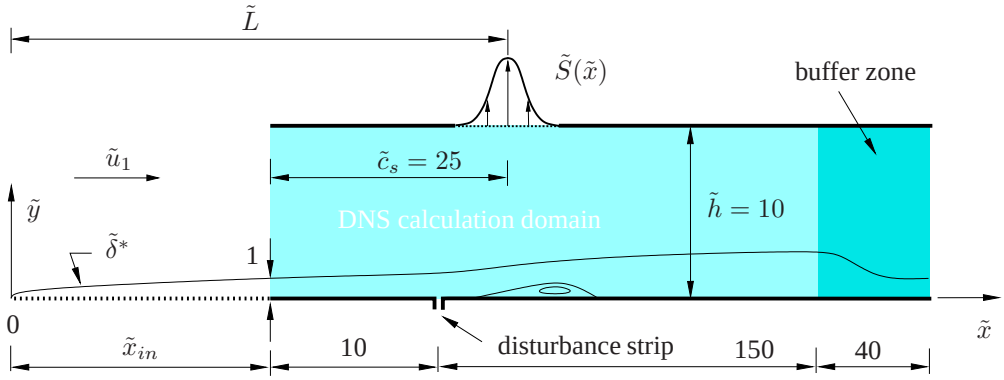

Figure 16: Channel flow of M. Alam & N.D. Sandham, [1] (not to scale); all measures in multiples of the displacement thickness $\tilde{\delta}^*_{in} = \tilde{\delta}^*(\tilde{x}_{in})$ of a Blasius boundary layer; channel width $= 30\,\tilde{\delta}^*_{in}$, $Re_{\tilde{\delta}^*_{in}} = 500$, mesh (max.): $x \times y \times z = 384 \times 160 \times 128$ grid points, computer: Cray (up to 128 CPU's), computing time: 20,000 PE h $\approx$ 6.5 days. $\tilde{L} \approx 193.85\,\tilde{\delta}^*_{in}$, $\tilde{x}_{in} \approx 168.85\,\tilde{\delta}^*_{in}$, $Re \approx 0.97 \times 10^5$ (based on calculations using Blasius solution); boundary conditions: no slip at lower wall, $u = 1$ *(!)*, cf. (86), $v = S(x)$ at upper bound, periodicity in x, z direction (Fourier series), Chebyshev collocation in y direction.

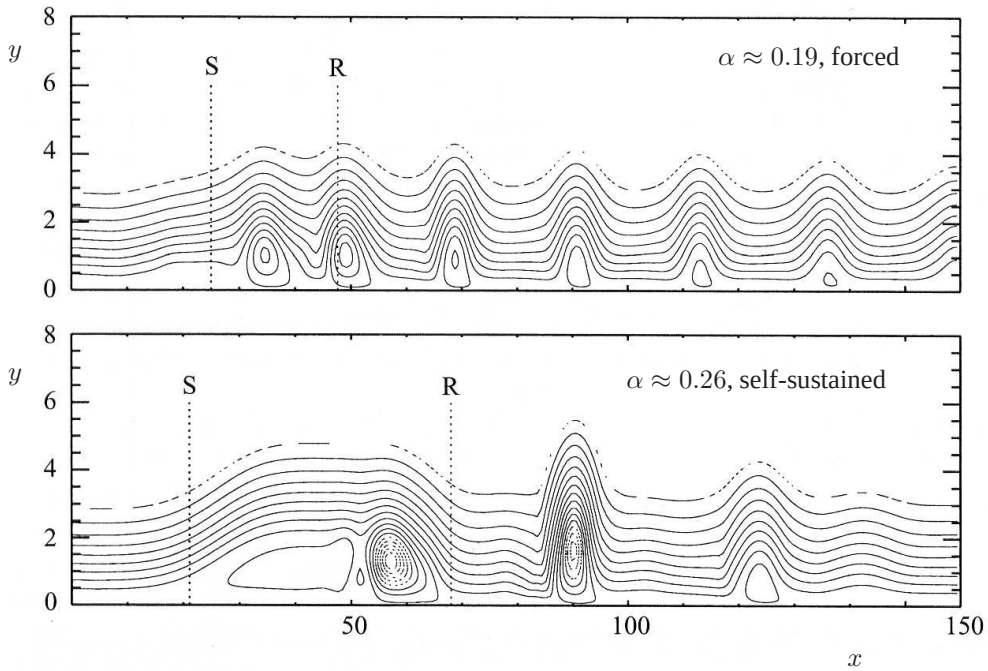

Figure 17: Instantaneous contours of stream function (2D flow), [1]: "... vortex shedding was found for large values of suction strength *(i.e. α)*, which persisted even *without* external forcing ...;
but: ... there is disagreement about a precise *shedding criterion*".
S/R mean separation/reattachment.

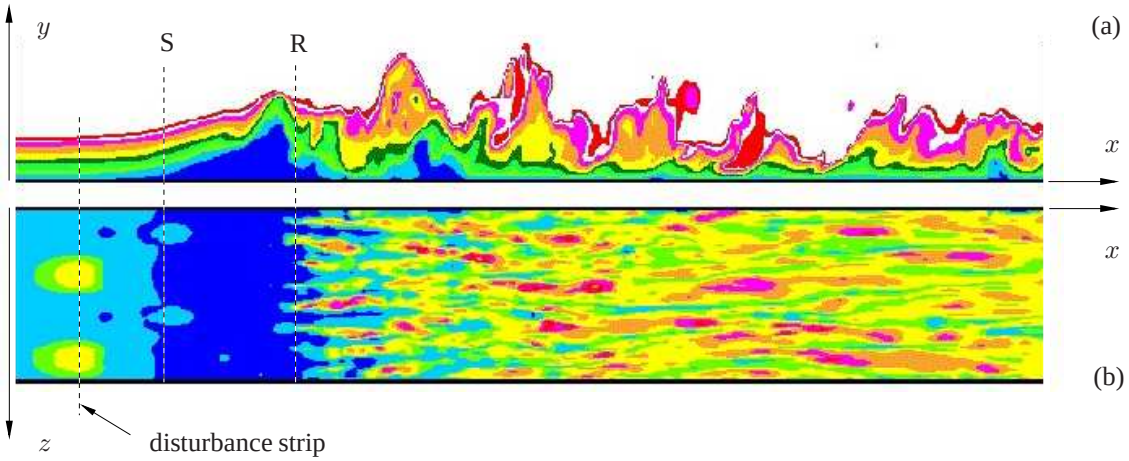

Figure 18: Instantaneous contours of stream-wise velocity $u(x, y, z, t)$, $\alpha \approx 0.19$; (a) side view, (b) top view of a section close to the wall; darkest areas denote reversed flow, S/R mean separation/reattachment, [1].

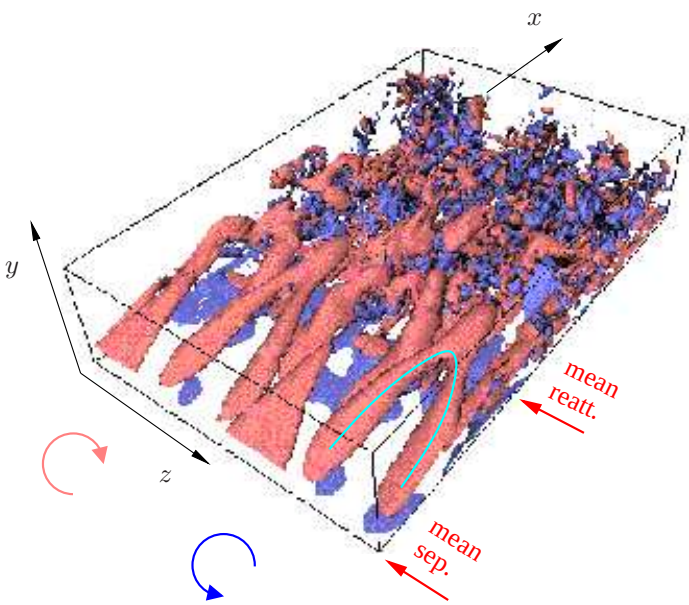

Figure 19: Instantaneous contours of span-wise vorticity component $\omega_z = \partial v/\partial x - \partial u/\partial y$, [1]. Λ-vortex structures within the mean separated region are associated with the generation of moving singularities (cyan lines) immediately after blow-up events.

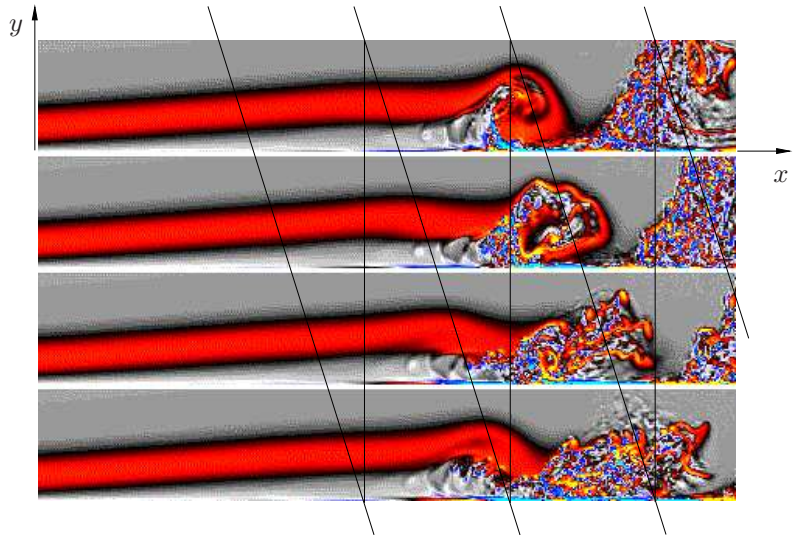

Figure 20: 'Shear-layer breakdown in reattachment zone of a laminar separation bubble': evolution of vorticity component ω_z; channel-like base flow, $Re_{\delta^*_{in}} \approx 10^3$; source: U. Maucher, U. Rist (1999), Institute of Aerodynamics and Gasdynamics, University of Stuttgart, Germany, see also [19].

3.3 Benchmark problem: channel flow

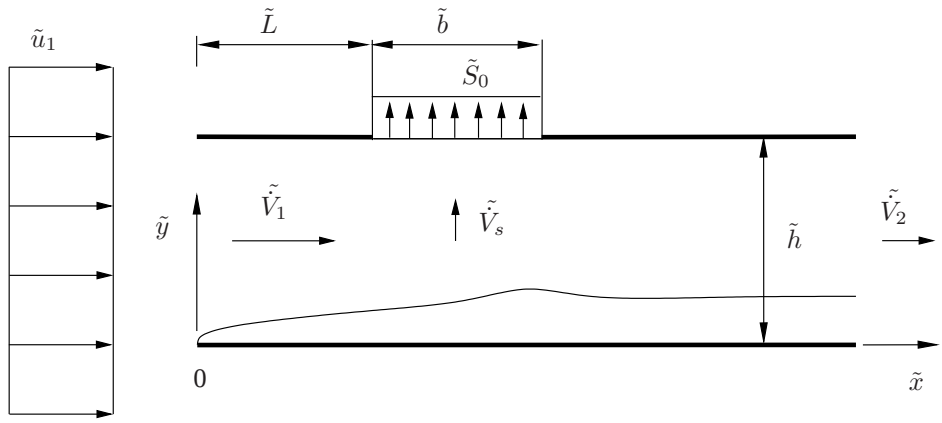

Figure 21: Channel flow of C.-T. Hsiao & L.L. Pauley, [16]; $\tilde{L} = 0.6135$m, $\tilde{h} = 0.1286$m, $\tilde{b} = 0.0381$m, $\tilde{u}_\infty = \tilde{u}_1 = 0.214$m/s; boundary conditions: no slip at lower wall, $\tilde{S}(x) = \tilde{S}_0 = const$ and impermeability/symmetry at upper boundary.

volume flux balance:

$$\dot{V}_s = \int_{-\infty}^{\infty} S(x)\,\mathrm{d}x = \dot{V}_1 - \dot{V}_2 = 2h\Delta u\,, \quad \dot{V}_1 = \underbrace{(u^* + \Delta u)}_{1}\,h\,, \quad \dot{V}_2 = (u^* - \Delta u)h\,. \tag{82}$$

relative suction rate (control parameter):

$$\alpha = \frac{\dot{V}_s}{\dot{V}_1} = 2\Delta u\,. \tag{83}$$

using method of *distributed singularities* and *images* for outer inviscid flow,

$$\phi_0(x,y) = x(1-\Delta u) - \frac{1}{\pi}\sum_{n=-\infty}^{\infty}\int_{-\infty}^{\infty} S(\xi)\ln\sqrt{(x-\xi)^2+[y-(2n+1)h]^2}\,\mathrm{d}\xi\,; \tag{84}$$

$$\begin{aligned} u_{0w}(x) &= \phi_{0x}(x,0) = 1-\Delta u - \frac{1}{2h}\int_{-\infty}^{\infty} S(\xi)\tanh\left(\frac{\pi(x-\xi)}{2h}\right)\mathrm{d}\xi\,, \\ u_{0h}(x) &= \phi_{0x}(x,h) = 1-\Delta u - \frac{1}{2h}\oint_{-\infty}^{\infty} S(\xi)\coth\left(\frac{\pi(x-\xi)}{2h}\right)\mathrm{d}\xi\,, \end{aligned} \tag{85}$$

$$u_0(x\to\pm\infty,y)\to\begin{cases}1-\alpha\,,\\ 1\,,\end{cases}\qquad v_0(x\to\pm\infty,y)\to 0\,. \tag{86}$$

channel flow according to Fig. 21, $S(x) = S_0\,\theta(x-1)\,\theta(1+b-x)$, where $\theta(x)$ denotes Heaviside's step function:

$$\begin{aligned} u_{0w}(x) &= 1-\frac{S_0 b}{2h}+\frac{S_0}{\pi}\ln\left[\frac{\cosh\left(\frac{\pi(x-1-b)}{2h}\right)}{\cosh\left(\frac{\pi(x-1)}{2h}\right)}\right]\,,\quad \alpha=\frac{S_0 b}{h}\,, \\ u_{0h}(x) &= 1-\frac{S_0 b}{2h}+\frac{S_0}{\pi}\ln\left|\frac{\sinh\left(\frac{\pi(x-1-b)}{2h}\right)}{\sinh\left(\frac{\pi(x-1)}{2h}\right)}\right|\,. \end{aligned} \tag{87}$$

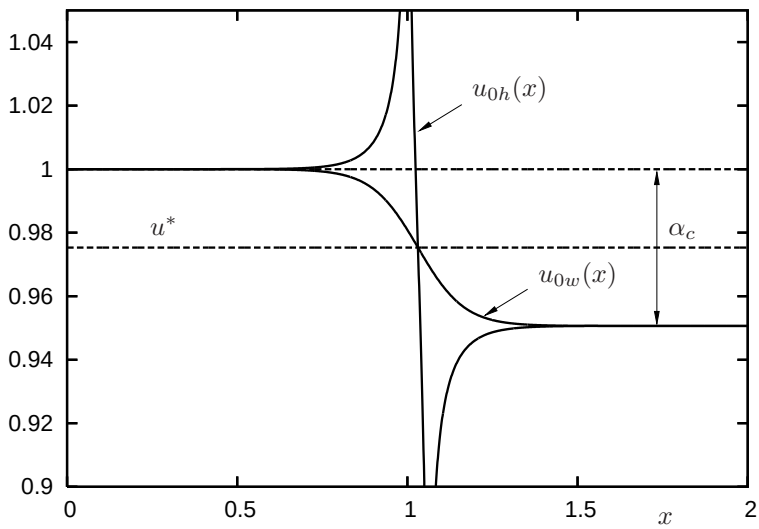

Figure 22: Lower and upper wall velocities $u_{0w}(x)$, $u_{0h}(x)$ in the case of critical suction $\alpha_c = 0.04935$ of the channel flow according to Fig. 21.

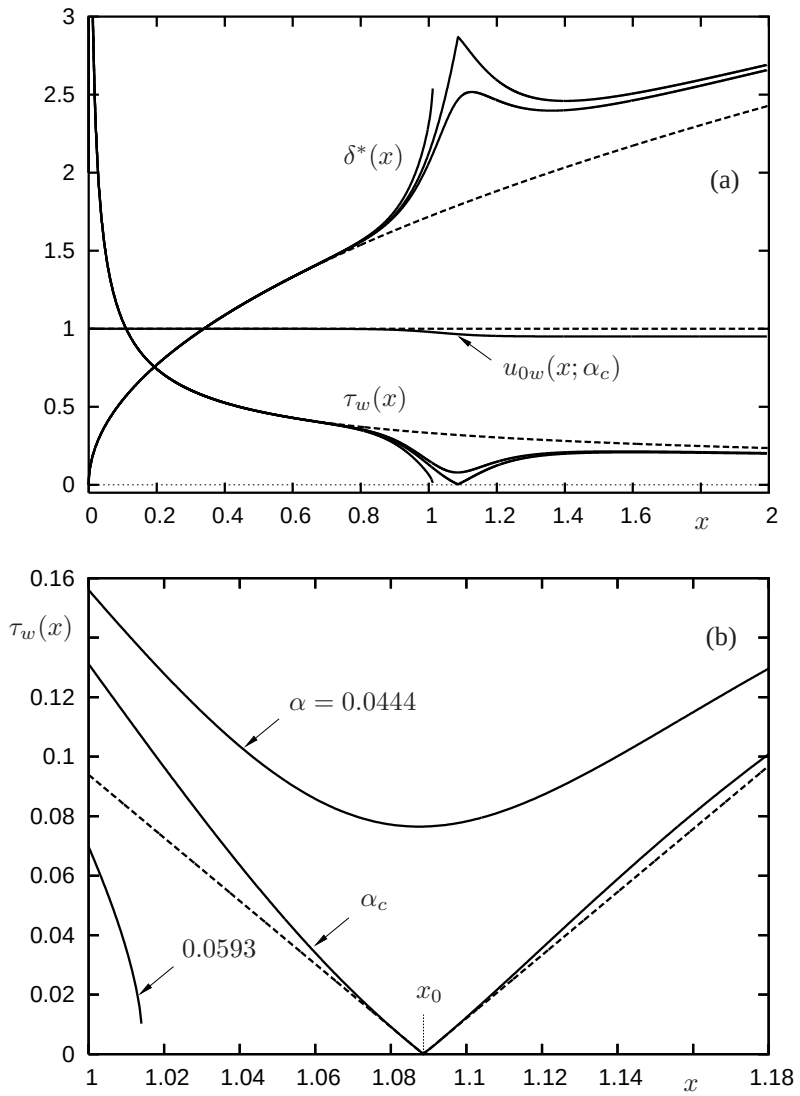

Figure 23: Boundary layer characteristics at the lower wall of the channel of Fig. 21, [16], depending on the relative suction rate $\alpha = S_0 b/h$; (a) overview, $\alpha = 0$ (dashed lines, Blasius-solution (21)), $\alpha = (0.0444, \alpha_c \approx 0.0494, 0.0593)$ (solid lines), (b) detail, dashed line: eqn. (29) or (117) with $a_0 = 1.06$ and $x_0 = 1.0886$.

3.4 Theory of marginal separation

steady, 2D flow: Ruban (1981), [21, 22] and Stewartson, Smith & Kaups (1982), [29], see also [30].

3.4.1 Classical boundary layer at the verge of separation

boundary layer equations (subscript '0' omitted):

$$\begin{gathered}\Psi_{\bar y}\Psi_{\bar y x} - \Psi_x \Psi_{\bar y\bar y} = -P_x + \Psi_{\bar y\bar y\bar y}\,, \quad P_{\bar y} = 0\,,\\ \bar y = 0: \quad \Psi = \Psi_{\bar y} = 0\,, \quad \bar y \to \infty: \quad \Psi_{\bar y} \to u_w(x)\,.\end{gathered} \tag{88}$$

local behaviour near a point x_0 of marginal separation $\tau_w(x_0) \to 0^+$ as $\Delta k = \alpha - \alpha_c \to 0^-$:

$$\Psi \sim \psi_0 + \Delta k\, \psi_1 + \cdots\,, \quad P \sim p_0 + \Delta k\, p_1 + \cdots\,; \tag{89}$$

$$\to \quad O(1): \quad \psi_{0\bar y}\psi_{0\bar y x} - \psi_{0x}\psi_{0\bar y\bar y} = -p_{0x} + \psi_{0\bar y\bar y\bar y}\,, \tag{90}$$

$$O(\Delta k): \quad (\psi_{0\bar y}\psi_{1\bar y})_x - \psi_{0x}\psi_{1\bar y\bar y} - \psi_{1x}\psi_{0\bar y\bar y} = -p_{1x} + \psi_{1\bar y\bar y\bar y}\,. \tag{91}$$

introduce $s = x - x_0 \to 0$; Taylor series expansion of imposed (adverse) pressure gradient:

$$p_{0x} \sim p_{00} + p_{01}\, s + \cdots\,; \quad p_{00} > 0\,, \quad p_{1x} \sim p_{10} + p_{11}\, s + \cdots\,. \tag{92}$$

viscous sub-layer 3:

local similarity, Goldstein (1948), [11] (cf. flat plate Goldstein near wake, eqn. (36))

$$\begin{gathered}\psi_0 \sim (-s)^a f_0(\eta) + \cdots\,, \quad \eta = \bar y/(-s)^b\,, \quad s \to 0^-\,,\\ \to \quad (-s)^{2a-2b-1}[-(a-b){f_0'}^2 + a f_0 f_0''\,] = -p_{00} + (-s)^{a-3b} f_0'''\,;\end{gathered} \tag{93}$$

presence of pressure gradient requires:

$$2a - 2b - 1 = a - 3b = 0 \quad \to \quad a = 3/4\,, \quad b = 1/4\,; \tag{94}$$

$$\begin{gathered}\psi_0 \sim (-s)^{3/4} f_0(\eta) + (-s)^\alpha f_1(\eta) + \cdots + (-s)^{2\alpha - 3/4} f_2(\eta) + \cdots\,,\\ \text{b.c.}: \ f_i(0) = f_i'(0) = 0\,, \quad i = 0, 1, 2, \cdots\,, \quad \eta \to \infty: \ \text{no exp. growth}\,;\end{gathered} \tag{95}$$

$$f_0''' - \frac{3}{4} f_0 f_0'' + \frac{1}{2}{f_0'}^2 = p_{00} \quad \to \quad f_0 = p_{00}\frac{\eta^3}{6}\,, \tag{96}$$

$$f_1''' - \frac{p_{00}}{8}\eta^3 f_1'' + (4\alpha + 1)\frac{p_{00}}{8}\eta^2 f_1' - \alpha p_{00}\eta\, f_1 = 0 \quad \to \quad f_1 = a_0\frac{\eta^2}{2}\,, \quad a_0 \in \mathbb{R}^+ \tag{97}$$

$$\begin{gathered}f_2''' - \frac{p_{00}}{8}\eta^3 f_2'' + (\alpha - \frac{1}{4})p_{00}\eta^2 f_2' - (2\alpha - \frac{3}{4})p_{00}\eta\, f_2 = (1 - 2\alpha)\frac{a_0}{4}\eta^2\\ \to \quad f_2 = b_0\frac{\eta^2}{2} + \frac{a_0^2}{2p_{00}}\frac{(1/4)!}{(-2\alpha)!}\sum_{n=1}^{2\alpha-1}\frac{(n-2\alpha)!}{(n+1/4)!\,n!\,(4n-1)}\left(\frac{p_{00}}{32}\right)^n \eta^{4n+1}\,, \quad b_0 \in \mathbb{R}\end{gathered} \tag{98}$$

with eigenvalue:

$$\alpha = k/2\,, \quad k = 1, 2, 3, \cdots\,, \tag{99}$$

where the value $k=1$ must be excluded; $z! = \Gamma(z+1) = z\,\Gamma(z)$.

$$\alpha = 1: \quad f_2 = b_0 \frac{\eta^2}{2} - a_0^2 \frac{\eta^5}{2\cdot 5!} \qquad \text{... Goldstein singularity}\,, \tag{100}$$

$$\alpha = 3/2: \quad f_2 = b_0 \frac{\eta^2}{2} - a_0^2 \frac{\eta^5}{5!} + a_0^2 p_{00} \frac{\eta^9}{8!} \qquad \text{... marginal separation singularity}\,. \tag{101}$$

Δk correction:

$$\begin{gathered} \psi_1 \sim (-s)^\beta g_1(\eta) + (-s)^{\beta+3/4} g_2(\eta) + \cdots\,, \\ g_i(0) = g_i'(0) = 0\,, \quad \eta \to \infty: \text{ no exp. growth}\,; \end{gathered} \tag{102}$$

eqn. for g_1 as that for f_1, i.e.

$$g_1 = a_1 \frac{\eta^2}{2}\,, \quad a_1 \in \mathbb{R} \tag{103}$$

eqn. for g_2 as that for f_2 with replacements $\alpha \to \beta/2 + 3/4$, $a_0^2 \to 2a_0 a_1$, i.e.

$$g_2 = b_1 \frac{\eta^2}{2} + \frac{a_0 a_1}{p_{00}} \frac{(1/4)!}{(-\beta-3/2)!} \sum_{n=1}^{\beta+1/2} \frac{(n-\beta-3/2)!}{(n+1/4)!\,n!\,(4n-1)} \left(\frac{p_{00}}{32}\right)^n \eta^{4n+1}\,, \quad b_1 \in \mathbb{R} \tag{104}$$

with eigenvalue

$$\beta = k - 3/2\,, \quad k = 1, 2, 3, \cdots\,. \tag{105}$$

finally, taking $\alpha = 3/2$ and the lowest e.v. $\beta = -1/2$,

$$\begin{gathered} \Psi \sim (-s)^{3/4} p_{00} \frac{\eta^3}{6} + (-s)^{3/2} a_0 \frac{\eta^2}{2} + \cdots + (-s)^{9/4} \left[b_0 \frac{\eta^2}{2} - a_0^2 \frac{\eta^5}{5!} + a_0^2 p_{00} \frac{\eta^9}{8!} \right] + \cdots \\ + \Delta k \left[(-s)^{-1/2} a_1 \frac{\eta^2}{2} + (-s)^{1/4} b_1 \frac{\eta^2}{2} + \cdots \right] + \cdots\,. \end{gathered} \tag{106}$$

rewriting in terms of $\bar{y}$ (match to region 2, $\eta \to \infty$, $\bar{y} \to 0$):

$$\begin{gathered} \Psi \sim p_{00} \frac{\bar{y}^3}{6} + \cdots + a_0^2 p_{00} \frac{\bar{y}^9}{8!} + \cdots + (-s) \left[a_0 \frac{\bar{y}^2}{2} + \cdots - a_0^2 \frac{\bar{y}^5}{5!} + \cdots \right] \\ + \Delta k \left[(-s)^{-1} a_1 \frac{\bar{y}^2}{2} + (-s)^{-1/4} b_1 \frac{\bar{y}^2}{2} + \cdots \right] + \cdots\,. \end{gathered} \tag{107}$$

region 2:

eqn. (107) suggests

$$\Psi \sim \psi_{00}(\bar{y}) + (-s)\psi_{01}(\bar{y}) + \cdots + \Delta k \left[(-s)^{-1} \psi_{10}(\bar{y}) + \cdots \right] + \cdots\,; \tag{108}$$

in b.l. eqn. (88)

$$\to \quad -\psi_{00}'\psi_{01}' + \psi_{01}\psi_{00}'' = -p_{00} + \psi_{00}'''\,, \quad \psi_{10}'\psi_{00}' - \psi_{10}\psi_{00}'' = 0\,, \quad \text{+ b.c.} \tag{109}$$

which reflects the inviscid character of the main part of the b.l.; solution, after matching to (107)

$$\psi_{01} = \psi_{00}' \left(\frac{a_0}{p_{00}} + \int_0^{\bar{y}} \frac{p_{00} - \psi_{00}'''}{\psi_{00}'^2}\, \mathrm{d}y \right)\,, \quad \psi_{10} = \frac{a_1}{p_{00}} \psi_{00}'\,. \tag{110}$$

region 3':

$s \to 0^+$, $\eta = \bar{y}/s^{1/4}$,

$$\Psi \sim s^{3/4} p_{00} \frac{\eta^3}{6} + s^{3/2} \bar{f}_1(\eta) + \cdots + s^{9/4} \bar{f}_2(\eta) + \cdots + \Delta k[\cdots] + \cdots \,; \tag{111}$$

$$\to \quad \Psi \sim s^{3/4} p_{00} \frac{\eta^3}{6} + s^{3/2} \bar{a}_0 \frac{\eta^2}{2} + \cdots + s^{9/4} \left[\bar{b}_0 \frac{\eta^2}{2} + \bar{a}_0 \frac{\eta^5}{5!} + p_{00} \bar{a}_0^2 \frac{\eta^9}{8!} \right] + \cdots + \Delta k[\cdots] + \cdots \,, \tag{112}$$

rewriting, $\eta \to \infty$, $\bar{y} \to 0$:

$$\Psi \sim p_{00} \frac{\bar{y}^3}{6} + \cdots + p_{00} \bar{a}_0^2 \frac{\bar{y}^9}{8!} + \cdots + s \left[\bar{a}_0^2 \frac{\bar{y}^2}{2} + \cdots \right] + \cdots \,, \tag{113}$$

i.e. matching 2-2' requires (compare with (107), $s \to 0$):

$$a_0^2 = \bar{a}_0^2 \quad \Rightarrow \quad a_0 = \begin{cases} -\bar{a}_0 & \text{... regular separation} \,, \\ \bar{a}_0 & \text{... marginal separation} \,. \end{cases} \tag{114}$$

region 2':

$$\Psi \sim \psi_{00}(\bar{y}) + s\, \bar{\psi}_{01}(\bar{y}) + \cdots + \Delta k[\cdots] + \cdots \,; \tag{115}$$

$$\to \quad \bar{\psi}_{01} = \psi_{00}' \left(\frac{a_0}{p_{00}} - \int_0^{\bar{y}} \frac{p_{00} - \psi_{00}'''}{\psi_{00}'^{\,2}} \, \mathrm{d}y \right) . \tag{116}$$

b.l. characteristics (combining results from reg. 2, 2'):

$$\delta^*(s) \sim \delta^*(0) - \frac{a_0}{p_{00}} |s| + O(s) \,, \quad \tau_w(s) \sim a_0 |s| + \cdots \quad \text{as} \quad s \to 0 \,; \;\; \Delta k = 0 \tag{117}$$

in agreement with (29).

expansion (108) needs to be modified if

$$|s| \sim \Delta k^{1/2} \sim \epsilon \ll 1 \quad \to \quad \Delta k = \alpha - \alpha_c = \epsilon^2 k_1 \,, \quad k_1 \sim O(1) \,. \tag{118}$$

region II:

see reg. 2, 2'; $x_* = s/\epsilon \sim O(1)$:

$$\Psi \sim \psi_0^*(x_*, \bar{y}) + \epsilon\, \psi_1^*(x_*, \bar{y}) + \cdots \,; \tag{119}$$

in b.l. eqns.:

$$\begin{aligned} &\to \quad \psi_{0\bar{y}}^* \psi_{0\bar{y}x_*}^* - \psi_{0x_*}^* \psi_{0\bar{y}\bar{y}}^* = 0 \quad \to \quad \psi_0^* = \psi_{00}(\bar{y}) \,, \\ &\psi_{1\bar{y}x_*}^* - \frac{\psi_{00}''}{\psi_{00}'} \psi_{1x_*}^* = \frac{\psi_{00}''' - p_{00}}{\psi_{00}'} \quad \to \quad \psi_1^* = \psi_{00}' \left(\frac{\bar{A}(x_*)}{p_{00}} + x_* \int_0^{\bar{y}} \frac{\psi_{00}''' - p_{00}}{\psi_{00}'^{\,2}} \, \mathrm{d}y \right) . \end{aligned} \tag{120}$$

here $\bar{A}(x_*)$ remains *unknown*, from the match 2-II, $s \to 0^-$, $x_* \to -\infty$:

$$\bar{A}(x_* \to -\infty) \sim a_0(-x_*) + \frac{a_1 k_1}{(-x_*)} + \cdots \,. \tag{121}$$

region III:

cf. reg. 3, 3'; $y_* = \bar{y}/\epsilon^{1/4} \sim O(1)$:

$$\Psi \sim \epsilon^{3/4} p_{00} \frac{{y_*}^3}{6} + \epsilon^{3/2} \Psi_1^*(x_*, y_*) + \cdots + \epsilon^{9/4} \Psi_2^*(x_*, y_*) + \cdots \,,$$
$$y_* = 0: \quad \Psi_i^* = \Psi_{iy_*}^* = 0 \,, \quad y_* \to \infty: \quad \text{no exp. growth}\,; \tag{122}$$

$$\to \quad p_{00} \frac{y_*^2}{2} \Psi_{1y_*x_*}^* - p_{00}\, y_* \Psi_{1x_*}^* - \Psi_{1y_*y_*y_*}^* = 0 \quad \to \quad \Psi_1^* = \bar{A}(x_*) \frac{y_*^2}{2} \tag{123}$$

suggested from the match to reg. II.

$$p_{00} \frac{y_*^2}{2} \Psi_{2y_*x_*}^* - p_{00}\, y_* \Psi_{2x_*}^* - \Psi_{2y_*y_*y_*}^* = -\bar{A}\bar{A}' \frac{y_*^2}{2}\,; \tag{124}$$

match to reg. 3 requires

$$\Psi_2^*(x_* \to -\infty, y_*) \sim p_{00} a_0^2 \frac{y_*^9}{8!} + a_0^2 x_* \frac{y_*^5}{5!} + A_2(x_*) \frac{y_*^2}{2} + \cdots \,,$$
$$A_2(x_* \to -\infty) \sim b_0 (-x_*)^{7/4} + b_1 k_1 (-x_*)^{-1/4} + \cdots \tag{125}$$

with the transformation

$$\Psi_2 = \Psi_2^* - p_{00} a_0^2 \frac{y_*^9}{8!} - a_0^2 x_* \frac{y_*^5}{5!} - A_2(x_*) \frac{y_*^2}{2} - \frac{\bar{A}^2 - a_0^2 x_*^2 - 2 a_0 a_1 k_1}{2 p_{00}}\, y_* \,, \tag{126}$$

where $A_2 y_*^2/2$ is a homogeneous and $\bar{A}^2 y_*/(2p_{00})$ a particular solution of (124), the *fundamental problem* reads

$$p_{00} \frac{y_*^2}{2} \Psi_{2y_*x_*} - p_{00}\, y_* \Psi_{2x_*} - \Psi_{2y_*y_*y_*} =: -F'(x_*) = 0 \,,$$
$$y_* = 0: \quad \Psi_2 = 0 \,, \quad \Psi_{2y_*} = -\frac{\bar{A}^2 - a_0^2 x_*^2 - 2 a_0 a_1 k_1}{2 p_{00}} =: L(x_*) \,, \tag{127}$$
$$\Psi_2(x_* \to -\infty, y_*) \to 0 \,.$$

following Stewartson (1970), [28], eqn. (127) can be solved subject to the *solvability condition*

$$L(x_*) = \frac{\lambda}{2 p_{00}^{1/2}} \int_{-\infty}^{x_*} \frac{F'(\xi)}{\sqrt{x_* - \xi}}\, \mathrm{d}\xi \,, \quad \lambda = \frac{(-1/4)!}{\sqrt{2}\,(1/4)!} \,. \tag{128}$$

here $L(x_*) = 0$, i.e.

$$\bar{A} = a_0 \sqrt{x_*^2 + \frac{2 a_1 k_1}{a_0}} = \frac{a_0}{\epsilon} \sqrt{s^2 + \frac{2 a_1 \Delta k}{a_0}} \tag{129}$$

using the previous variables $s = \epsilon x_*$, $\Delta k = \alpha - \alpha_c = \epsilon^2 k_1$; a comparison with e.g. Fig. 23 indicates $a_1 < 0$.

boundary layer characteristics:

$$\delta^*(s) \sim \delta^*(0) - \epsilon \frac{\bar{A}(s)}{p_{00}} + O(s) \,, \quad \tau_w(s) \sim \epsilon \bar{A}(s) + \cdots \quad \text{as} \quad s \to 0 \tag{130}$$

suggesting the notion *(negative correction) displacement function* or *(local) wall shear stress* $\bar{A}$.

the limiting solution $\Delta k = 0$ which can be continued beyond the point of (marginal) separation $s = 0$ indicates a *local breakdown* of the hierarchical b.l. concept: thin airfoil theory yield u, p perturbations $\propto Re^{-1/2} \ln|s|$ as $s \to 0$ in the external inviscid flow field.

3.4.2 Interaction

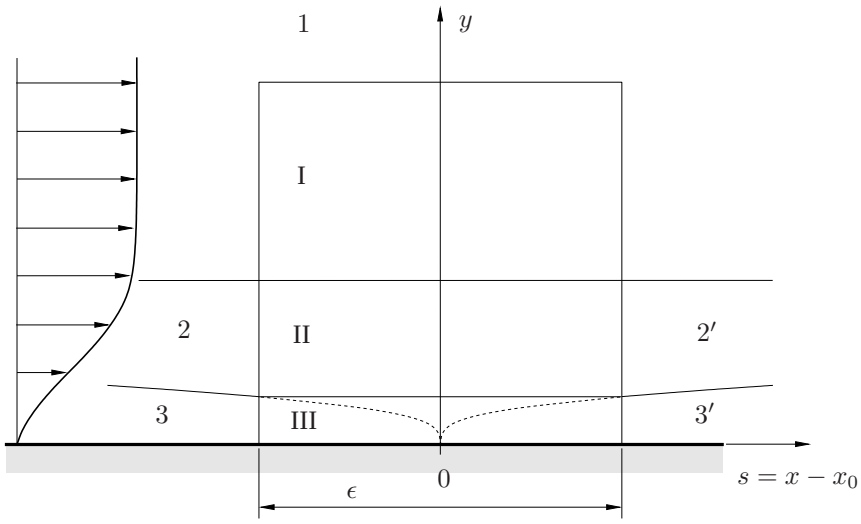

Figure 24: Triple deck of marginal separation.

in the limit $\Delta k \to 0$, $s \to 0$ the displacing effect caused by the viscous sublayer start to interact with the external inviscid pressure perturbation; to allow for a modification of the displacement function $\bar{A}$, the induced pressure gradient $p_i'(x_*) = F'(x_*)$ must enter the fundamental problem (127):

$$p_x \sim \Psi_{\bar{y}\bar{y}\bar{y}}: \quad Re^{-1/2}\epsilon^{-1} \sim \epsilon^{9/4}(\underbrace{\partial y_*/\partial \bar{y}}_{\epsilon^{-1/4}})^3 \quad \Rightarrow \quad \epsilon = Re^{-1/5} \tag{131}$$

leading to the interaction length scaling.

solvability condition (128):

$$\bar{A}^2 - a_0^2 x_*^2 - 2a_0 a_1 k_1 = -p_{00}^{1/2}\lambda \int_{-\infty}^{x_*} \frac{p_i'(\xi)}{\sqrt{x_* - \xi}}\,\mathrm{d}\xi\,. \tag{132}$$

to close problem (132), a second $\bar{A}$, p_i - relation is needed:

region I:

$(x_*, \hat{y}) = Re^{1/5}(x, y), \quad \hat{y} = Re^{-3/10}\bar{y},$

$$\begin{aligned} u &\sim U_{00} + Re^{-1/5}U_{01}x_* + \cdots + Re^{-1/2}\hat{u}_1(x_*, \hat{y}) + \cdots\,, \\ v &\sim -Re^{-1/5}U_{01}\hat{y} + \cdots + Re^{-1/2}\hat{v}_1(x_*, \hat{y}) + \cdots\,, \\ p &\sim (1 - U_{00}^2)/2 + Re^{-1/5}p_{00}x_* + \cdots + Re^{-1/2}\hat{p}_1(x_*, \hat{y}) + \cdots \end{aligned} \tag{133}$$

with $U_{00} = u_w(x_0) = \psi_{00}'(\infty)$ and $U_{01} = -p_{00}/U_{00}$.

$$\to \quad \hat{u}_{1x_*} + \hat{v}_{1\hat{y}} = 0\,, \quad U_{00}\,\hat{u}_{1x_*} = -\hat{p}_{1x_*}\,, \quad U_{00}\,\hat{v}_{1x_*} = -\hat{p}_{1y_*}\,, \tag{134}$$

i.e. the linearised Euler equations; b.c. from the match I-II, $\hat{y} \to 0$, $\bar{y} \to \infty$:

$$\hat{v}_1(x_*, 0) = -\Psi_x\Big|_{\bar{y}\to\infty} \sim -U_{00}\left(\frac{\bar{A}'}{p_{00}} + \int_0^\infty \frac{\psi_{00}''' - p_{00}}{\psi_{00}'^2}\,\mathrm{d}y\right) + \cdots\,. \tag{135}$$

finally, thin airfoil theory leads to the *interaction law*

$$-U_{00}\hat{u}_{1x_*}(x_*,0) = \hat{p}_{1x_*}(x_*,0) = p_i'(x_*) = \frac{U_{00}^2}{p_{00}\pi} \oint\limits_{-\infty}^{\infty} \frac{\bar{A}''(s)}{x_* - s}\,\mathrm{d}s\,. \tag{136}$$

combination of (132), (136) and the transformation

$$x_* = a_0^{-2/5} p_{00}^{-1/5} U_{00}^{4/5} X\,, \quad \bar{A} = a_0^{3/5} p_{00}^{-1/5} U_{00}^{4/5} A\,, \quad k_1 = -2^{-1} a_0^{1/5} p_{00}^{-2/5} U_{00}^{8/5} a_1^{-1} \Gamma \tag{137}$$

leads to the *fundamental equation* of marginal separation

$$A^2 - X^2 + \Gamma = \lambda \int\limits_X^{\infty} \frac{A''(s)}{\sqrt{s-X}}\,\mathrm{d}s\,, \tag{138}$$

which represents a *similarity law:* the specific problem under consideration (flow past airfoil, channel flow, backward facing step, etc.) affects the constants p_{00}, U_{00}, α_c, x_0, a_0, a_1 in (118), (137) only, see Tab. 1 on p. 42; asymptotic behaviour:

$$A(X \to \pm\infty) \sim |X| - \frac{\Gamma}{2|X|} + \cdots\,. \tag{139}$$

consequences of eqn. (138):

- interaction – i.e. rhs – *negligible* for $\Gamma \to -\infty$ and/or $X \to \pm\infty$,
- rescaling for $\Gamma \to \infty$ leads to Stewartson's result [28],
- interaction *delays* separation,
- solutions exist within the range $\Gamma \in (-\infty, \Gamma_c \approx 2.66]$,
- *non-unique* solutions within the range $\Gamma \in [0, \Gamma_c)$,
- point of separation $X_s \to 0$, reattachment $X_r \to \infty$ as $\Gamma \to 0$ at *lower* solution branch.

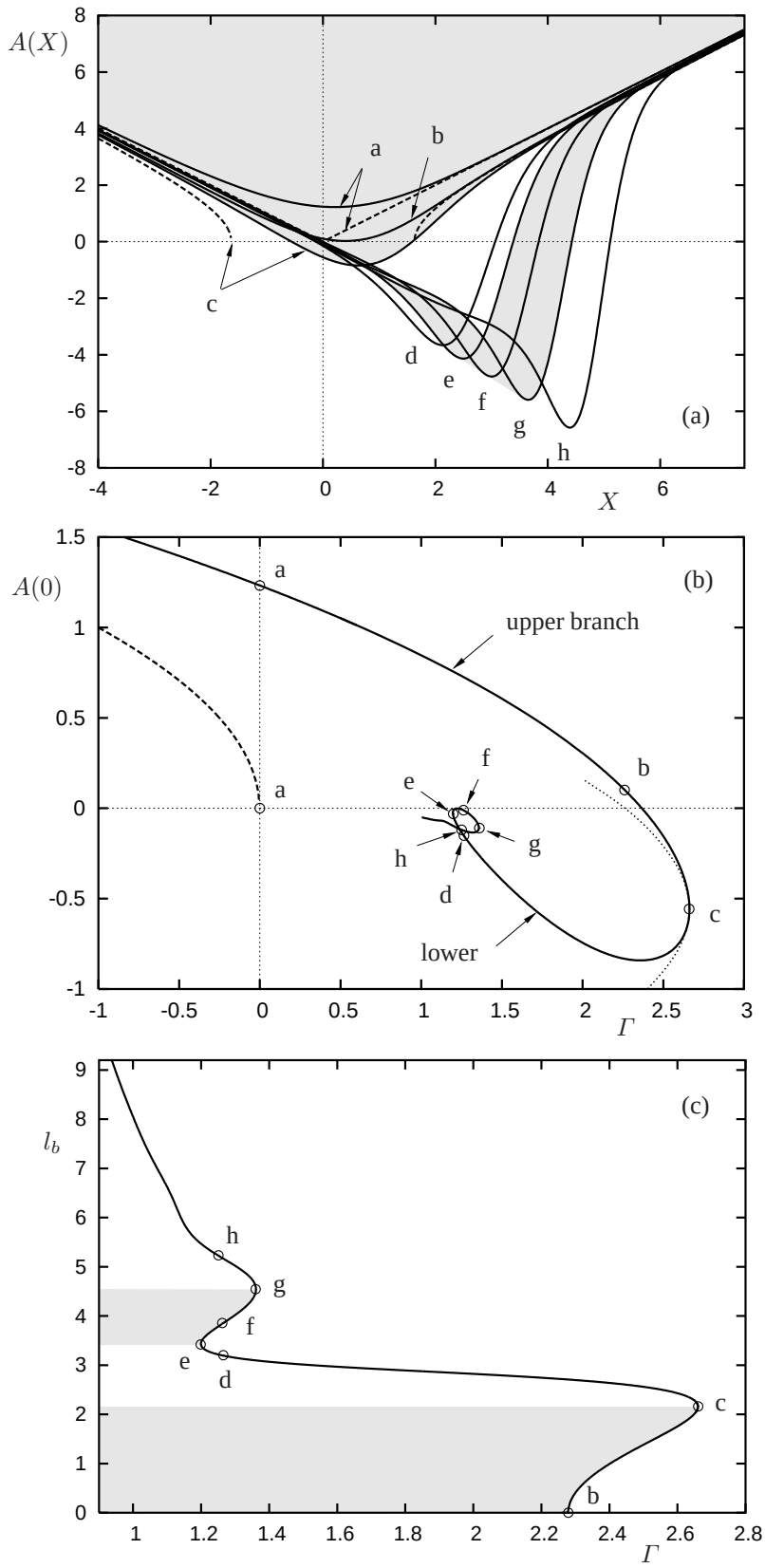

Figure 25: (a) Wall shear distributions according to (138), dashed lines: local solutions of classical boundary layer theory $A = \sqrt{X^2 - \Gamma}$, (b) *fundamental curve* of marginal separation; dashed line: local solution of classical boundary layer theory (asymptote for $\Gamma \to -\infty$), dotted line: parabola approximation near the bifurcation point, (c) separation bubble length $l_b = X_r - X_s$.

3.4.3 Extension to unsteady, 3D interacting flows including control devices

the idea is to restrict transient, three-dimensional effects ('perturbations' of the basic steady 2D flow) caused by control devices to the interaction process – described by the fundamental problem (127) and expressed through $\bar{A}$ – only; scaling from lower deck expansions:

$$\begin{aligned} u &= Re^{-1/2}\Psi_y \sim Re^{-1/10}p_{00}\frac{y_*^2}{2} + Re^{-1/4}\bar{A}y_* + \cdots + Re^{-2/5}u_2^* + \cdots\,, \quad \partial_y = Re^{11/20}\partial_{y_*}\,, \\ v &= -Re^{-1/2}\Psi_x \sim -Re^{-3/5}\bar{A}_{x_*}\frac{y_*^2}{2} + \cdots + Re^{-3/4}v_2^* + \cdots\,, \quad \partial_x = Re^{1/5}\partial_{x_*}\,, \\ p &\sim (1-U_{00}^2)/2 + Re^{-1/5}p_{00}x_* + \cdots + Re^{-1/2}p_i + \cdots\,. \end{aligned} \tag{140}$$

- *time t:* Ruban (1982), [23], Smith (1982), [26]

$$u_t \sim Re^{-1}u_{yy} \quad \Rightarrow \quad t = \frac{|\tilde{\boldsymbol{u}}_\infty|\tilde{t}}{\tilde{L}} \sim O(Re^{1/20})\,. \tag{141}$$

- *spanwise coordinate z & velocity w:* assumption: induced pressure in x and z direction of equal magnitude:

$$\Rightarrow \quad z = \frac{\tilde{z}}{\tilde{L}} \sim O(Re^{-1/5})\,; \quad uw_x \sim p_z \quad \Rightarrow \quad w = \frac{\tilde{w}}{|\tilde{\boldsymbol{u}}_\infty|} \sim O(Re^{-2/5})\,. \tag{142}$$

- *surface mounted obstacle h:* height/length ratio such that pressure perturbations are of the same order as induced pressure; according to thin airfoil theory, Hackmüller, Kluwick (1991), [13]:

$$h/Re^{-1/5} \sim Re^{-1/2} \quad \Rightarrow \quad h = \frac{\tilde{h}}{\tilde{L}} \sim O(Re^{-7/10})\,, \tag{143}$$

which is of the same order as the thickness of the separation bubble: from (140)

$$Re^{-1/10}h_*^2 \sim Re^{-1/4}\bar{A}h_* \quad \Rightarrow \quad h = Re^{-11/20}h_* \sim O(Re^{-7/10})\,. \tag{144}$$

- *suction/blowing v_w at the wall $y=0$:* from (140), Hackmüller, Kluwick (1990), [12]

$$\Rightarrow \quad v_w \sim O(Re^{-3/4})\,. \tag{145}$$

modified expansions for the triple deck of marginal separation:

upper deck I:

$$x = x_0 + Re^{-1/5}x_*\,, \quad y = Re^{-1/5}\hat{y}\,, \quad z = Re^{-1/5}z_*\,, \quad t = Re^{1/20}t_*\,; \tag{146}$$

$$\begin{aligned} u &\sim U_{00} + Re^{-1/5}U_{01}x_* + \cdots + Re^{-1/2}\hat{u}_1(x_*,\hat{y},z_*,t_*) + \cdots\,, \\ v &\sim -Re^{-1/5}U_{01}\hat{y} + \cdots + Re^{-1/2}\hat{v}_1(x_*,\hat{y},z_*,t_*) + \cdots\,, \\ w &\sim Re^{-1/2}\hat{w}_1(x_*,\hat{y},z_*,t_*) + \cdots\,, \\ p &\sim (1-U_{00}^2)/2 + Re^{-1/5}p_{00}x_* + \cdots + Re^{-1/2}\hat{p}_1(x_*,\hat{y},z_*,t_*) + \cdots\,. \end{aligned} \tag{147}$$

$$\rightarrow \quad \hat{u}_{1x_*} + \hat{v}_{1\hat{y}} + \hat{w}_{1z_*} = 0\,, \quad U_{00}\hat{u}_{1x_*} = -\hat{p}_{1x_*}\,, \quad U_{00}\hat{v}_{1x_*} = -\hat{p}_{1\hat{y}}\,, \quad U_{00}\hat{w}_{1x_*} = -\hat{p}_{1z_*}\,; \tag{148}$$

$$\hat{p}_1(x_*,0,z_*,t_*) = -\frac{U_{00}}{2\pi}\int_{-\infty}^{\infty}\int_{-\infty}^{\infty}\frac{\hat{v}_{1\xi}(\xi,0,\eta,t_*)}{\sqrt{(\xi-x_*)^2+(\eta-z_*)^2}}\,\mathrm{d}\xi\mathrm{d}\eta\,. \tag{149}$$

main deck II:

$$y = Re^{-1/2}\bar{y} + Re^{-7/10}\bar{h}(x_*, z_*, t_*) \quad \text{... Prandtl's transposition theorem}\,; \tag{150}$$

$$\begin{aligned} u &\sim U_0(\bar{y}) + Re^{-1/5}\bar{u}_1(x_*, \bar{y}, z_*, t_*) + \cdots\,, \\ v &\sim Re^{-1/2}[\bar{v}_1(x_*, \bar{y}, z_*, t_*) - U_0\bar{h}_{x_*}] + \cdots\,, \\ w &\sim Re^{-1/2}\bar{w}_1(x_*, \bar{y}, z_*, t_*) + \cdots\,, \\ p &\sim (1 - U_{00}^2)/2 + Re^{-1/5}p_{00}x_* + \cdots + Re^{-1/2}p_i(x_*, z_*, t_*) + \cdots\,; \end{aligned} \tag{151}$$

$$\rightarrow \quad \bar{u}_{1x_*} + \bar{v}_{1\bar{y}} = 0\,, \quad U_0\bar{u}_{1x_*} + \bar{v}_1 U_0' = U_0'' - p_{00} \quad \text{(cf. 2D case)}\,, \quad U_0\bar{w}_{1x_*} = -p_{iz_*}\,. \tag{152}$$

lower deck III:

$$y = Re^{-11/20}y_* + Re^{-7/10}\bar{h}\,; \tag{153}$$

$$\begin{aligned} u &\sim Re^{-1/10}p_{00}\frac{y_*^2}{2} + Re^{-1/4}\bar{A}(x_*, z_*, t_*)y_* + \cdots + Re^{-2/5}u_2^*(x_*, y_*, z_*, t_*) + \cdots\,, \\ v &\sim Re^{-3/5}[-\bar{A}_{x_*} + p_{00}\bar{h}_{x_*}]\frac{y_*^2}{2} + \cdots + Re^{-3/4}[v_2^*(x_*, y_*, z_*, t_*) + \bar{A}y_*\bar{h}_{x_*}] + \cdots\,, \\ w &\sim Re^{-2/5}w_2^*(x_*, y_*, z_*, t_*) + \cdots\,, \end{aligned} \tag{154}$$

$$\begin{gathered} p \sim (1 - U_{00}^2)/2 + Re^{-1/5}p_{00}x_* + \cdots + Re^{-1/2}p_i + \cdots\,, \\ \rightarrow \quad u_{2x_*}^* + v_{2y_*}^* + w_{2z_*}^* = 0\,, \\ p_{00}\frac{y_*^2}{2}u_{2x_*}^* + p_{00}y_*v_2^* - u_{2y_*y_*}^* = -p_{ix_*} + (-\bar{A}_{t_*} + p_{00}\bar{h}_{t_*})y_* - \bar{A}\bar{A}_{x_*}\frac{y_*^2}{2}\,, \\ p_{00}\frac{y_*^2}{2}w_{2x_*}^* - w_{2y_*y_*}^* = -p_{iz_*}\,, \\ y_* = 0: \quad u_2^* = w_2^* = 0\,, \quad v_2^* = v_{2w}^*(x_*, z_*, t_*)\,, \quad \ldots \end{gathered} \tag{155}$$

finally, after the transformations (137) and

$$\begin{gathered} z_* = a_0^{-2/5}p_{00}^{-1/5}U_{00}^{4/5}Z\,, \quad t_* = a_0^{-9/10}p_{00}^{3/10}U_{00}^{-1/5}T\,, \quad p_i = a_0p_{00}^{-1}U_{00}^2P\,, \\ \bar{h} = a_0^{3/5}p_{00}^{-6/5}U_{00}^{4/5}h\,, \quad v_{2w}^* = a_0^{3/2}p_{00}^{-3/2}U_{00}v_w\,, \end{gathered} \tag{156}$$

the solvability condition reads

$$\begin{aligned} A^2 - X^2 + \Gamma = &-\frac{\lambda}{2\pi}\int_{-\infty}^{X}\frac{\mathrm{d}s}{\sqrt{X-s}}\int_{-\infty}^{\infty}\int_{-\infty}^{\infty}\frac{(s-\xi)}{[(s-\xi)^2 + (Z-\eta)^2]^{3/2}}\left(\frac{\partial^2}{\partial\xi^2} + \frac{\partial^2}{\partial\eta^2}\right)(A-h)\,\mathrm{d}\xi\mathrm{d}\eta \\ &-\gamma\int_{-\infty}^{X}\frac{1}{(X-\xi)^{1/4}}\frac{\partial(A-h)}{\partial T}\,\mathrm{d}\xi - \kappa\int_{-\infty}^{X}\frac{v_w}{(X-\xi)^{1/4}}\,\mathrm{d}\xi \end{aligned} \tag{157}$$

with the positive constants

$$\gamma = \frac{2^{3/4}}{(-3/4)!}\,, \quad \kappa = \frac{2^{3/4}}{(1/4)!}\,. \tag{158}$$

interaction law

$$P(X, Z, T) = -\frac{1}{2\pi}\int_{-\infty}^{\infty}\int_{-\infty}^{\infty}\frac{1}{\sqrt{(X-\xi)^2 + (Z-\eta)^2}}\frac{\partial^2(A-h)}{\partial\xi^2}\,\mathrm{d}\xi\mathrm{d}\eta\,. \tag{159}$$

numerical solutions and analytical investigations for:

• *unsteady 2D flow without control devices:* Smith (1982), [26], Ryzhov & Smith (1984), [25], Elliott & Smith (1987), [8]:

conclusion: for $\Gamma > \Gamma_c$ *finite time breakdown*, which, depending on the initial conditions, is also possible for $\Gamma < \Gamma_c$, ...“marginally separated flows are very sensitive and should be considered to be in danger with regard to the unsteady stall process and the associated sudden change of the whole flow structure” ...

• *steady 3D flow with surface mounted obstacle:* Braun & Kluwick (2002), [3]:

$$\text{decomposition:} \quad A(X,Z) = A_\infty(X) + A_1(X,Z)\,, \quad h(X,Z) = h_\infty(X) + h_1(X,Z)\,; \tag{160}$$

$$h_1(X,Z) = H(1-X^2)^3\,\theta(1-|X|)\,\mathrm{e}^{-(Z/B)^2}\,. \tag{161}$$

conclusion, see Fig. 26: solutions in the limit $\Delta\Gamma = \Gamma_c - \Gamma \to 0^+$ can only be found if localized 3D perturbations $h_1(X,Z) \to 0$, response $A_1(X,Z) \to 0$ and corresponding wave length $\to \infty$, i.e. $A(X,Z) \to A_\infty(X)|_{\Gamma=\Gamma_c} =: A_{\infty c}(X)$ indicating the appearance of a *bifurcation problem*.

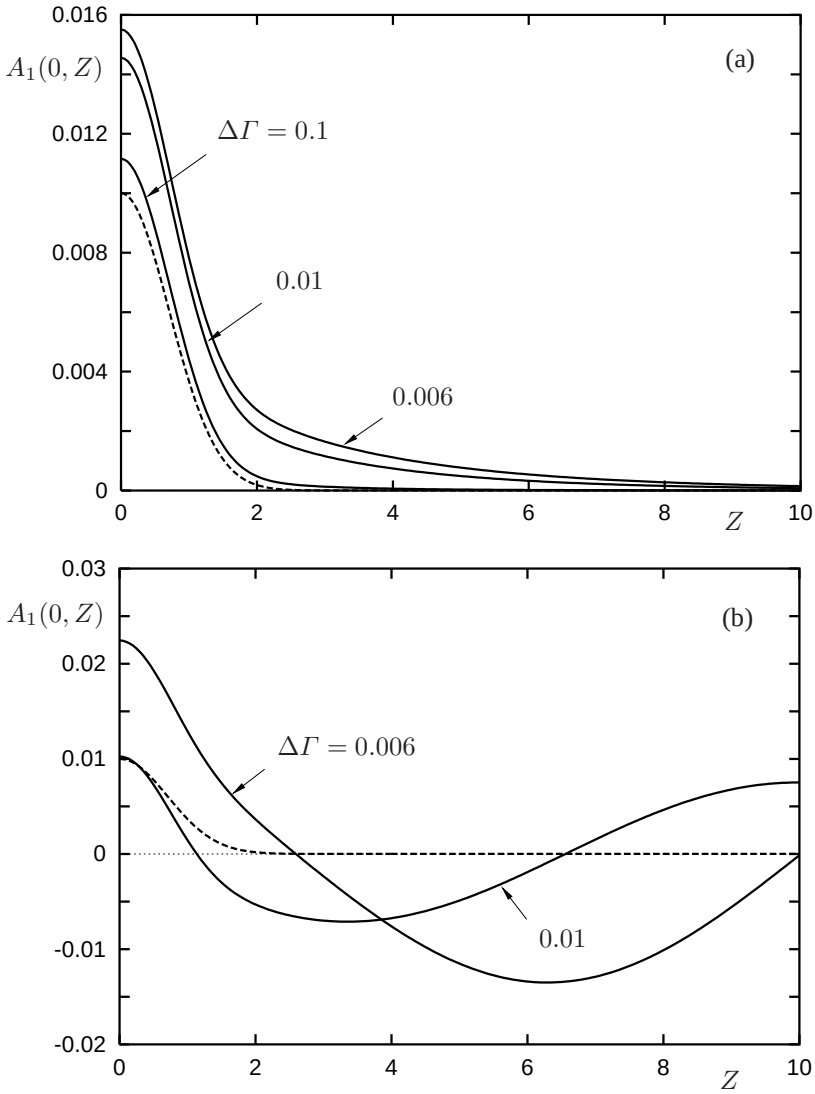

Figure 26: Numerical solutions of (157) for $\partial/\partial T = 0$, $h_\infty = v_w = 0$ and h_1 according to (161) with $H = 0.01$, $B = 1$ (dashed line) and near critical conditions $\Delta\Gamma \to 0^+$: (a) upper, (b) lower branch.

3.5 Bifurcation analysis

observation: methods of bifurcation theory applied to nonlinear stability problems generally indicate a strong *dimension reduction (degeneration)* in the neighbourhood of a bifurcation point: the spatial structure (here: with respect to the X-coordinate) is determined by (here: one) *active* or *critical (eigen-) mode(s)* and the evolution of the system is given by a *bifurcation equation* for the other (inactive) variables (here: Z, T) which determines the amplitude of the active mode(s), [31].

introduce perturbation parameter measuring distance from *critical point* Γ_c *(turning point* or *saddle-node bifurcation)*, [3]- [6]:

$$\varepsilon = |\Gamma_c - \Gamma|^{1/4} \to 0^+ \; ; \tag{162}$$

the parabolic shape of the fundamental curve, Fig. 25(b), suggests

$$A(X, Z, T) \sim A_{\infty c}(X) + \varepsilon^2 a_1(X, \bar{Z}, \bar{T}) + \cdots \tag{163}$$

with appropriate *slow* variables

$$\bar{Z} = \varepsilon Z \, , \quad \bar{T} = \varepsilon^2 T \tag{164}$$

and 'perturbations'

$$h = h_\infty(X) + \varepsilon^4 h_1(X, \bar{Z}, \bar{T}) \, , \quad v_w = v_{w\infty}(X) + \varepsilon^4 v_{w1}(X, \bar{Z}, \bar{T}) \tag{165}$$

according to the *selection (reduction) principle*; numerical findings (cf. Fig. 26) suggest Fourier representation

$$a_1 = \int_0^\infty \left[\hat{a}(X, k, \bar{T}) \cos(k\bar{Z}) + \hat{b}(X, k, \bar{T}) \sin(k\bar{Z}) \right] \mathrm{d}k \, . \tag{166}$$

convenient abbreviations:

$$I\cdot = \lambda \int_X^\infty \frac{1}{\sqrt{\xi - X}} \frac{\partial^2 \cdot}{\partial \xi^2} \, \mathrm{d}\xi \, , \quad J\cdot = \lambda \int_X^\infty \frac{\cdot \, \mathrm{d}\xi}{\sqrt{\xi - X}} \, , \quad K\cdot = \gamma \int_{-\infty}^X \frac{\cdot \, \mathrm{d}\xi}{(X - \xi)^{1/4}} \, . \tag{167}$$

crucial part of (157):

$$\begin{aligned} &-\frac{\lambda}{2\pi} \int_{-\infty}^X \frac{\mathrm{d}s}{\sqrt{X - s}} \int_{-\infty}^\infty \int_{-\infty}^\infty \frac{(s - \xi)}{[(s - \xi)^2 + (Z - \eta)^2]^{3/2}} \left(\frac{\partial^2}{\partial \xi^2} + \frac{\partial^2}{\partial \eta^2} \right) (A - h) \, \mathrm{d}\xi \mathrm{d}\eta \\ &\qquad \sim I(A_{\infty c} - h_\infty) + \varepsilon^2 I a_1 + \varepsilon^4 \left(\frac{\partial^2}{\partial \bar{Z}^2} J a_1 - I h_1 \right) \\ &-\frac{\lambda}{\pi} \int_{-\infty}^X \frac{\mathrm{d}s}{\sqrt{X - s}} \int_{-\infty}^\infty \mathrm{d}\xi \int_0^\infty \varepsilon^2 \, \mathrm{sgn}(s - \xi) \, k\varepsilon \, \mathcal{K}_1(k\varepsilon|s - \xi|) \, \tilde{\Delta} \left[\hat{a} \cos(k\bar{Z}) + \hat{b} \sin(k\bar{Z}) \right] \mathrm{d}k + \cdots \; ; \end{aligned} \tag{168}$$

here

$$\tilde{\Delta} = \frac{\partial^2}{\partial \xi^2} - \varepsilon^2 k^2 \, , \quad \mathcal{K}_1(x) = K_1(x) - \frac{1}{x} \tag{169}$$

and K_1 denotes the modified Bessel function; asymptotic behaviour

$$\mathcal{K}_1(x \to 0^+) \sim \frac{x}{4} (2 \ln x - \ln 4 - 1 + 2\gamma_e) + \frac{x^3}{64} (4 \ln x - 4 \ln 2 - 5 + 4\gamma_e) + O(x^5 \ln x) \tag{170}$$

(where γ_e is Euler's constant) indicates the structure

$$A \sim A_{\infty c} + \varepsilon^2 a_1 + \varepsilon^4(\ln\varepsilon\, b_2 + a_2) + O(\varepsilon^6 \ln^2\varepsilon) \quad \text{as} \quad \varepsilon \to 0^+ \,. \tag{171}$$

substitution in (157) leads to the staggered system (172)-(174), where orders involving $\ln\varepsilon$-terms have been omitted: for more details see [4, 5]; a more general and systematic method to deduce the asymptotic structure (171) avoiding (166) is *matching of integrals*, see [2], pp. 341.

the leading order problem

$$A_{\infty c}^2 - X^2 + \Gamma_c = I(A_{\infty c} - h_\infty) - \frac{\kappa}{\gamma} K v_{w\infty} \tag{172}$$

is the steady 2D solution at Γ_c indicating the possibility of flow control $\Gamma_c = \Gamma_c(h_\infty, v_{w\infty})$: see chapter 3.6;

$$(2A_{\infty c} - I)a_1 = 0 \quad \Rightarrow \quad a_1 = b(X)c(\bar{Z}, \bar{T}) \,, \tag{173}$$

$$(2A_{\infty c} - I)a_2 = \operatorname{sgn}(\Gamma_c - \Gamma) - b^2c^2 + \frac{Jb}{2}\frac{\partial^2 c}{\partial \bar{Z}^2} - Kb\frac{\partial c}{\partial \bar{T}} - Ih_1 - \frac{\kappa}{\gamma} K v_{w1} \,. \tag{174}$$

Fredholm alternative (solvability condition): if $\mathcal{L}$ is a bounded linear operator in a Hilbert space with closed range (image), the equation $\mathcal{L}a = f$ has a solution if and only if the inner product $\langle\, n, f \,\rangle = 0$ for every n in the nullspace (kernel) of the adjoint operator $\mathcal{L}^*$,

$$\langle\, n, f \,\rangle = \langle\, n, \mathcal{L}a \,\rangle = \langle\, \underbrace{\mathcal{L}^* n}_{0}, a \,\rangle = 0 \,. \tag{175}$$

in the present case, $\mathcal{L} = (2A_{\infty c} - I)$ is the (singular) Fréchet derivative $\mathcal{N}_A|_{\varepsilon=0}$ of the nonlinear problem $\mathcal{N}(A, \Gamma) = 0$ given by (157) or (138) evaluated at the bifurcation point Γ_c; $b(X)$ and $n(X)$ are the critical right and left eigenfunctions of $\mathcal{L}$ corresponding to the critical eigenvalue 0, respectively:

$$\begin{aligned} \langle\, n, (2A_{\infty c} - I)b \,\rangle &= \int_{-\infty}^{\infty} n(X) \left(2A_{\infty c}(X)b(X) - \lambda \int_X^{\infty} \frac{b''(\xi)}{\sqrt{\xi - X}} \,\mathrm{d}\xi \right) \mathrm{d}X \\ &= \int_{-\infty}^{\infty} b(\xi) \left(2A_{\infty c}(\xi)n(\xi) - \lambda \frac{\mathrm{d}^2}{\mathrm{d}\xi^2} \int_{-\infty}^{\xi} \frac{n(X)}{\sqrt{\xi - X}} \,\mathrm{d}X \right) \mathrm{d}\xi = \langle\, (2A_{\infty c} - I)^* n, b \,\rangle = 0 \,. \end{aligned} \tag{176}$$

application of (175) to (174) leads to the evolution (bifurcation) equation for the *shape function* $c(\bar{Z}, \bar{T})$:

$$\langle\, n, (2A_{\infty c} - I)a_2 \,\rangle = 0 \quad \Rightarrow \quad \frac{\partial c}{\partial \bar{T}} - \nu \frac{\partial^2 c}{\partial \bar{Z}^2} + \mu c^2 - \operatorname{sgn}(\Gamma_c - \Gamma)\delta = \bar{g}(\bar{Z}, \bar{T}) \,, \tag{177}$$

where

$$\nu = \frac{\langle\, n, Jb \,\rangle}{2\langle\, n, Kb \,\rangle} \,, \quad \mu = \frac{\langle\, n, b^2 \,\rangle}{\langle\, n, Kb \,\rangle} \,, \quad \delta = \frac{\langle\, n, 1 \,\rangle}{\langle\, n, Kb \,\rangle} \,, \quad \bar{g} = -\frac{\gamma\langle\, n, Ih_1 \,\rangle + \kappa\langle\, n, Kv_{w1} \,\rangle}{\gamma\langle\, n, Kb \,\rangle} \,. \tag{178}$$

without loss of generality the normalization condition $\langle\, n, 1 \,\rangle = 1$ is imposed; numerical calculations yield

$$\nu \approx 3.0 \,, \quad \mu \approx 2.07 \,, \quad \delta \approx 1.60 \quad \text{for} \quad h_\infty = v_{w\infty} = 0 \,. \tag{179}$$

stationary points of (177):

$$\Gamma < \Gamma_c : \quad c = \pm c_s \,, \quad c_s = \sqrt{\delta/\mu} \,; \qquad \Gamma > \Gamma_c : \quad c = \pm \mathrm{i} c_s \,, \tag{180}$$

corresponding to planar upper and lower branch solutions for below critical conditions.

to eliminate various constants the transformation

$$c(\bar{Z},\bar{T})+c_s=2c_s u(z,t)\,,\quad \bar{Z}=\sqrt{\frac{\nu}{2\mu c_s}}\,z\,,\quad \bar{T}=\frac{t}{2\mu c_s}\,,\quad g=\frac{\bar{g}}{4\delta} \tag{181}$$

is applied to end up with the *forced Fisher–Kolmogoroff, Petrovsky, Piscounoff-equation* (1937), [9]

$$u_t-u_{zz}=u-u^2-\theta(\Gamma-\Gamma_c)/2+g(z,t)\,. \tag{182}$$

finally, solutions of (157) in the limit $|\Gamma-\Gamma_c|\to 0$ are given by

$$A\sim A_{\infty c}(X)+\varepsilon^2 b(X)c_s[2u(z,t)-1]+\cdots\quad \text{as}\quad \varepsilon\to 0\,. \tag{183}$$

flow field quantities:

• interaction pressure: combination of (159) and (171)

$$P\sim P_{\infty c}+\varepsilon^2 P_b\,c+O(\varepsilon^4\ln\varepsilon)\,,$$

$$P_{\infty c}(X)=\frac{1}{\pi}\oint_{-\infty}^{\infty}\frac{(A_{\infty c}-h_\infty)'}{X-\xi}\,\mathrm{d}\xi\,,\quad P_b(X)=\frac{1}{\pi}\oint_{-\infty}^{\infty}\frac{b'}{X-\xi}\,\mathrm{d}\xi\,. \tag{184}$$

the far field behaviour of $P_{\infty c}$ is given by Hadamard's finite part of the corresponding divergent integral in (184),

$$P_{\infty c}\sim\frac{2}{\pi}\ln|X|+\cdots\,,\quad P_b\sim O(X^{-2})\quad \text{as}\quad X\to\pm\infty\,. \tag{185}$$

• spanwise vorticity:

$$\omega_z=\frac{\partial v}{\partial x}-\frac{\partial u}{\partial y}\sim -Re^{9/20}p_{00}y_*-Re^{3/10}\bar{A}+\cdots\,. \tag{186}$$

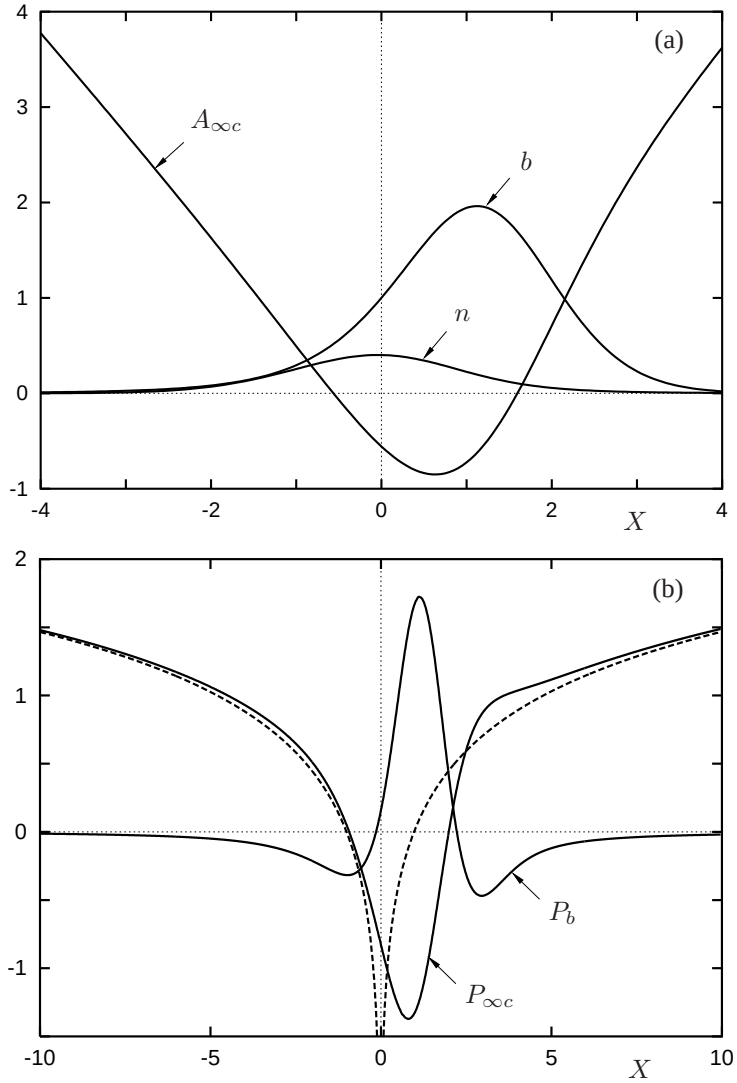

Figure 27: Near critical marginally separated flows ($h_\infty = v_{w\infty} = 0$): (a) wall shear $A_{\infty c}(X)$, right and left eigenfunctions $b(X)$ and $n(X)$, (b) interaction pressure, dashed lines: far-field asymptotes (185).

3.6 Flow control

specify control devices:

$$h_\infty(X) = \mathcal{H}\left[1 - \left(\frac{2(X - X_c)}{\mathcal{L}}\right)^2\right]^3 \theta\left(\frac{\mathcal{L}}{2} - |X - X_c|\right), \tag{187}$$

$$v_{w\infty}(X) = \mathcal{V}\,\theta\left(\frac{\mathcal{L}}{2} - |X - X_c|\right), \tag{188}$$

where the parameters X_c, $\mathcal{L}$, $\mathcal{H}$ and $\mathcal{V}$ denote the location, length of the device, height of the obstacle and the suction rate, see Figs. 28 and 29.

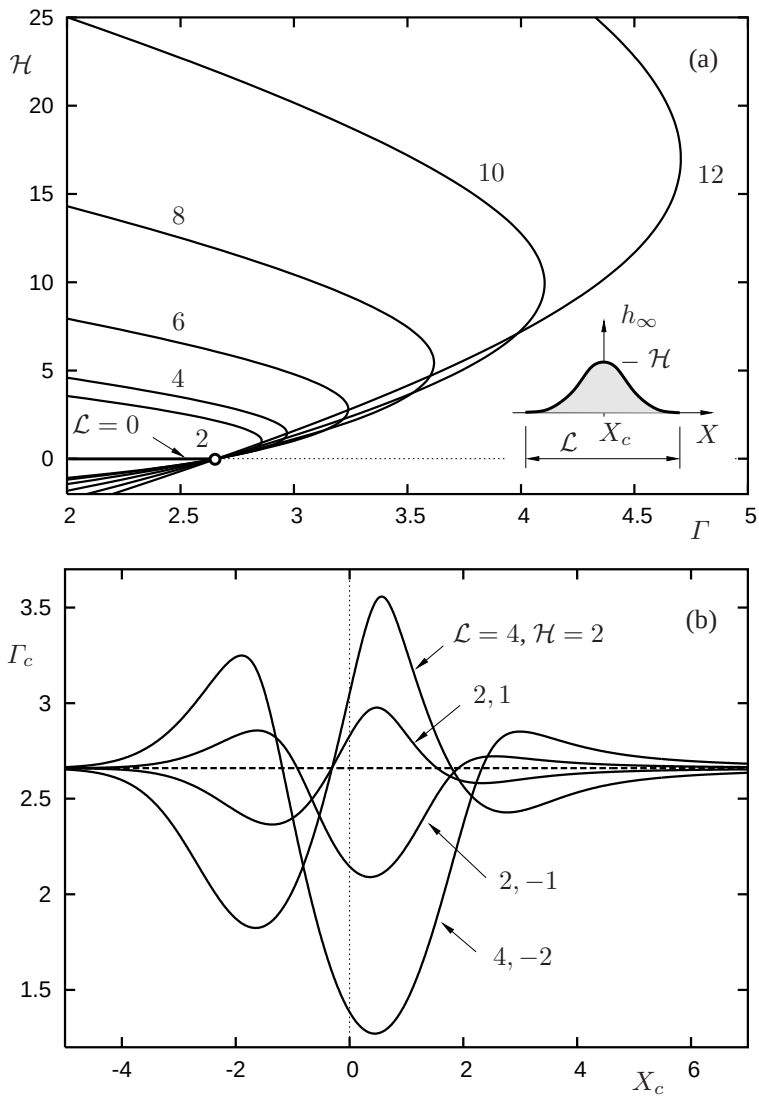

Figure 28: Effect of $h_\infty(X)$ on Γ_c, eqns. (172) and (187) with $v_{w\infty} = 0$: (a) variation of $\mathcal{H}$, $\mathcal{L}$ for $X_c = 0$; solutions for fixed $\mathcal{L}$ can be found in the left-hand domain of the drawn limiting curves $\Gamma = \Gamma_c$ only, (b) variation of X_c; dashed line: $\Gamma_c \approx 2.66$ for uncontrolled flow $h_\infty = v_{w\infty} = 0$.

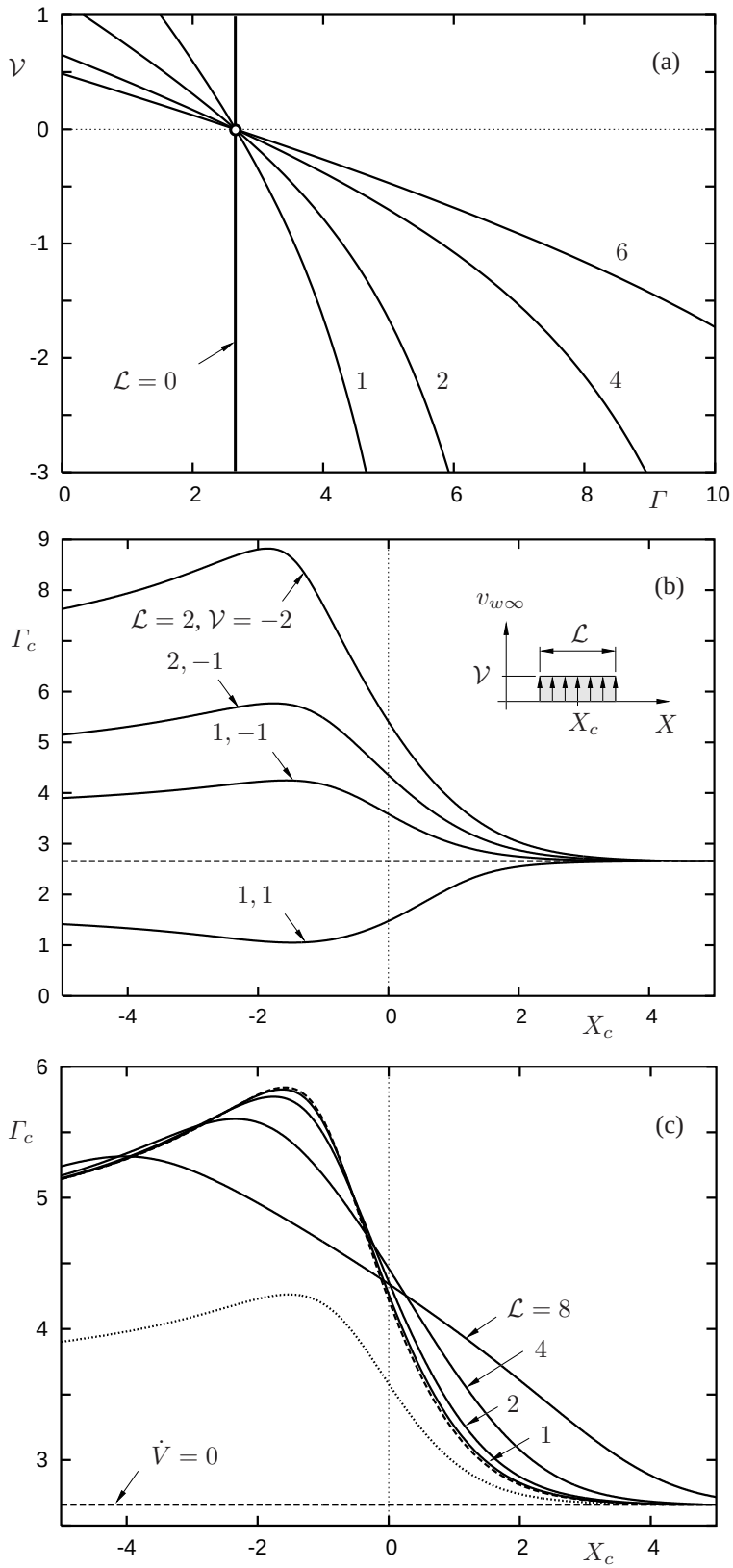

Figure 29: Effect of $v_{w\infty}(X)$ on Γ_c, eqns. (172) and (188) with $h_\infty = 0$: (a) variation of $\mathcal{V}$, $\mathcal{L}$ for $X_c = 0$; solutions for fixed $\mathcal{L}$ can be found in the left-hand domain of the drawn limiting curves $\Gamma = \Gamma_c$ only, (b) variation of X_c; dashed line: $\Gamma_c \approx 2.66$ for uncontrolled flow $v_{w\infty} = h_\infty = 0$, (c) optimization of Γ_c for given suction rate $\dot{V} = \mathcal{V}\mathcal{L} = -2$ (solid lines); limiting curves for $\mathcal{L} \to 0$: $\dot{V} = -2$ (dashed), $\dot{V} = -1$ (dotted).

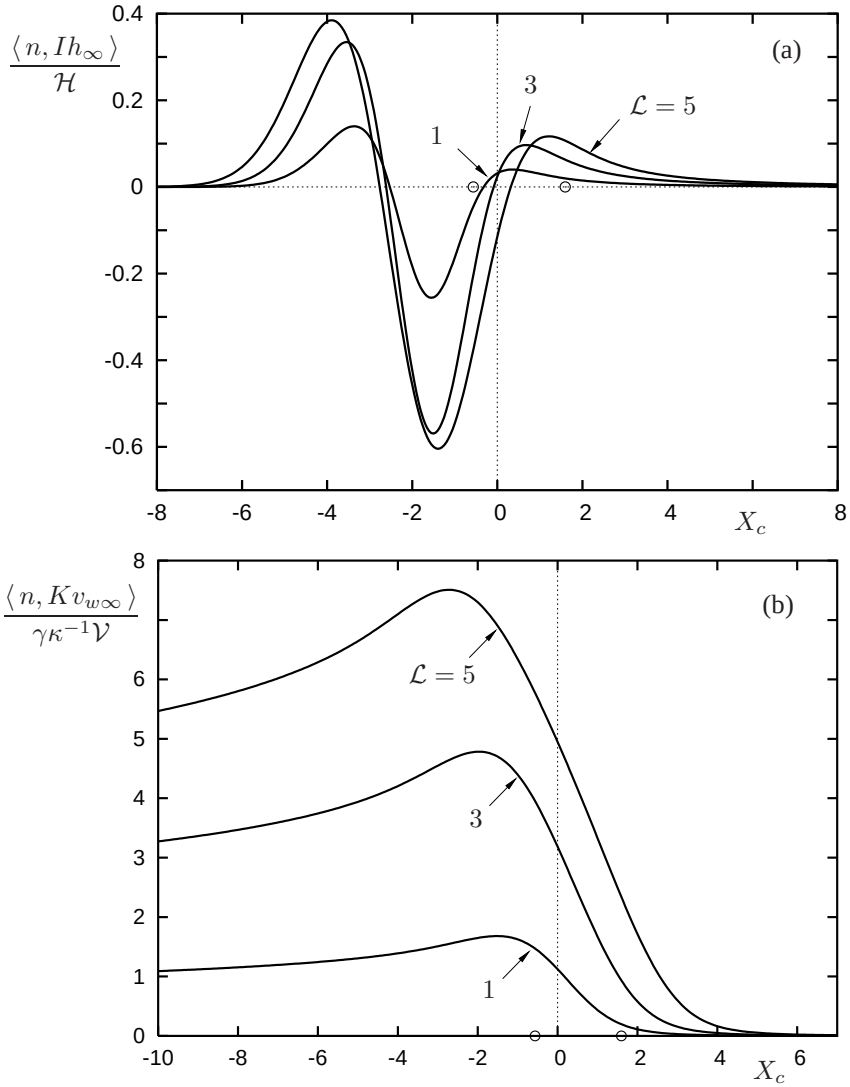

Figure 30: Forcing amplitude (178) in dependence of location X_c and length $\mathcal{L}$ of (a) an obstacle defined by (187), (b) suction distribution according to (188); open circles denote leading order separation and reattachment positions for $h_\infty = v_{w\infty} = 0$.

	(a)	(b)	(c)
U_{00}	0.965	0.983	1.42
p_{00}	0.148	0.221	6.66
α_c	0.04935	0.02458	3.373°
x_0	1.0886	1.0194	0.0287
a_0	1.06	3.61	31.2
a_1	-0.441	-0.499	-0.039

Table 1: *Fundamental constants* for various marginally separated flows: (a) channel flow of Hsiao & Pauley [16], cf. Fig. 21, (b) channel flow of Alam & Sandham [1], cf. Fig. 16, (c) symmetric airfoil with parabola nose of Figs. 6, 7.

example: airfoil of Fig. 6 & Tab. 1 at $Re = 2 \times 10^4$:

uncontrolled flow; maximum angle of attack associated with steady limiting solution:

$$\alpha_m = \alpha_c - Re^{-2/5} \frac{a_0^{1/5} U_{00}^{8/5}}{2 p_{00}^{2/5} a_1} \Gamma_c \approx 4.44^\circ \, ; \tag{189}$$

application of control devices:

$$\mathcal{L} = 1 \mathrel{\hat{=}} 3.2\% \, (\tilde{L}) \, , \quad \mathcal{H} = 1 \mathrel{\hat{=}} 0.1\% \, (\tilde{L}) \, , \quad \mathcal{V} = 1 \mathrel{\hat{=}} 0.86\% \, (\tilde{u}_\infty) \, .$$

4 Fisher's equation

the bifurcation equation for *near critical* marginally separated flows $\Gamma \approx \Gamma_c$ is the forced Fisher-KPP equation

$$\frac{\partial u}{\partial t} - \frac{\partial^2 u}{\partial z^2} = u - u^2 - \frac{\theta(\Gamma - \Gamma_c)}{2} + g(z,t)\,, \tag{190}$$

a nonlinear evolution equation of *reaction-diffusion type*, known from mathematical biology: population dynamics: travelling waves, where the 'concentration' is restricted to $u \in [0,1]$;

here: *no* restrictions: $u \in (-\infty, \infty)$.

questions associated with the problem of *finite time blow-up* in nonlinear parabolic equations, see the review by Galaktionov, Vázquez (2002), [10]:

- *does blow-up occur?*
- *when?*
- *where?*
- *how?*
- *what happens later?*
- *how to compute it numerically?*

it should be noted that the appearance of singularities in the solutions of (190) inevitably leads to a *break-down* of expansion (183); the author, however, believes that these *'bursts'* or *'spikes' remain localized* in space and time and indicate the *transition process* to turbulent boundary layer flow (which is confined to the near wall flow regime) but *do not* destroy the whole (outer inviscid) flow structure; it is further believed that blow-up associated with (190) is *not complete*, i.e. continuation of the solution *beyond* the blow-up time is physically meaningful while the immediate vicinity of singularities needs to be addressed separately by reconsidering the full Navier–Stokes equations.

4.1 2D flow

• without forcing, $g \equiv 0$; here (190) reduces to a Bernoulli equation:

$$\Gamma < \Gamma_c : \quad u(t) = \frac{u_0 + u_0 \tanh[(t-t_0)/2]}{1 + (2u_0 - 1)\tanh[(t-t_0)/2]}\,; \tag{191}$$

for initial conditions $u(t_0) = u_0 > 0$ the steady planar upper branch solution $u_s = 1$ is approached as $t \to \infty$, whereas for values of u_0 below the lower branch $u_s = 0$ finite time blow-up occurs at the blow-up time

$$t^* = t_0 + 2\,\mathrm{artanh}[1/(1-2u_0)]\,. \tag{192}$$

conclusion, see Fig. 31(a): upper/lower branch solutions are attracting/repelling, i.e. stable/unstable in general.

$$\Gamma > \Gamma_c : \quad u(t) = \frac{u_0 + (u_0 - 1)\tan[(t-t_0)/2]}{1 + (2u_0 - 1)\tan[(t-t_0)/2]}\,. \tag{193}$$

Strouhal number associated with *self-sustained oscillations* of the separation bubble (repetitive blow-up solutions):

$$Str = \frac{\tilde{L}}{|\tilde{\boldsymbol{u}}_\infty|\Delta\tilde{t}^*} \sim \frac{a_0^{9/10} U_{00}^{1/5} \mu c_s \sqrt{\Gamma - \Gamma_c}}{p_{00}^{3/10} \pi Re^{1/20}} + \cdots \quad \text{as} \quad \Gamma - \Gamma_c \to 0^+ \,, \tag{194}$$

which – in the absence of any disturbance – reflects the *"shedding criterion":* $\Gamma > \Gamma_c$.

example: channel flow of Alam & Sandham, *Re* $\approx 0.97 \times 10^5$, from Tab. 1 and (189): self-sustained vortex shedding expected for

$$\alpha > \alpha_m \approx 0.09 \,, \tag{195}$$

which differs from the value found by DNS: $\alpha > 0.2 \div 0.25$, cf. Fig. 17.

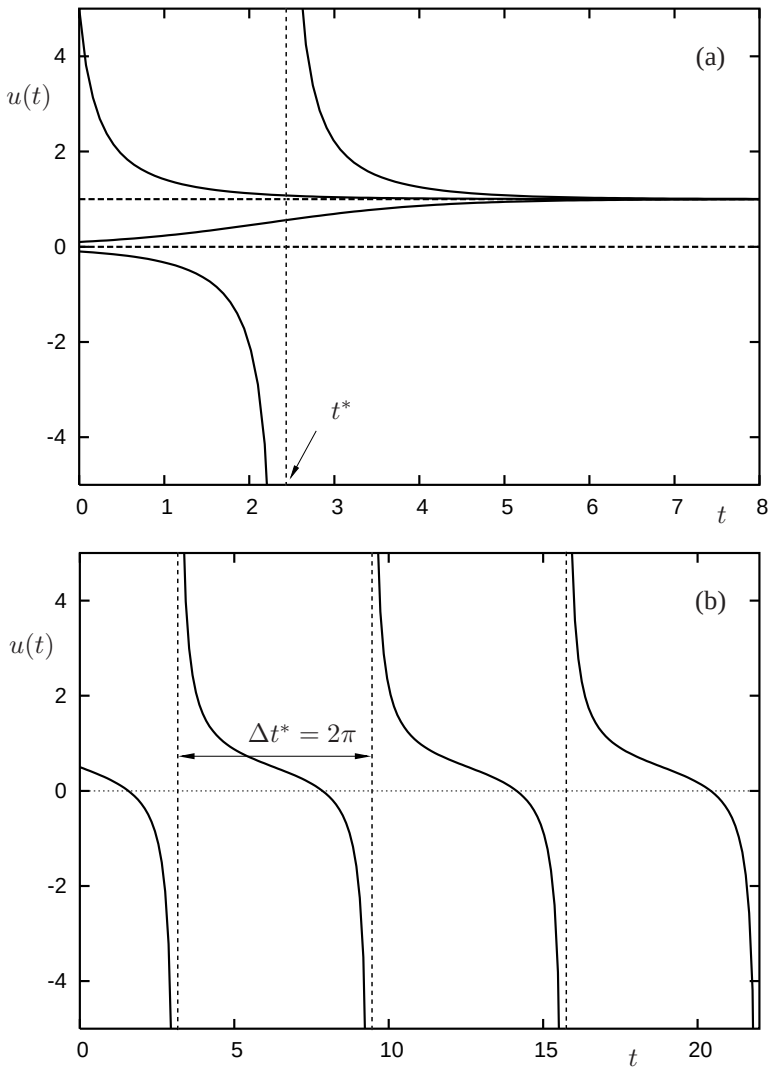

Figure 31: Solutions of (190) for unforced planar flow; (a) sub-critical conditions $\Gamma < \Gamma_c$, (191); dashed lines: steady states corresponding to upper and lower branch solutions; blow-up time t^*, (b) self-sustained bubble bursting associated with super-critical conditions $\Gamma > \Gamma_c$, (193), (194).

• periodic forcing, subcritical flow $\Gamma < \Gamma_c$:

$$u_t = u - u^2 + g\,, \quad g(t) = a\sin(\omega t)\theta(t)\,, \tag{196}$$

a Riccati equation, which can be converted into a second order linear equation, [2].

numerics: first order implicit Euler finite-differencing scheme with *fixed (!)* time step Δt:

$$\left(\frac{1}{\Delta t} + 2u_{j-1} - 1\right) u_j = \frac{u_{j-1}}{\Delta t} + u_{j-1}^2 + g_j + O(\Delta t)\,, \tag{197}$$

where $u_j = u(t_0 + j\Delta t)\,,\ j = 1, 2, \cdots$ and $u_0 = 1$.

near blow-up $t \to t^*$ where $|u_j| \gg 1$:

$$u_j \sim \frac{\left(\dfrac{1}{\Delta t} + u_{j-1}\right) u_{j-1}}{\dfrac{1}{\Delta t} + 2u_{j-1}}\,, \tag{198}$$

i.e. numerical solution u_j 'jumps' if

$$u_{j-1} < -\frac{1}{2\Delta t}\,. \tag{199}$$

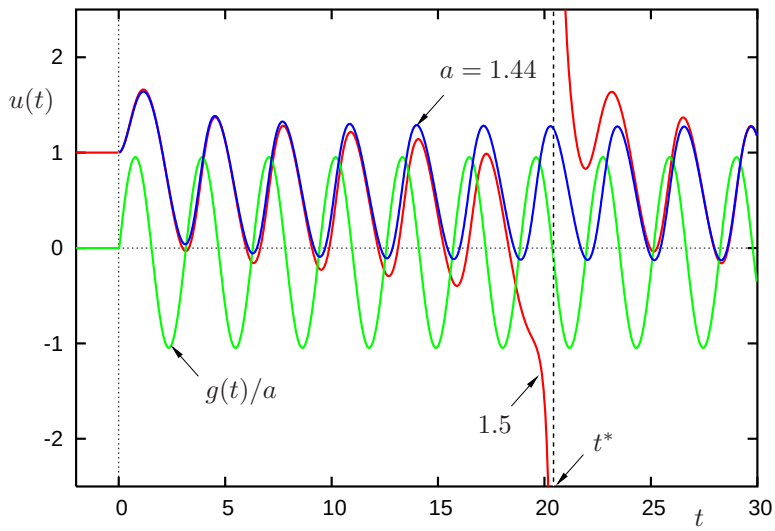

Figure 32: Planar forced flow: numerical solutions of (190) in the form (197) with (196) and $\omega = 2$; for $a > a_c(\omega = 2) \approx 1.45216$ repeated blow-up occurs.

conclusion: if the forcing amplitude is less than a critical value $a < a_c(\omega)$, a bounded response is obtained; $a > a_c$ leads to periodic bubble bursting, Fig. 32.

analytics: E.A. Cox (2006, private communication): transformation

$$u(t) = \frac{1}{2}\left[1 + \omega\,\frac{R'(\bar{t})}{R}\right]\,, \quad 2\bar{t} = \omega t - \pi/2 \tag{200}$$

leads to canonical form of Mathieu's equation

$$R'' + \left[-\frac{1}{\omega^2} - \frac{4a}{\omega^2}\cos(2\bar{t})\right] R = 0\,. \tag{201}$$

blow-up of solutions of (196) are from (200) associated with zeros of solutions of (201); multiple blow-up is associated with oscillatory solutions of (201):

repetitive blow-up if (shedding criterion):

$$\frac{2a}{\omega^2} > q_0 \quad \text{where} \quad -\frac{1}{\omega^2} = a_0(q_0)\,; \tag{202}$$

here $a_0(q_0)$ denotes the characteristic value which yields an even π-periodic solution of (201) which has no zeros.

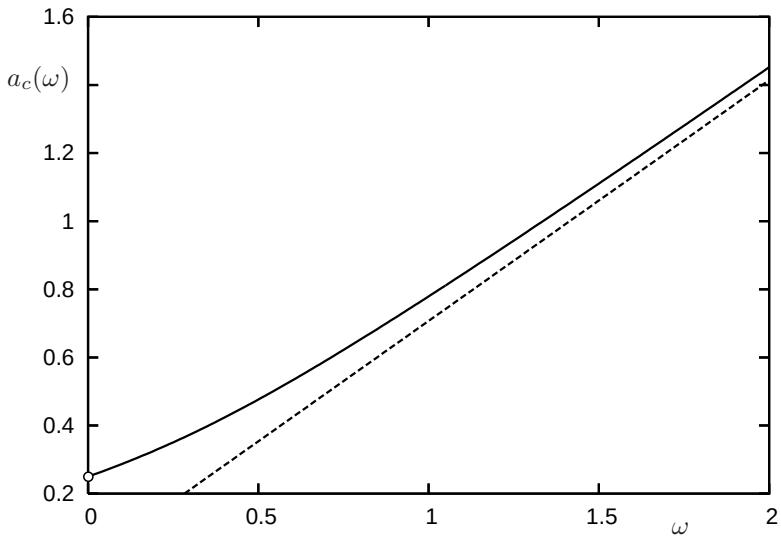

Figure 33: Critical forcing amplitude for planar flow (196) according to (202): $a > a_c$ leads to repetitive blow-up; $a_c(0) = 1/4$, $a_c(\omega \to \infty) \sim \omega/\sqrt{2} + \cdots$ (dashed line).

4.2 3D flow

• *steady bounded* solutions for $\Gamma < \Gamma_c$, $g \equiv 0$:

$$u(z) = \sin^2\left(\frac{\varphi}{2}\right) + \sqrt{3}\sin\varphi\left[\frac{1}{2} - \mathrm{cn}^2\left(\sqrt{\cos\varphi + \frac{\sin\varphi}{\sqrt{3}}}\,\frac{z}{2}\,\middle|\,\frac{2\tan\varphi}{\sqrt{3}+\tan\varphi}\right)\right], \quad \varphi \in [0, \pi/3] \tag{203}$$

containing Jacobian elliptic function $\mathrm{cn}(z|m)$ and a constant of integration φ indicating an infinite number of solutions in the absence of the forcing term, Fig. 34; the second constant of integration reflects the translation invariance of the solution: it is chosen such that $u(z) = u(-z)$; the non-periodic limiting case $\varphi = \pi/3$ is the *homoclinic orbit*

$$u(z) = 1 - \frac{3}{2}\cosh^{-2}\left(\frac{z}{2}\right). \tag{204}$$

for $\varphi \to 0$ (203) yields

$$u(z) \sim -\frac{\sqrt{3}}{2}\,\varphi\cos z + O(\varphi^2)\,. \tag{205}$$

• *steady singular* solutions, $g \equiv 0$

$$u(z) = 6\wp\left(z; \frac{\mathrm{sgn}(\Gamma_c - \Gamma)}{12}, g_3\right) + \frac{1}{2}, \quad g_3 \in \mathbb{R} \tag{206}$$

expressed in terms of Weierstraß elliptic function $\wp(z; g_2, g_3)$ where the invariant g_3 remains arbitrary; in the case of sub-critical flow conditions the non-periodic limiting solution is obtained for $g_3 = -1/216$:

$$u(z) = 1 + \frac{3}{2}\sinh^{-2}\left(\frac{z}{2}\right). \tag{207}$$

in sharp contrast, solutions for super-critical flow are always periodic, where the maximum *'streak spacing'* is given by

$$\frac{\Delta\tilde{z}_{max}}{\tilde{L}} \sim 2\omega_{2max}\sqrt{\frac{\nu}{2\mu c_s}}\,\frac{U_{00}^{4/5}}{a_0^{2/5}p_{00}^{1/5}Re^{1/5}(\Gamma - \Gamma_c)^{1/4}} \quad \text{as} \quad \Gamma - \Gamma_c \to 0^+\,, \tag{208}$$

since they can't decay to a 'planar' steady state, Fig. 35.

• *travelling wave* solutions, $\Gamma < \Gamma_c$, $g \equiv 0$

$$u(z,t) = v(\xi)\,, \quad \xi = z - Ut - \xi_0 \tag{209}$$

where ξ, U denote the wave coordinate, wave speed and the arbitrary constant ξ_0 accounts for the translation invariance of the wave profile, (190) reduces to

$$v'' + Uv' + v - v^2 = 0\,; \tag{210}$$

because of the invariance property $u(z,t;-U) = u(-z,t;U)$ it is sufficient to consider right running waves only; bounded solutions join the stationary states $u_s = 1, 0$ *(heteroclinic orbit)* and the lower limit of the wave speed for positive valued functions v is $U = 2$, Fig. 36(a); the (single, isolated) *singular travelling waves*, which are of special interest in the present context, deviate from and return to the stable upper branch level $u_s = 1$ having the decay behaviour

$$v(\xi) \sim 1 \mp a\,\exp\left[-\left(\frac{U}{2} \pm \sqrt{\frac{U^2}{4} + 1}\right)\xi\right], \quad a \ll 1 \quad \text{as} \quad \xi \to \pm\infty \tag{211}$$

and the structure

$$v(\xi) \sim \frac{6}{(\xi-\xi_s)^2} - \frac{6U}{5(\xi-\xi_s)} + \frac{25-U^2}{50} + O(\xi-\xi_s)\,, \quad \xi \to \xi_s \tag{212}$$

near the pole where ξ_s denotes the location of the singularity, Fig. 36(b).

the limiting form of (210) for $U \to \infty$ can be obtained by the transformation $v(\xi) = U^2\phi(\zeta)$, $\xi = \zeta/U$,

$$\phi'' + \phi' - \phi^2 \sim O(U^{-2})\,, \tag{213}$$

and the solution corresponding to the stationary limit $U = 0$ is given by (207).

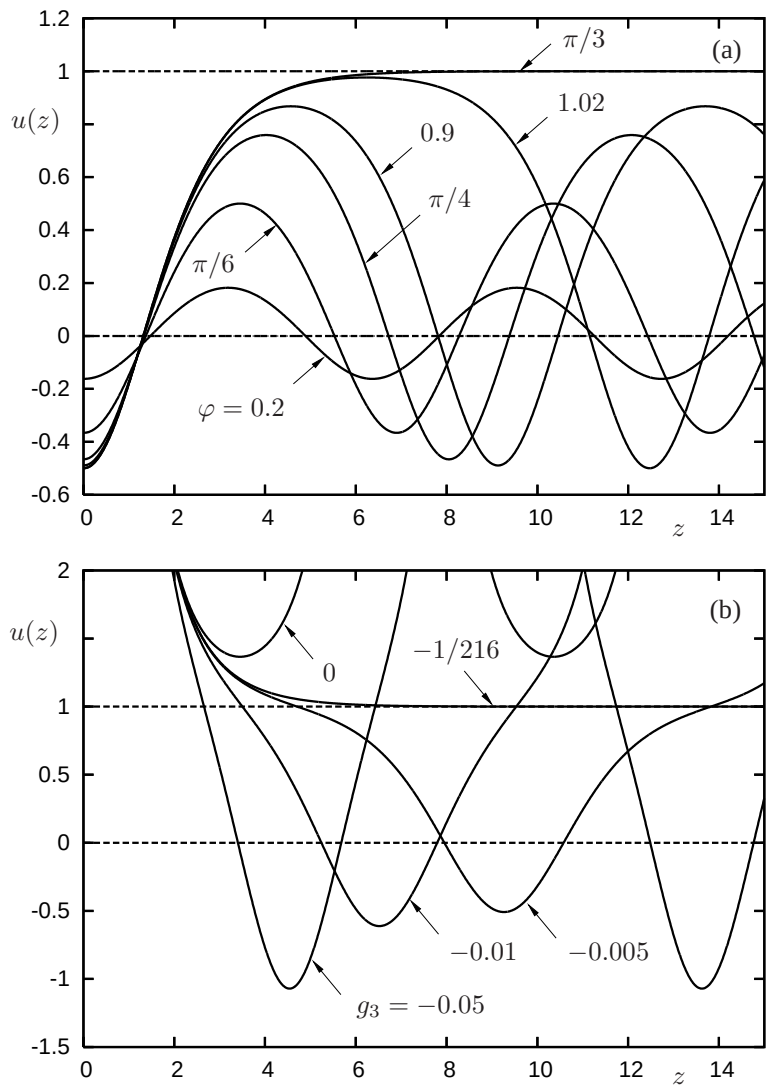

Figure 34: Steady sub-critical solutions of (190) without forcing; dashed lines: $u_s = 0, 1$; (a) bounded, eqns. (203), (204), (b) singular, eqns. (206), (207).

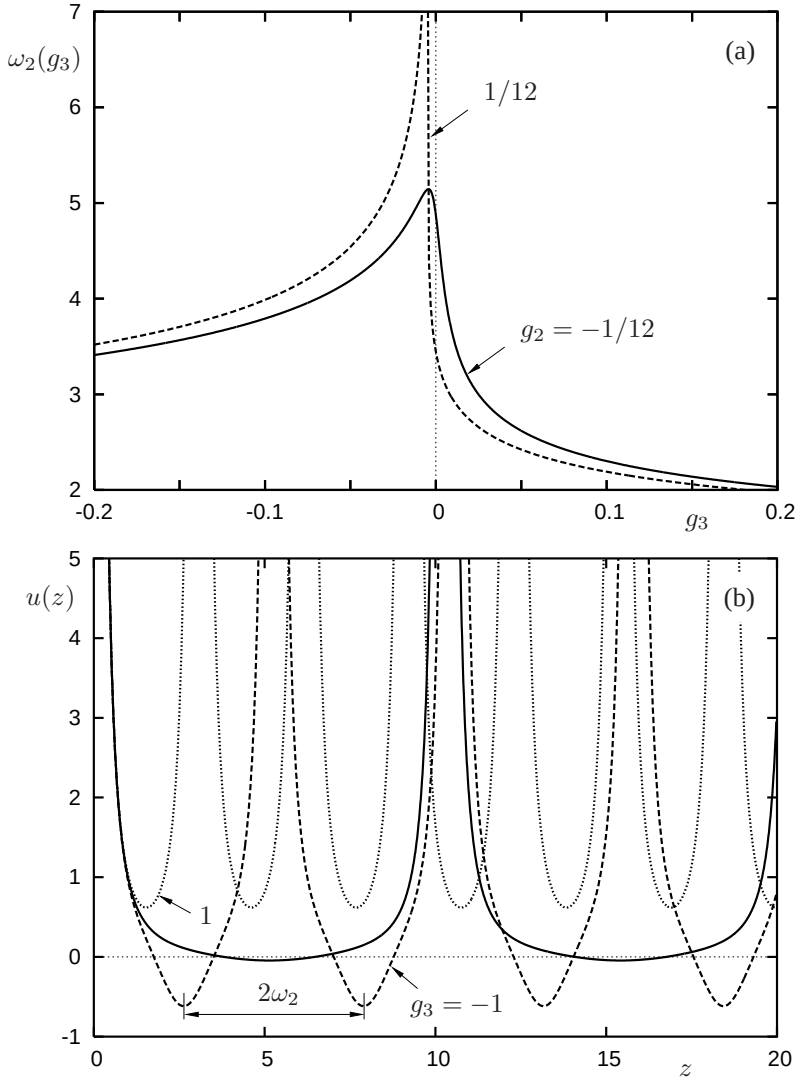

Figure 35: (a) Half-period ω_2 in dependence of the invariants g_2 and g_3, (b) singular steady super-critical solutions; solid line: limiting case with maximum period $2\omega_{2\max} \approx 10.2909$ ($g_3 \approx -0.00423616$).

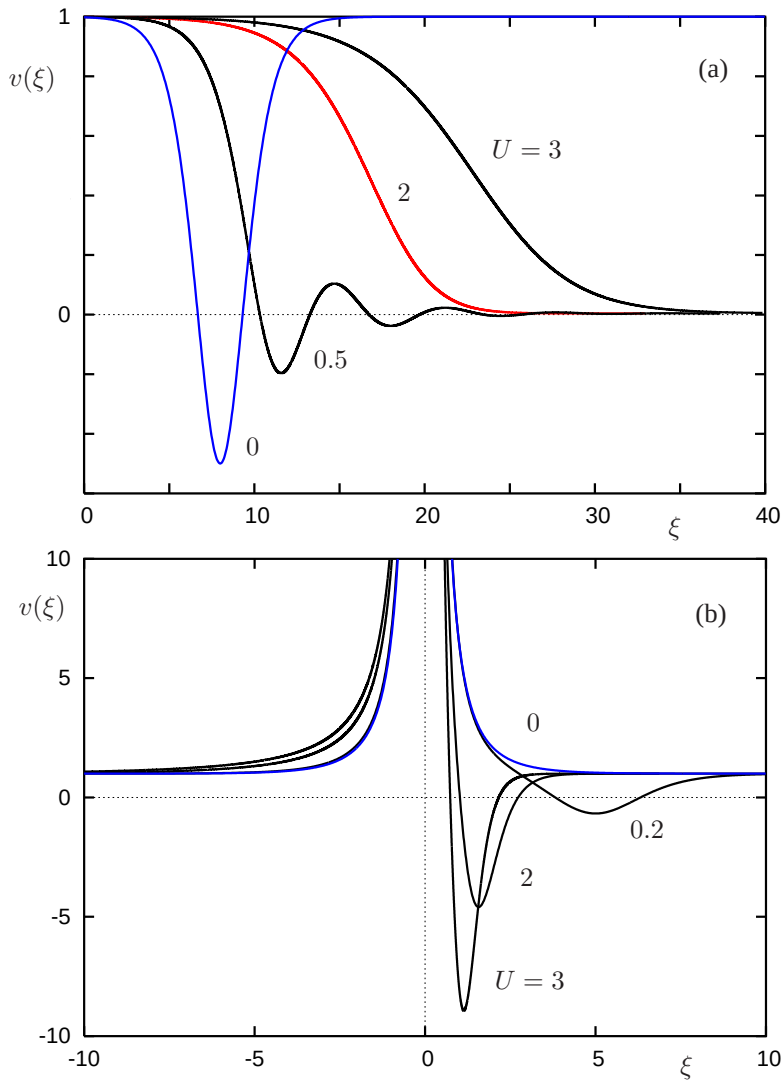

Figure 36: (a) bounded and (b) singular travelling (right running) wave solutions of Fisher's equation (210) depending on the wave speed U.

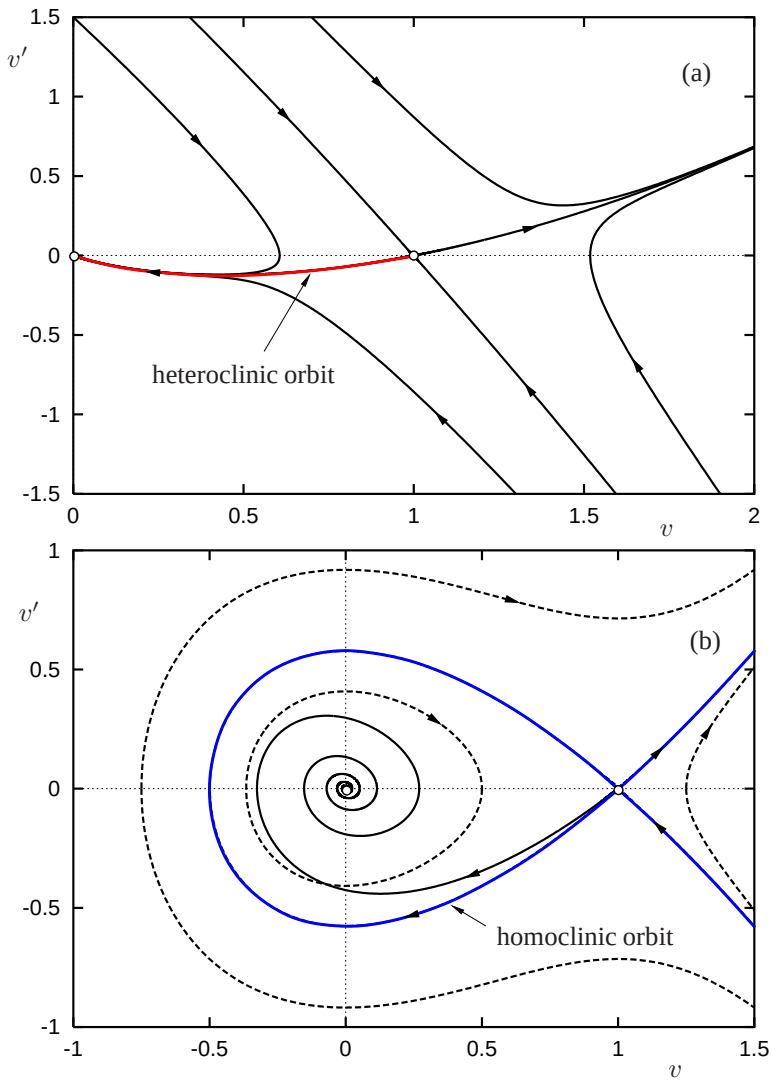

Figure 37: Poincaré's phase portrait of equation (210): (a) $U = 2$; bounded travelling wave solutions join the saddle point $(1, 0)$, $\xi \to -\infty$ and the node $(0, 0)$, $\xi \to \infty$, (b) $U = 0$ (dashed and blue lines, the steady limit), $U = 0.25$ (solid line): $(0, 0)$ now is a spiral point.

4.3 Blow-up asymptotics

comment on the continuation of the solution beyond blow-up, suggested by A.I. Ruban (2006, private communication):

near blow-up – where $|u| \gg 1$ – Fisher's equation can be written in conservative form

$$u_t \sim -u^2 \quad \Rightarrow \quad \frac{\mathrm{d}}{\mathrm{d}t}\left(\frac{1}{u} - t\right) = 0\,. \tag{214}$$

using the concept of weak solutions, following *jump condition* can be derived

$$\frac{1}{u^-} - t^- = \frac{1}{u^+} - t^+\,; \tag{215}$$

here $u^{\mp}$, $t^{\mp}$ denote values immediately before/beyond the blow-up time t^*.

without loss of generality finite time blow-up is located at $t = 0$ and for 3D flow additionally at $z = 0$, i.e.

$$t - t^* \to t\,, \quad z - z^* \to z\,. \tag{216}$$

• 2D flow:

$$u(t) \sim \frac{1}{t} + \frac{1}{2} + \frac{1}{3}\left[\frac{1}{4} - \frac{\theta(\Gamma - \Gamma_c)}{2} + g(0)\right] t + \frac{g'(0)}{4}\, t^2 + O(t^3) \quad \text{as} \quad t \to 0\,. \tag{217}$$

• 3D flow:

since Fisher's equation is of diffusion type, the fundamental solution suggests

$$u(z,t) \sim \frac{1}{t}\, f(\eta) + \cdots\,, \quad \eta = \frac{z}{\sqrt{t}} \quad \Rightarrow \quad f'' - \frac{\eta}{2}\, f' - f - f^2 = 0\,; \tag{218}$$

it can be shown that there is *no* solution; modifying the approach of Hocking et al. (1972), [15] for an equation with cubic non-linearity give the *approximate similarity* ansatz

$$u(z,t) \sim \frac{1}{t}\, f(\eta,\tau) + \cdots\,, \quad \eta = \frac{z}{\sqrt{|t|\,\tau}}\,, \quad \tau = -\ln|t| \to \infty \quad \text{as} \quad t \to 0\,, \tag{219}$$

resulting in

$$f + \frac{\eta}{2}\, f_\eta - f^2 = \frac{\eta}{2\tau}\, f_\eta - f_\tau - \frac{\mathrm{sgn}(t)}{\tau}\, f_{\eta\eta} - \mathrm{sgn}(t)\,\mathrm{e}^{-\tau} f + \mathrm{e}^{-2\tau}\left[\frac{\theta(\Gamma - \Gamma_c)}{2} - g\right]. \tag{220}$$

the setup of an uniformly valid expansion for $t \to 0^-$ (avoiding logarithmic singularities at $\eta = 0$) requires the introduction of $\ln\tau$ terms,

$$f(\eta,\tau) \sim f_0(\eta) + g_1(\eta)\frac{\ln\tau}{\tau} + \frac{f_1(\eta)}{\tau} + O\left(\frac{\ln^2\tau}{\tau^2}\right), \tag{221}$$

where f_0 represents the *blow-up profile*, see Fig. 38(a).

near blow-up – where exponentially small terms in (220) can be neglected – important *symmetry properties* hold:

$$f(\eta,\tau) \to f(\mathrm{i}\eta,\tau) \quad \text{if} \quad t \to -t\,; \quad f(\eta,\tau) = f(-\eta,\tau)\,. \tag{222}$$

as a result

$$f_0^{\mp} = \frac{8}{8 \pm \eta^2}\,, \quad g_1^{\mp} = \mp\frac{10\,\eta^2}{(8 \pm \eta^2)^2}\,, \quad f_1^{\mp} = \frac{16 \mp c_1\eta^2 \mp 8\eta^2 \ln|8 \pm \eta^2|}{(8 \pm \eta^2)^2}\,, \tag{223}$$

where c_1 is an arbitrary constant depending on initial conditions and the upper/lower sign corresponds to $t \to 0^{\mp}$; the *focussing* of the solution for $t \to 0^-$ is associated with the generation of a pair of *moving singularities* immediately beyond blow-up $t > 0$: their path is determined by

$$\eta_s(\tau) = \frac{z_s(t)}{\sqrt{t\tau}} = \pm\sqrt{8} + O(\ln\tau/\tau)\,, \tag{224}$$

see Figs. 38, 39; from a physical point of view it is just this phenomenon which is believed to explain the appearance of *coherent structures* (Λ-vortices, see e.g. Fig. 19) in transitional separation bubbles.

expansion (221) loses its uniform validity in the vicinity of the singularities suggesting the introduction of an inner region (here for the right running sing.)

$$f(\eta,\tau) = F(q,\tau) \sim \tau F_0(q) + O(\tau^0)\,, \quad q = (\eta - \sqrt{8})\tau \tag{225}$$

leading to

$$F_0'' + \sqrt{2}F_0' - F_0^2 = 0\,, \quad F_0(q \to q_s) \sim \frac{6}{(q-q_s)^2} + \cdots\,, \quad F_0(q \to \pm\infty) \sim -\frac{\sqrt{2}}{q} + \cdots\,, \tag{226}$$

which describes a singular travelling wave (with pole location q_s) in the limit of infinite wave speed, cf. (213); the next order term cannot be matched to (221): a correction of the location of a singularity would need stronger singular higher order terms, a contradiction to the usual requirement of uniformly valid expansions.

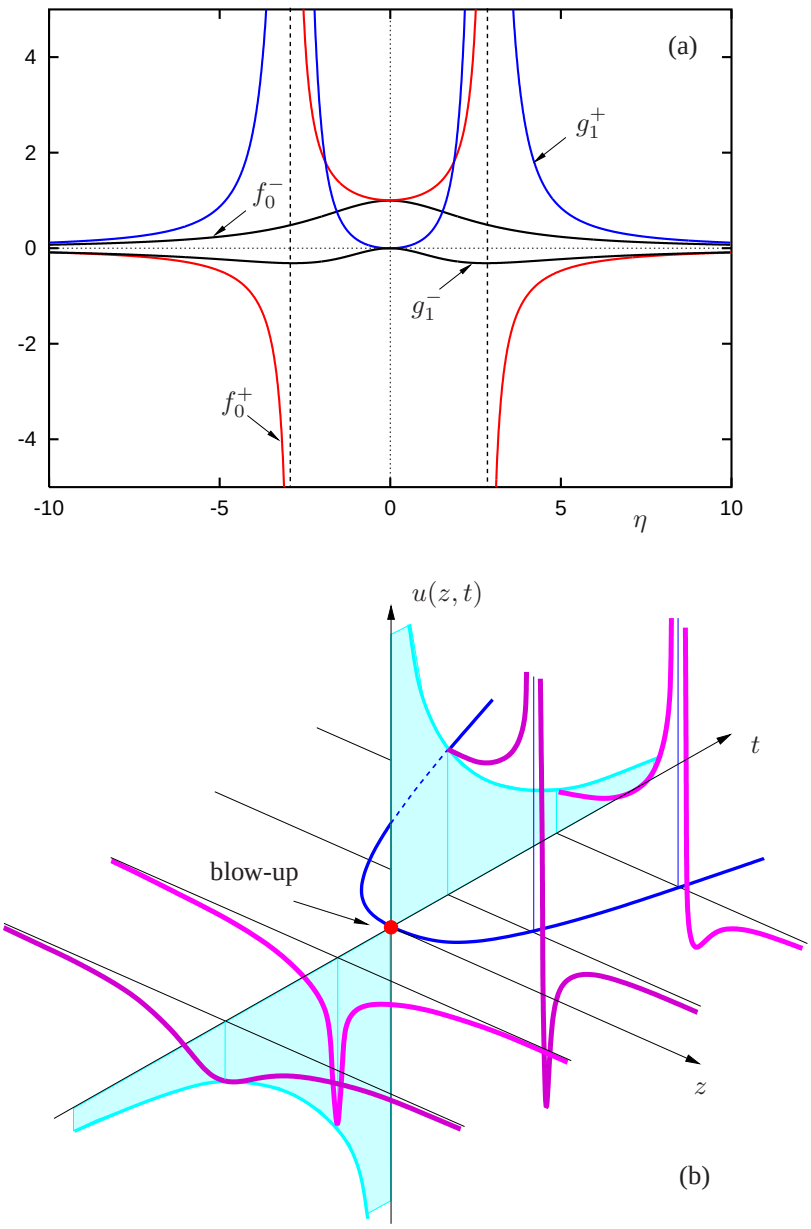

Figure 38: Local blow-up behaviour of solutions to Fisher's equation (190): (a) first and second order spatiotemporal structure (223); dashed lines: leading order singularity location $\eta_s \sim \pm\sqrt{8} + \cdots$, (b) schematic; for $t > 0$ the solution is shown in the right half plane only.

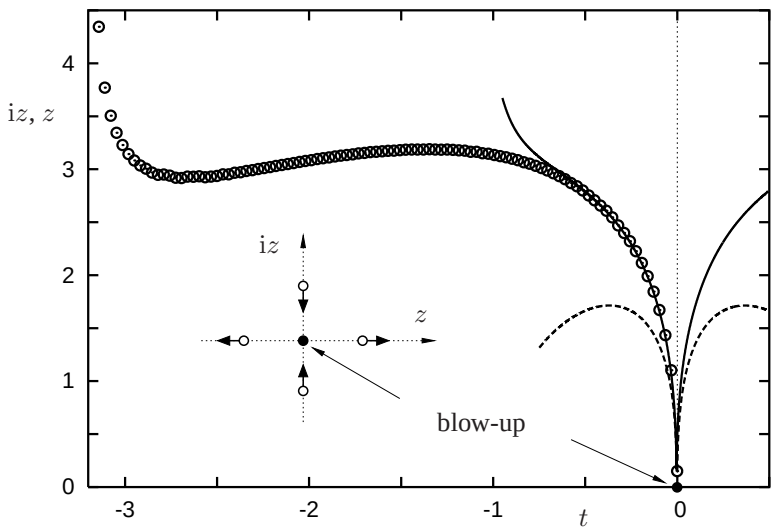

Figure 39: Trajectories of moving complex ($t < 0$) and real ($t > 0$) singularities; open circles: numerical data of Weideman [33], dashed lines: leading order asymptotic prediction $\eta_s \sim \pm\sigma\sqrt{8}$, solid lines: least squares fit $\eta_s(\tau) \sim \pm\sigma(\sqrt{8} + 0.236 \ln \tau/\tau + 1.41/\tau)$ suggested by expansion (221), ($\sigma = \mathrm{i}$ for $t < 0$, $\sigma = 1$ for $t > 0$).

5 Bifurcations in triple deck flows

for the derivation and solution of the triple deck equations for various flow problems see [30], [14]; this chapter contains unpublished work in progress jointly with A. Kluwick.

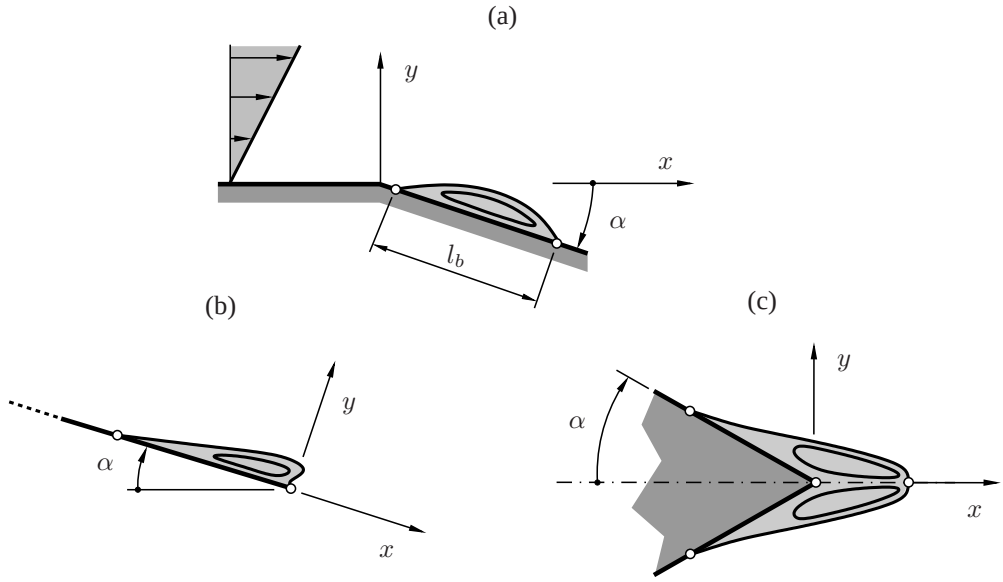

Figure 40: Various subsonic triple deck flows with flow separation (schematic; control parameter α):
(a) expansion ramp, [18], (b) trailing edge of inclined flat plate, [17], (c) symmetric wedge-shaped airfoil.

5.1 Subsonic expansion ramp flow

introduction of dimensionless quantities for the viscous sub-layer; transient and cross flow effects (e.g. due to control devices) are restricted to the interaction process only:

$$\begin{gathered}
\tilde{x} = \tilde{L}(1 + Re^{-3/8}\lambda^{-5/4}x)\,, \quad \tilde{u} = \tilde{u}_\infty\, Re^{-1/8}\lambda^{1/4}u\,, \\
\tilde{y} = \tilde{L}Re^{-5/8}\lambda^{-3/4}(y+f)\,, \quad \tilde{v} = \tilde{u}_\infty\, Re^{-3/8}\lambda^{3/4}(v + uf_x + wf_z + f_t)\,, \\
\tilde{z} = \tilde{L}Re^{-3/8}\lambda^{-5/4}z\,, \quad \tilde{w} = \tilde{u}_\infty Re^{-1/8}\lambda^{1/4}w\,, \\
\tilde{t} = \tilde{L}\tilde{u}_\infty^{-1}Re^{-1/4}\lambda^{-3/2}t\,, \quad \tilde{p} = \tilde{p}_\infty + \tilde{\rho}\tilde{u}_\infty^2\, Re^{-1/4}\lambda^{1/2}p\,, \quad \bar{\alpha} = Re^{-1/4}\lambda^{1/2}\alpha
\end{gathered} \tag{227}$$

here $\lambda \approx 0.32206$ is Blasius' constant and $f(x,z,t)$ denotes the ramp shape; lower deck equations for 3D unsteady flow:

$$\begin{gathered}
\frac{\partial u}{\partial t} + u\frac{\partial u}{\partial x} + v\frac{\partial u}{\partial y} + w\frac{\partial u}{\partial z} = -\frac{\partial p}{\partial x} + \frac{\partial^2 u}{\partial y^2}\,, \\
\frac{\partial p}{\partial y} = 0\,, \\
\frac{\partial w}{\partial t} + u\frac{\partial w}{\partial x} + v\frac{\partial w}{\partial y} + w\frac{\partial w}{\partial z} = -\frac{\partial p}{\partial z} + \frac{\partial^2 w}{\partial y^2}\,, \\
\frac{\partial u}{\partial x} + \frac{\partial v}{\partial y} + \frac{\partial w}{\partial z} = 0\,,
\end{gathered} \tag{228}$$

subject to the no-slip boundary and matching conditions

$$\begin{aligned} y=0: &\quad u=w=0\,, \quad v=v_w(x,z,t)\,, \\ y\to\infty: &\quad u\sim y+A(x,z,t)+\cdots\,, \quad w\sim\frac{B(x,z,t)}{y}+\cdots\,, \quad B=-\int\limits_{-\infty}^{x}\frac{\partial p}{\partial z}\,\mathrm{d}\xi\,, \\ x\to-\infty: &\quad u\sim y+\cdots \end{aligned} \tag{229}$$

and the interaction law

$$p(x,z,t)=-\frac{1}{2\pi}\int\limits_{-\infty}^{\infty}\int\limits_{-\infty}^{\infty}\frac{\partial^2(A-f)/\partial\xi^2}{\sqrt{(x-\xi)^2+(z-\eta)^2}}\,\mathrm{d}\xi\mathrm{d}\eta\,, \tag{230}$$

where $f(x,z,t)=\alpha h(x,z,t)$ and

$$p\sim-\frac{\alpha}{\pi}\ln|x|+\cdots\,, \quad A\to 0\,, \quad h\sim x\,\theta(x)+\cdots \quad \text{as} \quad x\to\pm\infty\,. \tag{231}$$

expansions for *near critical flow* according to the reduction principle (omitting $\ln\varepsilon$ terms induced by (230)):

$$\varepsilon=|\alpha-\alpha_c|^{1/4}\to 0^+\,, \quad \bar z=\varepsilon z\,, \quad \bar t=\varepsilon^2 t\,, \tag{232}$$

$$\begin{aligned} &[u,v]\sim[u_c,v_c](x,y)+\varepsilon^2[u_1,v_1](x,y,\bar z,\bar t\,)+\cdots+\varepsilon^4[u_2,v_2](x,y,\bar z,\bar t\,)+\cdots\,, \\ &[p,A]\sim[p_c,A_c](x)+\varepsilon^2[p_1,A_1](x,\bar z,\bar t\,)+\cdots+\varepsilon^4[p_2,A_2](x,\bar z,\bar t\,)+\cdots\,, \\ &w\sim\varepsilon^3 w_1(x,y,\bar z,\bar t)+\cdots\,, \\ &B\sim\varepsilon^3 B_1(x,\bar z,\bar t)+\cdots\,, \\ &[v_w,f]\sim[v_{wc},f_c](x)+\varepsilon^4[v_{w2},f_2](x,\bar z,\bar t\,)+\cdots\,, \end{aligned} \tag{233}$$

with

$$f_c=\alpha_c h_c(x)\,, \quad f_2=\operatorname{sgn}(\alpha-\alpha_c)\,h_2(x,\bar z,\bar t\,)\,. \tag{234}$$

• $O(\varepsilon^0)$, leading order problem (steady planar flow for $\alpha=\alpha_c$, where α_c may be affected by f_c, v_{wc}), see Fig. 41:

$$\begin{aligned} u_c\frac{\partial u_c}{\partial x}+v_c\frac{\partial u_c}{\partial y}&=-p_c'+\frac{\partial^2 u_c}{\partial y^2}\,, \\ \frac{\partial u_c}{\partial x}+\frac{\partial v_c}{\partial y}&=0\,, \end{aligned} \tag{235}$$

$$\begin{aligned} y=0: &\quad u_c=0\,, \quad v_c=v_{wc}(x)\,, \\ y\to\infty: &\quad u_c\sim y+A_c+\cdots\,, \quad v_c\sim -A_c'\,y+\cdots\,, \\ x\to-\infty: &\quad u_c\sim y+\cdots\,, \end{aligned} \tag{236}$$

$$p_c(x)=\frac{1}{\pi}\oint\limits_{-\infty}^{\infty}\frac{(A_c-f_c)'}{x-\xi}\,\mathrm{d}\xi\,. \tag{237}$$

higher order problems $O(\varepsilon^{2i})$, $i=1,2,\cdots$ can be expressed in the form

$$\begin{aligned} u_c\frac{\partial u_i}{\partial x}+u_i\frac{\partial u_c}{\partial x}+v_c\frac{\partial u_i}{\partial y}+v_i\frac{\partial u_c}{\partial y}+\frac{1}{\pi}\oint\limits_{-\infty}^{\infty}\frac{\partial^2 A_i/\partial\xi^2}{x-\xi}\,\mathrm{d}\xi-\frac{\partial^2 u_i}{\partial y^2}&=b_{i,1}\,, \\ \frac{\partial u_i}{\partial x}+\frac{\partial v_i}{\partial y}&=b_{i,2}\,, \\ \frac{\partial A_i}{\partial y}&=b_{i,3}\,, \end{aligned} \tag{238}$$

subject to

$$
\begin{aligned}
y=0: &\quad u_i=0\,, \quad v_1=0\,, \quad v_2=v_{w2}\,,\\
y\to\infty: &\quad u_i\sim A_i+\cdots\,, \quad v_i\sim -A_i'\,y+\cdots\,,\\
x\to-\infty: &\quad u_i\to 0\,.
\end{aligned}
\tag{239}
$$

• $O(\varepsilon^2)$, critical eigenmode:

$$
\mathcal{M}\boldsymbol{r}_1=\boldsymbol{b}_1=\boldsymbol{0} \quad\Rightarrow\quad \boldsymbol{r}_1=c(\bar{z},\bar{t}\,)\,\boldsymbol{r}(x,y)\,, \quad p_1(x,\bar{z},\bar{t}\,)=c(\bar{z},\bar{t}\,)\,p_r(x)\,,
\tag{240}
$$

where $\mathcal{M}$ is a singular linear operator matrix determined by (238), $\boldsymbol{r}_i=(u_i,v_i,A_i)^T$, $\boldsymbol{b}_i=(b_{i,1},b_{i,2},b_{i,3})^T$ and $\boldsymbol{r}=(u_r,v_r,A_r)$ the perturbation vector of the field quantities, right hand side and right eigenvector of $\mathcal{M}$:

$$
\mathcal{M}\boldsymbol{r}=\begin{pmatrix} u_c\partial_x+u_{cx}+v_c\partial_y-\partial_{yy} & u_{cy} & \dfrac{1}{\pi}\displaystyle\oint_{-\infty}^{\infty}\dfrac{\mathrm{d}^2\cdot/\mathrm{d}\xi^2}{x-\xi}\,\mathrm{d}\xi\\ \partial_x & \partial_y & 0\\ 0 & 0 & \partial_y \end{pmatrix}\begin{pmatrix} u_r\\ v_r\\ A_r\end{pmatrix}=\boldsymbol{0}\,.
\tag{241}
$$

introduction of left eigenvector $\boldsymbol{l}^T=(m,n,q)$, flow domain $D=\{x\in(-\infty,\infty),y\in[0,\infty)\}$, surface element $\mathrm{d}D=\mathrm{d}x\mathrm{d}y$ and adjoint operator $\mathcal{M}^*$,

$$
\int_D \boldsymbol{l}^T\mathcal{M}\boldsymbol{r}\,\mathrm{d}D=\int_D \boldsymbol{r}^T\mathcal{M}^*\boldsymbol{l}\,\mathrm{d}D+\mathcal{B}(\boldsymbol{r})=0\,,
\tag{242}
$$

where the condition $\mathcal{B}(\boldsymbol{r})=0$ is required for the boundary term; explicitly, using integration by parts:

$$
\begin{aligned}
&\int_D\Big\{\,[m(u_c\partial_x+u_{cx}+v_c\partial_y-\partial_{yy})+n\partial_x]\,u_r+[mu_{cy}+n\partial_y]\,v_r+\Big[\frac{m}{\pi}\oint_{-\infty}^{\infty}\frac{\mathrm{d}^2\cdot/\mathrm{d}\xi^2}{x-\xi}\,\mathrm{d}\xi+q\partial_y\Big]A_r\Big\}\mathrm{d}D\\
&\quad=\int_D\Big\{u_r\,[-m_xu_c-m_yv_c-mv_{cy}-m_{yy}-n_x]+v_r\,[mu_{cy}-n_y]\\
&\qquad\qquad +A_r\Big[-\frac{1}{\pi}\frac{\partial^2}{\partial x^2}\oint_{-\infty}^{\infty}\frac{m}{x-\xi}\,\mathrm{d}\xi-q_y\Big]\Big\}\mathrm{d}D+\mathcal{B}(\boldsymbol{r})=0
\end{aligned}
\tag{243}
$$

with

$$
\mathcal{B}(\boldsymbol{r})=\int_{-\infty}^{\infty}[mv_cu_r-mu_{ry}+m_yu_r+nv_r+qA_r]\Big|_{y=0}^{\infty}\mathrm{d}x\,,
\tag{244}
$$

$$
\mathcal{M}^*\boldsymbol{l}=\begin{pmatrix} -u_c\partial_x-v_c\partial_y-v_{cy}-\partial_{yy} & -\partial_x & 0\\ u_{cy} & -\partial_y & 0\\ -\dfrac{1}{\pi}\dfrac{\partial^2}{\partial x^2}\displaystyle\oint_{-\infty}^{\infty}\dfrac{\cdot\,\mathrm{d}\xi}{x-\xi} & 0 & -\partial_y \end{pmatrix}\begin{pmatrix} m\\ n\\ q\end{pmatrix}=\boldsymbol{0}\,.
\tag{245}
$$

adjoint system:

$$
\begin{aligned}
u_c\frac{\partial m}{\partial x}+v_c\frac{\partial m}{\partial y}+m\frac{\partial v_c}{\partial y}+\frac{\partial^2 m}{\partial y^2}+\frac{\partial n}{\partial x}&=0\,,\\
m\frac{\partial u_c}{\partial y}-\frac{\partial n}{\partial y}&=0\,,\\
\frac{1}{\pi}\frac{\partial^2}{\partial x^2}\oint_{-\infty}^{\infty}\frac{m}{x-\xi}\,\mathrm{d}\xi+\frac{\partial q}{\partial y}&=0\,,
\end{aligned}
\tag{246}
$$

from which, taking into account (236),

$$m \sim \frac{\mu(x)}{y^2} + \cdots\,, \quad n \sim -\frac{\mu}{y} + \cdots\,, \quad q \sim \frac{1}{\pi y}\frac{\mathrm{d}^2}{\mathrm{d}x^2}\oint\limits_{-\infty}^{\infty} \frac{\mu}{x-\xi}\,\mathrm{d}\xi + \cdots \quad \text{as} \quad y \to \infty \tag{247}$$

can be deduced; behaviour near solid wall:

$$\begin{gathered} u_c \sim u_{c1}(x)\,y + \cdots\,, \quad v_c \sim v_{wc}(x) - u'_{c1}\frac{y^2}{2} + \cdots\,, \\ u_r \sim \tau_{wr}(x)\,y + \cdots\,, \quad v_r \sim -\tau'_{wr}\frac{y^2}{2} + \cdots\,, \\ m \sim \sum_{i=0} m_i(x)\,y^i\,, \quad n \sim \sum_{i=0} n_i(x)\,y^i\,, \quad q \sim \sum_{i=0} q_i(x)\,y^i\,, \quad \text{as} \quad y \to 0\,. \end{gathered} \tag{248}$$

from (246)

$$2m_2 + m_1 v_{wc} + n'_0 = 0\,, \quad m_0 u_{c1} - n_1 = 0\,, \quad \frac{1}{\pi}\frac{\mathrm{d}^2}{\mathrm{d}x^2}\oint\limits_{-\infty}^{\infty} \frac{m_0}{x-\xi}\,\mathrm{d}\xi + q_1 = 0\,; \tag{249}$$

from (244)

$$\mathcal{B}(\boldsymbol{r}) = \int\limits_{-\infty}^{\infty} \left[\mu A'_r + m_0\tau_{wr} - q_0 A_r\right]\mathrm{d}x = 0\,. \tag{250}$$

• $O(\varepsilon^3)$, cross flow:

$$\begin{gathered} u_c\frac{\partial w_1}{\partial x} + v_c\frac{\partial w_1}{\partial y} = -\frac{\partial c}{\partial \bar{z}}\,p_r + \frac{\partial^2 w_1}{\partial y^2}\,, \\ y = 0: \quad w_1 = 0\,, \quad y \to \infty: \quad w_1 \sim \frac{B_1}{y} + \cdots\,, \end{gathered} \tag{251}$$

resulting in the decomposition

$$w_1 = \frac{\partial c}{\partial \bar{z}}\,w_r(x,y)\,, \quad B_1 = -\frac{\partial c}{\partial \bar{z}}\int\limits_{-\infty}^{x} p_r\,\mathrm{d}\xi\,. \tag{252}$$

• $O(\varepsilon^4)$, bifurcation equation from Fredholm alternative:

$$\int_D \boldsymbol{l}^T\mathcal{M}\boldsymbol{r}_2\,\mathrm{d}D = \int_D \boldsymbol{r}_2^T\underbrace{\mathcal{M}^*\boldsymbol{l}}_{0}\,\mathrm{d}D + \mathcal{B}(\boldsymbol{r}_2) = \int_D \boldsymbol{l}^T\boldsymbol{b}_2\,\mathrm{d}D\,, \tag{253}$$

where

$$\mathcal{B}(\boldsymbol{r}_2) = \int\limits_{-\infty}^{\infty}\left[\mu A_{2x} + m_0 u_{21} - n_0 v_{w2} - q_0 A_2\right]\mathrm{d}x\,, \tag{254}$$

$$\boldsymbol{b}_2^T = \left(-\frac{\partial c}{\partial \bar{t}}\,u_r - c^2(u_r u_{rx} + v_r u_{ry}) + \frac{\mathrm{sgn}(\alpha-\alpha_c)}{\pi}\oint\limits_{-\infty}^{\infty}\frac{h_{2\xi\xi}}{x-\xi}\,\mathrm{d}\xi, -\frac{\partial^2 c}{\partial \bar{z}^2}\,w_r, 0\right) \tag{255}$$

with

$$u_2 \sim u_{21}(x,\bar{z},\bar{t}\,)\,y + \cdots\,, \quad v_2 \sim v_{w2}(x,\bar{z},\bar{t}\,) - u_{21x}\frac{y^2}{2} + \cdots\,. \tag{256}$$

to *avoid secular terms* in (254):

$$m_0 = 0\,, \quad \mu = kA_r\,, \quad q_0 = -kA_r'\,, \quad k = const., \quad n_1 = q_1 = 0 \tag{257}$$

as a consequence of (249), (250).

finally, from (253):

$$\begin{aligned}\frac{\partial c}{\partial \bar{t}} \int_D m u_r \,\mathrm{d}D + c^2 \int_D m(u_r u_{rx} + v_r u_{ry})\,\mathrm{d}D + \frac{\partial^2 c}{\partial \bar{z}^2} \int\limits_D n w_r \mathrm{d}D \\ - \operatorname{sgn}(\alpha - \alpha_c) \int_D \left(\frac{m}{\pi} \oint\limits_{-\infty}^{\infty} \frac{h_{2\xi\xi}}{x - \xi}\,\mathrm{d}\xi \right) \mathrm{d}D = \int\limits_{-\infty}^{\infty} n_0 v_{w2}\,\mathrm{d}x\,,\end{aligned} \tag{258}$$

which is a *Fisher type equation*; for steady 2D unforced ramp flow past a sharp corner $h(x) = x\theta(x)$ it reduces to

$$c^2 \int_D m(u_r u_{rx} + v_r u_{ry})\,\mathrm{d}D - \frac{\operatorname{sgn}(\alpha - \alpha_c)}{\pi} \int_D \frac{m}{x}\,\mathrm{d}D = 0\,, \tag{259}$$

where

$$c_s^2 = \int_D \frac{m}{x}\,\mathrm{d}D \Big/ \left(\pi \int_D m(u_r u_{rx} + v_r u_{ry})\,\mathrm{d}D \right) > 0\,. \tag{260}$$

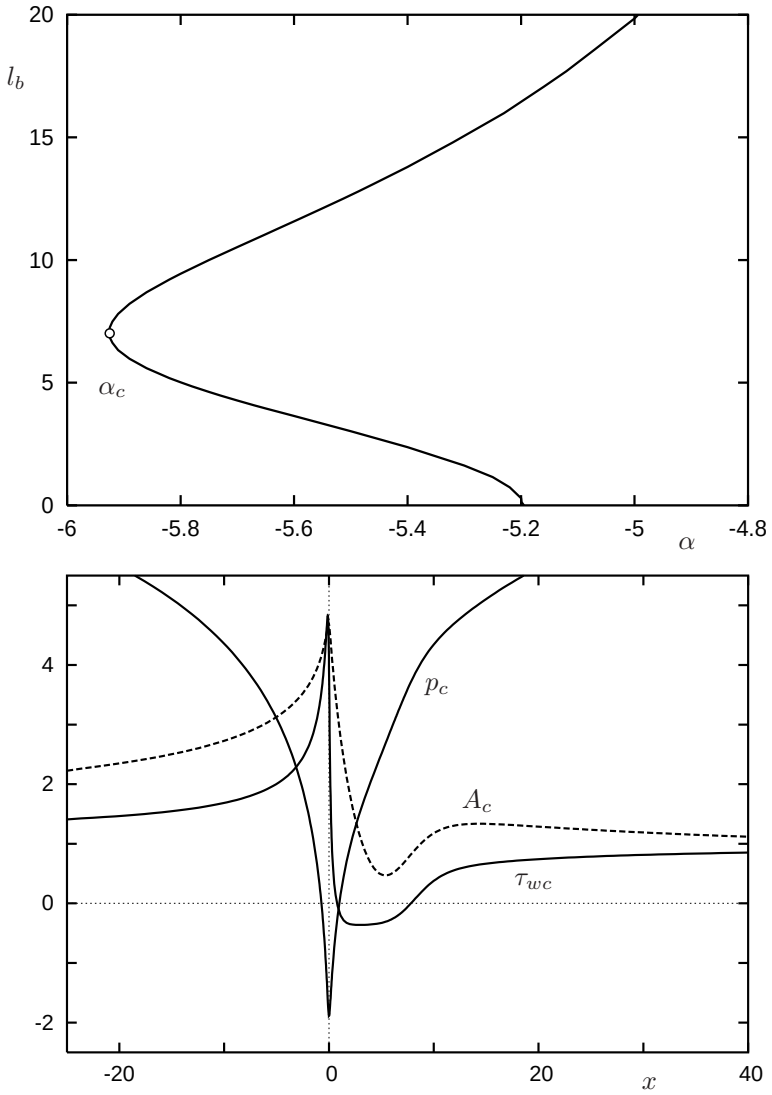

Figure 41: (a) non-uniqueness of the planar ramp flow: bubble length l_b versus ramp angle α for $h = (x + \sqrt{x^2 + r^2})/2$ with $r = 0.1$ and $v_w = 0$, (b) wall shear stress $\tau_{wc}(x) = u_{c1}(x)$, displacement function $A_c(x)$ and interaction pressure $p_c(x)$ at the turning point $\alpha_c \doteq -5.92631$, eqn. (235); source: V.B. Zametaev (2003, private communication).

5.2 Subsonic symmetric wedge shaped trailing edge flow

assume turning point bifurcation;

$\Rightarrow$ observation: symmetry properties of components of right/left eigenfunctions with respect to y coordinate:

$$\text{even:} \quad u_r, n, q\,; \qquad \text{odd:} \quad v_r, m \qquad (y \to -y) \tag{261}$$

bifurcation equation, $D = \{x, y \in (-\infty, \infty)\}$:

$$\frac{\partial c}{\partial t} \underbrace{\int_D m u_r \,\mathrm{d}D}_{0} + c^2 \underbrace{\int_D m(u_r u_{rx} + v_r u_{ry}) \,\mathrm{d}D}_{0} + \cdots = 0 \tag{262}$$

consequence: *no* turning point bifurcation expected!

conclusion: *existence of turning point bifurcation* within the framework of high Reynolds number boundary layer (triple deck) flows *seems to require* (at least):

- *flow separation,*
- *symmetry breaking steady base flow*.

if there is such a bifurcation, the resulting bifurcation equation turns out to be of Fisher's type as in the case of near critical marginally separated flows.

References

[1] Alam, M. & Sandham, N.D. 2000 Direct numerical simulation of 'short' laminar separation bubbles with turbulent reattachment. *J. Fluid Mech.* **410**, 1–28.

[2] Bender, C.M. & Orszag, S.A. 1999 *Advanced Mathematical Methods for Scientists and Engineers*, Springer.

[3] Braun, S. & Kluwick, A. 2002 The effect of three-dimensional obstacles on marginally separated laminar boundary layer flows. *J. Fluid Mech.* **460**, 57–82.

[4] Braun, S. & Kluwick, A. 2003 Analysis of a bifurcation problem in marginally separated laminar wall jets and boundary layers. *Acta Mech.* **161**, 195–211.

[5] Braun, S. & Kluwick, A. 2004 Unsteady three-dimensional marginal separation caused by surface-mounted obstacles and/or local suction. *J. Fluid Mech.* **514**, 121–152.

[6] Braun, S. & Kluwick, A. 2005 Blow-up and control of marginally separated boundary layer flows. In *New Developments and Applications in Rapid Fluid Flows* (Eds. J.S.B. Gajjar & F.T. Smith). *Phil. Trans. R. Soc. Lond.* A **363**, 1057–1067.

[7] Cowley, S.J. 2001 Laminar boundary-layer theory: a 20th century paradox? In *Proceedings of ICTAM 2000* (Eds. H. Aref and J.W. Phillips), Kluwer, pp. 389–411.

[8] Elliott, J.W. & Smith, F.T. 1987 Dynamic stall due to unsteady marginal separation. *J. Fluid Mech.* **179**, 489–512.

[9] Fisher, R.A. 1937 The wave of advance of advantageous genes. *Ann. Eugenics* **7**, 355–369.

[10] Galaktionov, V.A. & Vazquez, J.L. 2002 The problem of blow-up in nonlinear parabolic equations. *Discrete and continuous dynamical systems* **8**, 399–433.

[11] Goldstein, S. 1948 On laminar boundary-layer flow near a position of separation. *Q. J. Mech. Appl. Maths.* **179**, 489–512.

[12] Hackmüller, G. & Kluwick, A. 1990 Effects of surface geometry and suction/blowing on marginal separation. *Proc. 3rd Intl Congr. of Fluid Mechanics, Cairo 1990* (Eds. A.H. Nayfeh & A. Mobarak), Vol. I, Cairo University, pp. 1–6.

[13] Hackmüller, G. & Kluwick, A. 1991 Effects of 3-D surface mounted obstacles on marginal separation. In *Separated Flows and Jets* (Eds. V.V. Kozlov & A.V. Dovgal), Springer, pp. 55–65.

[14] Kluwick, A. 1998 Interacting laminar and turbulent boundary layers. In *Recent Advances in Boundary Layer Theory.* (Ed. A. Kluwick), Springer, pp. 231–330.

[15] Hocking, L.M., Stewartson, K., Stuart, J.T. & Brown, S.N. 1972 A nonlinear instability burst in plane parallel flow. *J. Fluid Mech.* **51**, 705–735.

[16] Hsiao, C.-T. & Pauley, L.L. 1994 Comparison of the triple-deck theory, interactive boundary layer method, and Navier–Stokes computation for marginal separation. *Trans. ASME J. Fluids Eng.* **116**, 22–28.

[17] Korolev, G.L. 1989 Contribution to the theory of thin-profile trailing edge separation. *Izv. Akad. Nauk SSSR: Mekh. Zhidk. Gaza* **4**, 55–59 (Engl. transl. *Fluid Dyn.* **24**, 534–537).

[18] Korolev, G.L. 1992 Non-uniqueness of separated flow past nearly flat corners. *Izv. Akad. Nauk SSSR: Mekh. Zhidk. Gaza* **3**, 178–180 (Engl. transl. *Fluid Dyn.* **27**, 442–444).

[19] Maucher, U., Rist, U., Kloker, M. & Wagner, S. 2000 DNS of laminar-turbulent transition in separation bubbles. In *High Performance Computing in Science and Engineering '99* (Eds. E. Krause & W. Jäger), Springer, pp. 279–294.

[20] Messiter, A.F. 1970 Boundary-layer flow near the trailing edge of a flat plate. *SIAM J. Appl. Math.* **18**, 241–257.

[21] Ruban, A.I. 1981a Singular solution of boundary layer equations which can be extended continously through the point of zero surface friction. *Izv. Akad. Nauk SSSR: Mekh. Zhidk. Gaza* **6**, 42–52 (Engl. transl. *Fluid Dyn.* **16** *(6)*, 835–843).

[22] Ruban, A.I. 1981b Asymptotic theory of short separation regions on the leading edge of a slender airfoil. *Izv. Akad. Nauk SSSR: Mekh. Zhidk. Gaza* **1**, 42–51 (Engl. transl. *Fluid Dyn.* **17** *(1)*, 33–41).

[23] Ruban, A.I. 1982 Stability of preseparation boundary layer on the leading edge of a thin airfoil. *Izv. Akad. Nauk SSSR: Mekh. Zhidk. Gaza* **6**, 55–63 (Engl. transl. *Fluid Dyn.* **17**, 860–867).

[24] Schlichting, H. & Gersten, K. 2000 *Boundary Layer Theory*, 8th ed., Springer.

[25] Ryzhov, O.S. & Smith, F.T. 1984 Short-length instabilities, breakdown and initial value problems in dynamic stall. *Mathematika* **31**, 163–177.

[26] Smith, F.T. 1982 Concerning dynamic stall. *Aeron. Quart.* **33**, 331–352.

[27] Stewartson, K. 1969 On the flow near the trailing edge of a flat plate II. *Mathematika* **16**, 106–121.

[28] Stewartson, K. 1970 Is the singularity at separation removable? *J. Fluid Mech.* **44**, 347–364.

[29] Stewartson, K., Smith, F.T. & Kaups, K. 1982 Marginal Separation. *Stud. in Appl. Math.* **67**, 45–61.

[30] Sychev, V.V., Ruban, A.I., Sychev, Vic.V. & Korolev, G.L. 1998 *Asymptotic Theory of Separated Flows*, Cambridge University Press.

[31] Troger, H. & Steindl, A. 1991 *Nonlinear Stability and Bifurcation Theory*, Springer.

[32] Van Dyke, M. 1962 Higher approximations in boundary-layer theory. Part 1. General analysis. *J. Fluid Mech.* **14**, 161–177.

[33] Weideman, J.A.C. 2003 Computing the dynamics of complex singularities of nonlinear PDEs. *SIAM J. Appl. Dyn. Sys.* **2**, 171–186.